Deliverable D19 (D3.4)

High resolution mapping over European urban areas

RI-URBANS

Research Infrastructures Services Reinforcing Air Quality Monitoring Capacities in European Urban & Industrial AreaS (GA n. 101036245)

By

INERIS, FORTH, FMI, MET Norway, TNO, CNRS & ENPC

26 March 2024

RI-URBANS (**www.RIURBANS.eu**) is supported by the European Commission under the Horizon 2020 – Research and Innovation Framework Programme, H2020-GD-2020, Grant Agreement number: 101036245

Deliverable D19 (D3.4): High resolution mapping over European urban areas

Authors: Augustin Colette (INERIS), Antoine Guion (INERIS), Florian Couvidat (INERIS), Karine Sartelet (ENPC), Soo-Jin Park (ENPC), Lya Lugon (ENPC), Astrid Manders (TNO), Floris Pekel (TNO), Renske Timmermans (TNO), Janot Tokaya (TNO), Richard Kranenburg (TNO), Hasna Chebaicheb (INERIS), Mohammed Gherras (INERIS), Victor Lannuque (INERIS), Alicia Gressent (INERIS), Benjamin Chazeau (AMU), David Simpson (MET Norway), Hilde Fagerli (MET Norway), Willem van Caspel (MET Norway), Bruce Denby (MET Norway), Ruud Janssen (TNO), Petros Vasilakos (PSI), Kaspar Dällenbach (PSI), Gaëlle Uzu (IGE), David Patoulias (FORTH), Elena Pouliki (FORTH), Ksakousti Skyllakou (FORTH), Evangelia Siouti (FORTH), Spyros Pandis (FORTH), Gilles Foret (LISA), Matthieu Vida (LISA), Guillaume Siour (LISA), Matthias Beekmann (LISA)

Work package (WP)	WP3 Improving modelling and emission inventories for policy assessment using advanced observation-based methodologies
Deliverable	D19 (D3.4)
Lead beneficiary	INERIS
Deliverable type	☐ R (document, report) ☐ DEC (websites, patent filings, videos, …) ■ Other: ORDP (open research data pilot)
Dissemination level	■ PU (public) ☐ CO (confidential, only members of consortium and European Commission))
Estimated delivery deadline	M30 (31/03/2024)
Actual delivery deadline	26/03/2024
Version	Final
Reviewed by	WP3 leaders and coordinators
Accepted by	Project coordination team
Comments	This deliverable presents the progress achieved within T3.3 of RI-URBANS by a consortium of 8 European air quality modelling teams (INERIS, FORTH, FMI, MET Norway, TNO, CNRS/CEREA, CNRS/LISA, ENPC) and in very close collaboration with observation providers.

RI-URBANS (**www.RIURBANS.eu**) is supported by the European Commission under the Horizon 2020 – Research and Innovation Framework Programme, H2020-GD-2020, Grant Agreement number: 101036245

Table of Contents

RI-URBANS (**www.RIURBANS.eu**) is supported by the European Commission under the Horizon 2020 – Research and Innovation Framework Programme, H2020-GD-2020, Grant Agreement number: 101036245

1 About this document

This deliverable presents the progress achieved within Task 3.3 of the Project RI-URBANS by a consortium of 8 European air quality modelling teams (INERIS, FORTH, FMI, MET Norway, TNO, CNRS/CEREA, CNRS/LISA, ENPC) and in very close collaboration with observation providers.

The task was designed originally to enhance selected chemistry-transport models (CTMs), PM Comprehensive AQ Model with eXtensions for UltraFines (PMCAMx-UF), CHIMERE, EMEP, LOTOS-EUROS, SILAM) to quantify source contributions to conventional and novel AQ health metrics (nanoparticles, OP). Besides modelling developments, an important focus was given to combine the CTMs with urban observational data of in situ atmospheric concentrations (in connection with RI-URBANS W1).

The goal of this task was to provide maps of source-specific information on health relevant air pollution indicators at high resolution (1x1 km2) over specific urban areas and over the remaining European regions. The improved modelling tools will subsequently be used in T3.4 and implemented in specific pilot tests-demonstrations (SP2) and in the roadmap for upscaling (SP3).

In the first part of this document (Section 2), we focus on development in regional models, but at a spatial resolution representative of urban background. The use of chemistry-transport models at regional scale is motivated by (i) the importance of secondary species at regional scale, (ii) the larger availability (for the time being) of observations and multi-model ensembles when including suburban areas, (iii) the importance of long-range background contributions. Bringing together high resolution and urban background modelling also allows building upon WP1 measurement of Source Apportionment for both PM mass and number (UFP) concentrations. This step is instrumental in developing the models and ensuring their evaluation with regards to source apportionment which are strong pre-requisite before engaging in the definition of advanced metrics for health and policy.

In Section 2, four main areas of work are covered:

2.1. BC evaluation. Here a new model/measurement methodology is proposed to compare the CAMS ensemble of models (8 models in this case) with aethalometer data. The difficulty to compare modelled Elemental Carbon (EC) to observed EC and equivalent Black Carbone (BC) is addressed, as well as the issue of comparing the source apportionment of solid fuel and liquid fuels. The proposed methodology builds upon information provided by the RI-URBANS measurement community to account for observation uncertainties in the model evaluation. The goal of this activity is to focus on source apportionment of primary constituents of atmospheric particulate matter (PM) before engaging to secondary species. The EC model results are already produced in the CAMS operational service, and observed eBC source apportionment is very close to operational nera real time (NRT) measurements delivery, making it a good candidate for an operational Service Tool (ST).

2.2. Organic Aerosol (OA) evaluation. In that section we use PMF analysis of online speciation by ACSM measurements versus model results. Detailed modelled OA is not yet available in the CAMS production, so we use four different model design (CHIMERE, CAMx, EMEP, and LOTOS-EUROS) to ensure that the comparison methodology is generic enough. The ACSM data are also close to become available in near real time, which opens the perspective for a Service Tool on the evaluation of hydrogenated, biomass burning and oxigenated organic aerosols (HOA, BBOA and OOA, respectively).

RI-URBANS (www.RIURBANS.eu) is supported by the European Commission under the Horizon 2020 – Research and Innovation Framework Programme, H2020-GD-2020, Grant Agreement number: 101036245

2.3. Oxidative Potential (OP) Modelling. The modelled source apportionment can be combined with the measured source-specific oxidative potential. The challenge lies in matching the sources in the models and observations. It also requires a good understanding of the methodologies and uncertainties in quantifying observed source specific OP. There is also a link with the demonstration of the capacity of models to reproduce the relative abundance of the sources, hence the link with eBC and Organic Carbon (OC) source apportionment in the first two items. Ultimately, the target is to produce maps and time series of OP over Europe which will be a key outcome in terms of health relevant indicators.

2.4. UFP Modelling. Here we focus on ultrafine particles, which are also a key indicator of relevance for health impacts. This activity also largely relies on data collected in WP1, including when it comes to the evaluation of modelled and measured source apportionment.

In the second part of the deliverable (Section 3), the focus is on high resolution mapping over selected European urban areas. We build upon the methodologies developed at regional scale (in Section 2) but increase the spatial resolution and couple regional and city scale models to provide close-up maps for eBC, OP and UFPs.

The work presented here is also related to other modelling endeavors in the RI-Urbans project which are documented in Deliverables D3.1 and D4.6 (also finalized in March 2024). D3.1 is a "Framework to cross-check methodologies to assess urban emissions", while it also relies on high resolution modelling in urban areas, the topic is on improving emissions rather than building health and policy relevant indicators. D4.6 is about "Air pollution variability in the pilot cities". There, the focus in on NO_2, PM2.5, eBC and UFP and intra-city variability by also comparing various modelling approaches (deterministic multi-scale models and LUR-based models) for the pilots of Paris, Birmingham, Bucharest, Athens and Rotterdam.

The present D3.4 shows the outcome of the development activities in T3.3 "Extending AQ modelling to health and policy relevant indicators down to urban scale". After March 2024, this work will be transferred to T3.4 where the demonstration of policy relevance will be consolidated, and to T 5.3 "Establishing the modelling framework supporting RI-URBANS services" where the methodologies will be translated in terms of Service Tools.

This document is a public document that will be distributed to all RI-URBANS partners for their use and submitted to the European Commission as an RI-URBANS deliverable D19 (D3.4). This document can be downloaded at https://riurbans.eu/work-package-3/#deliverables-wp3

Acknowledgements

Data providers are acknowledged, as far as Oxidative Potential Measurements are concerned, we are grateful to the following: for French data: Gaëlle Uzu (IGE), Jean-Luc Jaffrezo (IGE), Olivier Favez (INERIS / LCSQA), for Spanish data: Xavier Querol (CSIC), Gaëlle Uzu (IGE), for Swiss data: Christoph Hueglin (EMPA), Gaëlle Uzu (IGE).

RI-URBANS (www.RIURBANS.eu) is supported by the European Commission under the Horizon 2020 – Research and Innovation Framework Programme, H2020-GD-2020, Grant Agreement number: 101036245

1.1 Key Findings, Status and Future Plans

- Black Carbon Model / Observation evaluation. We developed a robust methodology to compare modelled elemental carbon to available equivalent black carbon measurement accounting for the data harmonization and uncertainty estimates consolidated by observations experts in RI-Urbans WP1. The evaluation accounting for model and observation uncertainties relies on FAIRMODE evaluation metrics. The comparison also extends to the source apportionment of solid/liquid fuel in eBC paving the way to the evaluation of source apportionment. We demonstrate the feasibility of the comparison using past reanalysis and daily operation production of the ensemble of CAMS models. A demonstrator of NRT evaluation is proposed as a first stage towards a future Service Tool to be further refined in WP5.
- Organic Aerosol Model / Observation evaluation. A first multi-model comparison to ACSM OA speciation (HOA, BBOA, OOA) is proposed. The work consisted in deriving a consistent comparison for 4 different models, accounting for the specificities of different SOA formation mechanisms and assumptions related to the volatility in emissions. We illustrate and discuss the performances of each models but the actual methodology to perform this evaluation constitutes an important step to deriving long standing Service Tools. Note that the configuration used in the models involved deviates from the standard operational setup (as in CAMS for instance). Further work will be required in the model to apply such evaluation techniques using NRT ACSM data consolidated in the pilot supersites.
- Modelling the Oxidative Potential of Particulate Matter. Three regional CTMs were developed to model the Oxidative Potential of PM. A close consideration of sector allocation of different PM component was undertaken to match the intrinsic OP obtained from measurement studies. Different OP metrics obtained from several field studies were considered. When giving an accurate level of scrutiny to the specific methodologies, these first results of multi-model and multi-methodologies OP modelling give broadly consistent results, while further work remains to fine tune the matching of model and observation.
- Ultrafine Particle Modelling in Europe. A new inventory for UFP emission were implemented in a new version of the PMCAMx-UFP model. The model was compared to observations and used to assess the main sector contributing to UFP at European scale.
- The development undertaken at European scale are further declined over city pilots at resolution equal or higher than 1km. Case studies are presented for Paris, Athens, Barcelona, and Rotterdam are presented, also including source apportionment of UFP modelling for some of these cities. The downscaling at high resolution of OP modelling is also introduced for selected target cities.

RI-URBANS (www.RIURBANS.eu) is supported by the European Commission under the Horizon 2020 – Research and Innovation Framework Programme, H2020-GD-2020, Grant Agreement number: 101036245

2 Mapping Urban Background Air Quality

2.1 Black Carbon Model/Observation evaluation (INERIS)

2.1.1 Design of the Model evaluation for the year 2018

2.1.1.1 Source of Model Results

Simulations of 8 chemistry-transport models (CTMs) are used for the evaluation of surface concentrations of BC. These simulations are part of a multi-model consistent modelling experiment conducted in 2021 as part of the CAMS_61 project led by TNO and MET Norway. The target year for the simulation was 2018, which is also convenient in terms of availability of observations. The participating CTMs are listed below with their referent institute:

- CHIMERE (INERIS, France)
- MONARCH (BSC, Spain)
- MINNI (ENEA, Italy)
- MATCH (SMHI, Sweden)
- LOTOS-EUROS (KNMI & TNO, the Netherlands)
- DEHM (AARHUS UNIVERSITY, Denmark)
- EURAD-IM (FZJ-IEK8, Germany)
- EMEP (MET Norway, Norway)

The regional simulations were carried out over the European domain with spatial coverage extending to 30°W-45°E, 30°N-75°N. Spatial resolution is 0.1° to 0.2° depending on the model, on a regular latitude-longitude grid. The Ensemble is calculated from the median of the models for each grid cell. Only EC simulated concentrations are considered here. The outputs of the concentration fields are at the hourly time steps for the whole of 2018.

All the models use the same emission inventory: CAMS REG AP_v2.2.1_2015_ REF2, where condensable PM are represented in a consistent way for all European countries. Two main source of emission temporalisation were considered in this experiment, depending on each model: GENEMIS (Ebel et al., 1997) and TNO (Denier van der Gon et al., 2011). Total annual emissions of PM are officially reported per country (based on official statistics) and then distributed in space and time based on specific proxies that vary between inventories. At the sector level, PM emissions are then split into various components (e.g. EC, OC). The EC source apportionment calculated from the model results is based on emission inventories that differentiate the residential sector (solid fuels) from the rest, i.e. mainly traffic (liquid fuels).

2.1.1.2 Source of Observations

The source of observations used for the model evaluation is provided by the RI-URBANS' D1.1 referenced in Savadkoohi et al. (2023). It compiles datasets of ambient eBC and EC measurements with instrumental and operational settings to determine the source contributions from biomass burning and traffic. Concentration time series are available for 53 sites in Europe over the period 2006-2022. For 2018, 18 stations report measurements of eBC and 6 stations report co-localised measurements of EC.

The EC and eBC measurement methods are very different and do not quantify black carbon concentrations in the same way. EC measurements are based on thermo-optical methods. While this type of method has the advantage of having a referenced technique (EUSAAR-II Protocol for Europe), it can be operated either off-line using (quartz) filters or continuously, as with the SUNSET Field Analyzer.

RI-URBANS (www.RIURBANS.eu) is supported by the European Commission under the Horizon 2020 – Research and Innovation Framework Programme, H2020-GD-2020, Grant Agreement number: 101036245

Instruments for measuring eBC (e.g. aethalometers, multi-angle absorption photometers) are based on a light absorption. They convert the measured light attenuation (B_{abs}) of black carbon particles into eBC concentration using the Mass Absorption Cross section (MAC) coefficient:

$$eBC = \frac{B_{abs,BC}}{MAC}$$

Although these instruments are easy to set up and have a high temporal resolution, they have the disadvantage of not being part of a reference method, as the MAC value is highly variable (in space and time). The MAC coefficient depends on many parameters that can vary (e.g. BC sources, the mixing state).

As a result, comparing model outputs of EC with observations can be challenging, as direct measurements of EC are rarer and those of eBC are indirect. eBC measurements must therefore be converted for comparison (see next section).

2.1.2 Results of the Model evaluation for the year 2018

2.1.2.1 Scores for EC and eBC

The performance scores of the CAMS models are first calculated for EC observations. ***Table** 1* presents the average scores for 6 stations. On average, the ENSEMBLE underestimates EC concentrations by –0.15µg/m^3 and has an RMSE of 0.51µg/m^3. The temporal correlation coefficients are greater than 0.6 for all stations except for Bern Bollwerk.

For almost half of EC measurements (48% of the total), the mean bias with the ENSEMBLE (mod. – obs.) is greater than the standard deviation of ENSEMBLE. In this case, it is difficult to identify which model fits the best, as the observed concentration do not even fall within the range of concentrations simulated by the models. Our analysis shows that this depends heavily on the site, concerning mainly sites in "urban" areas. **Figure** 1 illustrates this with the Athens NOA station (urban) where almost all the models underestimate the EC concentration throughout the year, while observations at Paris Sirta (suburban) are within the standard deviation of the ENSEMBLE. One possible explanation is the problem of sub-grid representativeness for urban and/or traffic stations, which concerns all models operating on a grid. Another discrepancy between simulated and measured concentrations concerns coastal towns with high port activity such as Marseille or Barcelona. This could be due to an underestimation of shipping emissions in the models.

The variability between models (standard deviation of 0.27µg/m^3 on average at the stations) reflects the significant uncertainty in the simulated EC concentrations. Model uncertainty can arise from different factors. The main one is the emissions inventory used. Emissions inventories are theoretically based on EC measurements but are probably a mixture of EC and eBC measurements. Another important factor is the diversity of the CTM formulation, especially concerning the PM distribution and the aerosol speciation.

To compare the eBC observations, which we have for 18 stations, with the simulated EC concentrations, the measurements were normalized by a constant harmonization factor (H) equal to 1.76 (Yus-Diez et al., 2021), as suggested by ACTRIS. Table 1 shows the performance scores of the models compared with the harmonised eBC measurements for 18 stations. The average bias is –0.14µg/m^3 and the RMSE 0.60µg/m^3. The correlation coefficient is lower (R= 0.53) than for EC measurements but it should be noted that we focus on different stations so the comparison is not direct.

eBC measurements are subject to considerable uncertainty. eBC measurements are very sensitive to the MAC used. **Figure 2** shows the distribution of the eBC with a MAC calculated specifically for the site concerned (local MAC) and the median values for the sites (median MAC). The values can vary by up to 50%. Given this additional uncertainty factor, the EC (compared with the eBC) appears to be a more relevant measure for assessing the model simulation.

RI-URBANS (www.RIURBANS.eu) is supported by the European Commission under the Horizon 2020 – Research and Innovation Framework Programme, H2020-GD-2020, Grant Agreement number: 101036245

***Table** 1. Performance scores for surface concentrations simulated by the model Ensemble from CAMS evaluated in 2018 for each EC and eBC measuring station.*

		Mean concentration of observations [μg/m^3]	Mean concentration of the model ensemble [μg/m^3]	Bias (mod.-obs.)	RMSE	Pearson correlation (R)
EC	Mean stations	0.73	0.58 (σ = 0.27)	-0.15	0.51	0.62
	Paris Sirta	0.50	0.79 (σ = 0.30)	0.29	0.48	0.71
	Athens NOA	1.16	0.66 (σ = 0.30)	-0.50	0.93	0.62
	Athens Demokritos	0.36	0.48 (σ = 0.29)	0.12	0.21	0.67
	Bern Bollwerk	0.86	0.54 (σ = 0.23)	-0.32	0.53	0.28
	Marseille Longchamp	0.96	0.34 (σ = 0.11)	-0.62	0.64	0.71
	Zurich Kaserne	0.54	0.68 (σ = 0.36)	0.14	0.28	0.74
eBC	Mean stations	0.74	0.60 (σ = 0.28)	-0.14	0.60	0.53
	Paris Sirta	0.37	0.78 (σ = 0.29)	0.41	0.63	0.43
	Athens NOA	1.02	0.65 (σ = 0.29)	-0.37	0.66	0.76
	Athens Demokritos	0.49	0.50 (σ = 0.30)	0.01	0.21	0.61
	Bern Bollwerk	0.50	0.54 (σ = 0.23)	0.04	0.30	0.47
	Marseille Longchamp	0.92	0.48 (σ = 0.17)	-0.43	0.53	0.85
	Zurich Kaserne	0.47	0.66 (σ = 0.33)	0.19	0.36	0.63
	Lille Villeneuve d'Ascq	0.41	1.25 (σ = 0.52)	0.84	1.29	-0.20
	Stockholm Torkel	0.17	0.29 (σ = 0.12)	0.12	0.20	0.50
	Barcelona Palau Reial	0.92	0.73 (σ = 0.31)	-0.18	0.49	0.58
	Helsinki Itä-Hakkila	0.54	0.30 (σ = 0.14)	-0.25	0.39	0.69
	Milan Pascal	1.10	1.29 (σ = 0.82)	0.19	0.35	0.89
	Stockholm Hornsgatan	0.55	0.29 (σ = 0.12)	-0.26	0.37	0.28
	Bucharest INO	1.10	0.88 (σ = 0.42)	-0.21	1.05	0.40
	Paris Blvd Haussman	1.36	0.88 (σ = 0.36)	-0.48	0.71	0.59
	SMEAR II Hyytiälä	0.18	0.11 (σ = 0.05)	-0.07	0.14	0.73
	Granada UGR	1.21	0.17 (σ = 0.08)	-1.04	1.25	0.36
	Madrid CIEMAT	1.19	0.11 (σ = 0.04)	-1.08	1.38	0.36
	Paris PA13	0.83	0.87 (σ = 0.35)	0.05	0.45	0.64

RI-URBANS (www.RIURBANS.eu) is supported by the European Commission under the Horizon 2020 – Research and Innovation Framework Programme, H2020-GD-2020, Grant Agreement number: 101036245

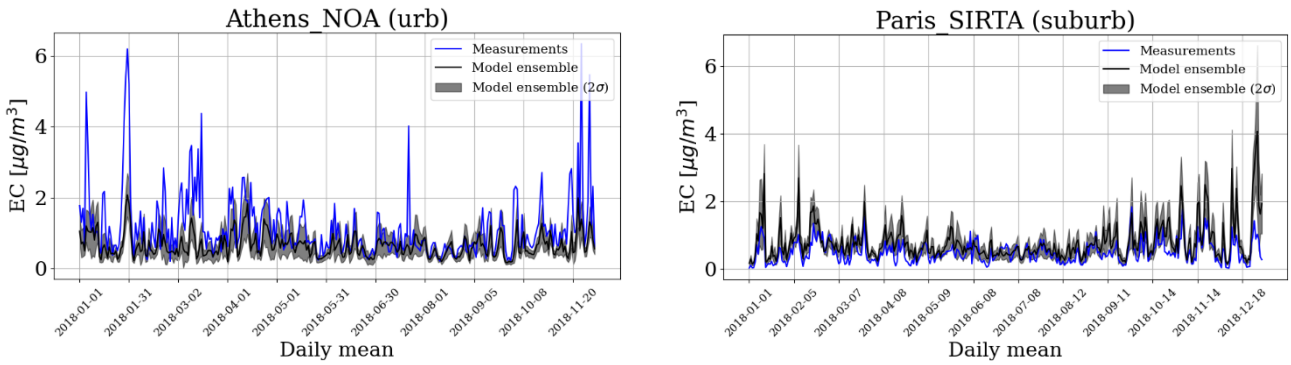

***Figure** 1. Daily time series of EC concentration in µg/m3 simulated by the CAMS Ensemble and measured for the whole 2018 at Athens-NOA and Paris Sirta stations (right and left panel respectively).*

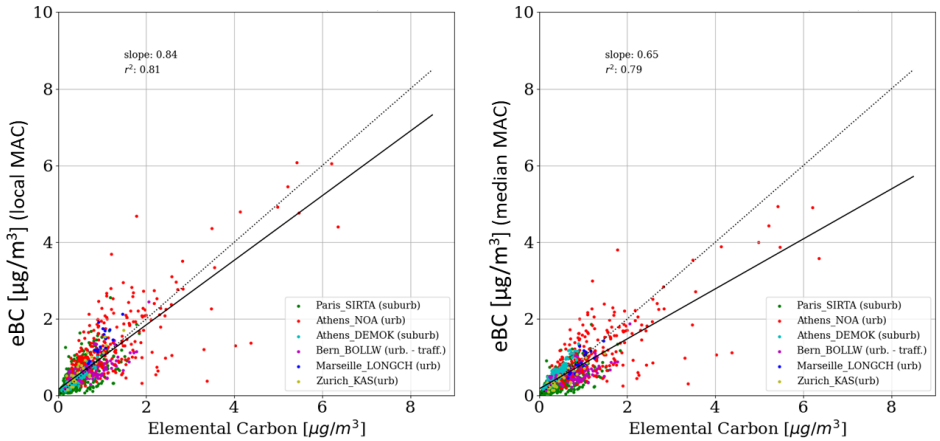

***Figure 2.** Scatter plot of co-localised measurements of eBC and EC at 6 stations with local MAC (left panel) and median MAC (right panel).*

2.1.2.2 Evaluation for sf/lf in eBC

Source apportionment between solid fuels (sf, mainly from the residential sector) and liquid fuels (lf, mainly from the traffic sector) can be estimated from aethalometer instruments and therefore used for model evaluation. Since different combustion sources exhibit a different light absorption wavelength dependence, this can be used for source apportionment of eBC. While emissions from liquid fuel sources contain predominantly pure eBC dominate at IR wavelengths and exhibit only a weak wavelength dependence, solid fuel combustions contain light absorbing organic substances, show an enhanced absorption in the N-UV range and are strongly wavelength dependent. The "Aethalometer model" (Sandradewi et al., 2008) based on source-specific Absorption Angstrom Exponents (AAE), is a method for separating these two combustion types when only two eBC sources are present.

Table 2 presents the scores of the model ENSEMBLE for the eBC fraction from liquid fuels (linked to the traffic sector). Scores vary widely between measurement sites. On average, the ENSEMBLE attributes a smaller fraction of the eBC to traffic (average bias of -14.7%) compared with the measurements. This may be linked to the problem of sub-grid representativeness. Although annual variability is generally well simulated, with a maximum of the solid fuels fraction in winter and a minimum in summer, the average temporal correlation coefficient is only 0.50. It varies from almost 0.1 for the "Lille Villeneuve d'Ascq" site to 0.84 for "Paris Sirta".

RI-URBANS (www.RIURBANS.eu) is supported by the European Commission under the Horizon 2020 – Research and Innovation Framework Programme, H2020-GD-2020, Grant Agreement number: 101036245

***Table** 2. CAMS Ensemble model performance scores for the average attribution of eBC to fossil fuels for 18 European sites assessed in 2018. Solid fuels are considered as the complementary source to traffic for a total eBC.*

	Mean source attribution to fossil fuel from observations [%]	Mean source attribution to fossil fuel from the model ensemble [%]	Bias (mod.-obs.)	RMSE	Pearson correlation (R)
Mean stations	77.2	62.5	-14.7	21.2	0.50
Paris Sirta	72.7	56.5	-16.2	18.1	0.84
Athens NOA	67.1	77.8	10.7	12.8	0.74
Athens Demokritos	75.1	77.2	2.0	7.2	0.73
Bern Bollwerk	70.0	59.1	-10.9	15.5	0.56
Marseille Longchamp	83.2	61.2	-21.7	23.7	0.74
Zurich Kaserne	76.2	58.4	-17.8	20.7	0.62
Lille Villeneuve d'Ascq	72.4	50.9	-21.5	23.1	0.06
Stockholm Torkel	74.9	53.8	-21.1	26.3	0.33
Barcelona Palau Reial	81.1	56.1	-25.0	26.5	0.58
Helsinki Itä-Hakkila	65.1	63.7	-1.4	11.9	0.63
Milan Pascal	85.0	74.9	-10.1	10.8	0.32
Stockholm Hornsgatan	85.8	53.9	-31.9	36.0	0.29
Bucharest INO	61.8	42.2	-19.6	23.0	0.60
Paris Blvd Haussman	87.8	65.7	-22.1	24.1	0.54
SMEAR II Hyytiälä	89.0	54.1	-34.9	37.5	0.39
Granada UGR	72.9	89.1	16.2	19.4	0.24
Madrid CIEMAT	81.2	65.0	-16.2	20.3	0.31
Paris PA13	88.1	65.0	-23.1	24.6	0.72

The predefined source specific AAE used for the source apportionment is an additional uncertainty factor. Several parameters are present in the literature. As an alternative to the parameters suggested by Sandradewi et al. (2008) (AAE of 2 and 1) used here in the validation, Zotter et al. (2017) proposed other values (1.68 and 0.9). We tested the values of Zotter et al. (2017) on several stations. While the temporal correlation coefficient hardly varies (because the variability of the response does not change), the RMSE score can increase or decrease by a factor of

RI-URBANS (www.RIURBANS.eu) is supported by the European Commission under the Horizon 2020 – Research and Innovation Framework Programme, H2020-GD-2020, Grant Agreement number: 101036245

two depending on the station (because the fraction of eBC attributed to traffic changes). **Figure** 3 show an example for the station "Athens NOA" with the different parameters.

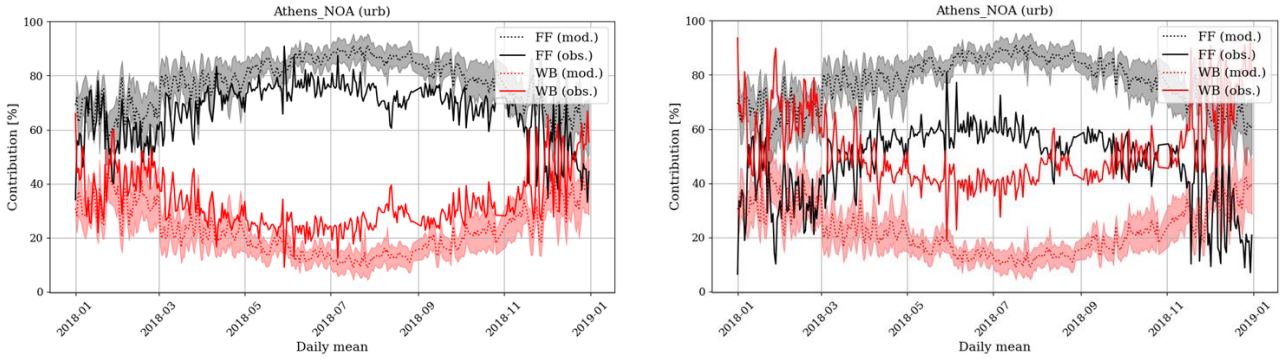

***Figure** 3. Source distribution of eBC based on aethalometers using the AAE values of Sandradewi et al. (2008) (left panel) and Zotter et al. (2017) (right panel) and compared with the model ENSEMBLE for the "Athens NOA" station in 2018.*

2.1.2.3 Factoring uncertainty in the evaluation (FAIRMODE Target Plots)

To provide a more relevant assessment, a factor incorporating the uncertainty of the observations was included using the FAIRMODE model evaluation protocol. To calculate the Modelling Quality Index (MQI), the measurement uncertainty must be included. Although the FAIRMODE Guidance Document on Modelling Quality Objectives and Benchmarking (Janssen et al., 2022) provides the necessary parameters to calculate the measurement uncertainty for the main pollutants (NO_2, O_3, $PM_{2.5}$ and PM_{10}), this is not the case for EC. Based on the scientific literature and the evaluation of EC and eBC performed over 2018, we propose here an innovative adaptation of the FAIRMODE target plots for the EC species.

The measurement uncertainty for a given pollutant depends on its concentration level, is estimated as the 95th percentile highest value from instrument inter-comparison results and is expresses for times series and yearly averaged values (Janssen et al., 2022). It uses the following parameters: the reference value in µg/m^3 (RV), the relative uncertainty around RV in % (U_r), the non-proportional fraction around RV in % (α). The RV for EC set at 1.6µg/m^3 is calculated from that defined for $PM_{2.5}$ (20µg/m^3) multiplied by the EC/$PM_{2.5}$ fraction (~6%) as reported from different measurements in Pérez et al. (2008) and Hussein et al. (2022). Based on several experimental studies on the characterisation of uncertainties in thermo-optical EC measurements, U_r was set at 25% for EC (e.g. Brown et al., 2017; Merico et al., 2019) and at 50% for eBC (e.g. Mbengue et al., 2020; Zhao et al., 2021). The value of 50% for the eBC is of the same order of magnitude as the differences obtained in the 2018 assessment with the different MACs used. Finally, the parameter α is the same as for $PM_{2.5}$ (50%) for EC and eBC.

Assessment target plots for EC and eBC are presented in **Figure 4**. Compared with the EC measurements, the ENSEMBLE model is outside the MQI target (MQI > 1) for 3 stations: "Athens NOA", "Marseille Longchamp" and "Paris Sirta". Nevertheless, the 90th percentile of the MQI for the 6 stations is close to the objective with 1.2. This plot directly shows that the simulated concentrations are underestimated at "Marseille Longchamp" and "Athens NOA", with a too low variability on the latter one. Compared with the eBC measurements, the ENSEMBLE model is in the target for all stations except for "Lille Villeneuve d'Ascq" (90th percentile of MQI of 0.9). As the measurement uncertainty for the eBC is large (50%), the simulations are more "easily" in the MQI target. A reduction in uncertainty for eBC measurements would allow a more relevant simulation evaluation. Finally, **Figure 5** summarizes the metric statistics for the evaluation by mixing all stations. This allows to know directly which metric of the

RI-URBANS (www.RIURBANS.eu) is supported by the European Commission under the Horizon 2020 – Research and Innovation Framework Programme, H2020-GD-2020, Grant Agreement number: 101036245

simulation must be improved to remain in the target of the MQI, such as correlation in time and space, standard deviation in time and space, bias, high percentile representations.

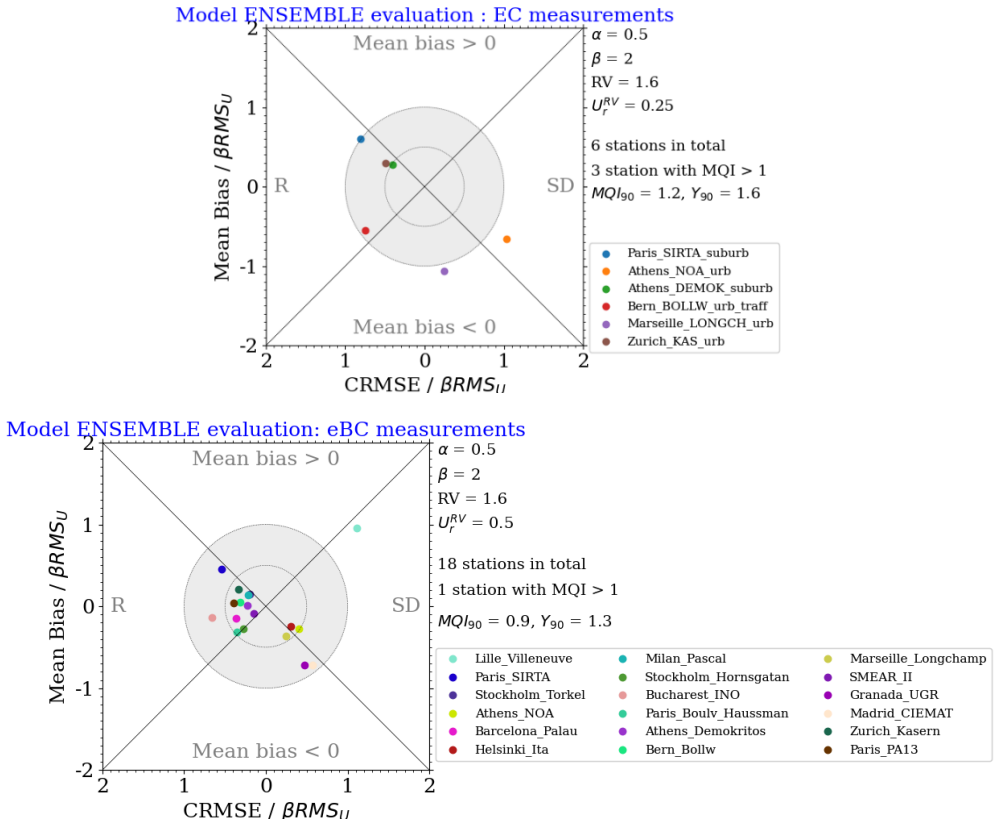

Figure 4. *Assessment target plot as defined in FAIRMODE for the ENSEMBLE model based on EC (top panel) and eBC (low panel) measurements in 2018.*

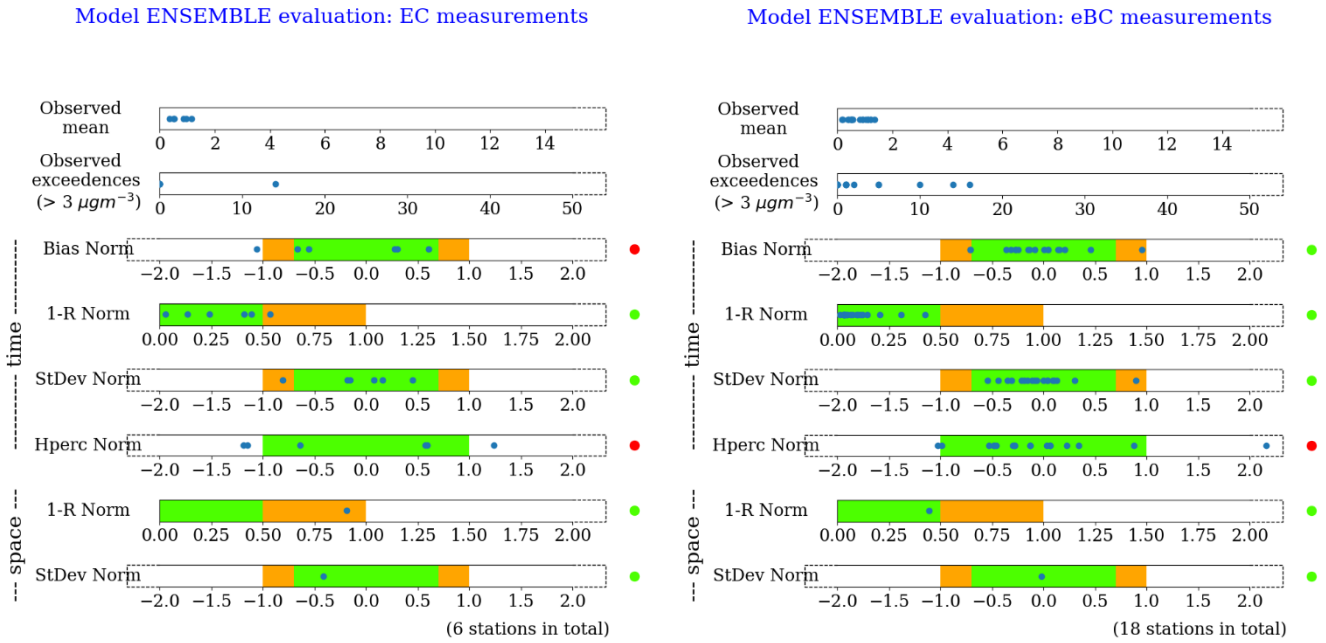

Figure 5. *Assessment plot of summary statistics as defined in FAIRMODE for the ENSEMBLE model based on EC (left panel) and eBC (right panel) measurements in 2018.*

RI-URBANS (www.RIURBANS.eu) is supported by the European Commission under the Horizon 2020 – Research and Innovation Framework Programme, H2020-GD-2020, Grant Agreement number: 101036245

2.1.3 Demonstrator for RI-Urbans Pilot Sites with NRT data

A programme for the evaluation in near-real time (NRT) of hourly BC concentrations and source distribution of CAMS models based on aethalometer measurements (hereinafter referred to as “EvaNRT - BC”) has been developed.

Currently at the demonstrator stage (beta version), the “EvaNRT - BC” programme provides daily evaluation of the air quality analyses (D-1) from the daily operation production of 11 CAMS air quality models obtained from the Atmosphere Data Store (CHIMERE, EMEP, LOTOS-EUROS, MATCH, MOCAGE, SILAM, EURA-IM, DEHM, GEM-AQ, MINNI and MONARCH) and its Ensemble (median) at the following RI-Urbans Pilot Sites : “Airparif BpEst”, “Airparif Chatelet”, “AMU Marseille-Longchamp", “APCG Athens-Noa", “APCG Athens-Demokritos", “CNR-ISAC Bologna”, “CNR-ISAC Milano”, “FMI Helsinki”, “PSI Zurich”, “RADO Bucharest” and “SIRTA Palaiseau”. “EvaNRT - BC” can handle missing observation data and a filter on outliers and observation quality flags can be set directly by the user.

eBC concentration observations are taken from AE33 aethalometers as obtained from the RI-Urban NRT Pilot cities and compared with EC concentrations from CTM simulations by applying a harmonization factor (H) equal to 1.76 (Yus-Diez et al., 2021). The data processing is documented in “Demonstrator for RI-URBANS Pilot Sites with NRT data” (INERIS & Datalystica, 2022).

The distribution of sources between "solid fuel" and "liquid fuel" is also evaluated, as detailed in the previous section (“Evaluation in sf/lf for eBC”). The aim of this demonstrator is to show that the evaluation in NRT of the EC simulated by the CTMs is possible, although certain points of the comparison method (e.g. MAC, H value) still need to be improved. **Figure** 6 shows an example of validation of the EC in NRT for the date 10-02-2024 at the "SIRTA Palaiseau (France)" site using analyses from several CAMS models and the Ensemble. This illustrates the diversity of EC concentrations simulated by the CTMs. For this day and site taken as an example, most models overestimate the EC concentration. The MATCH model has the lowest bias (+0.1 µg/m^3 on average). While all models use the same emission totals, and in most cases the same EC/OC splits, they use different temporal variation, and of course specific model processes. In that context it is interesting to emphasize that the LOTOS-EUROS model best reproduces the distribution of sources (compared with observations), but as many other of the models it overestimates almost all day long the total EC concentration (+0.4 µg/m^3 on average).

Relevant developments could be envisaged based on this demonstrator to improve our understanding of the dynamics of EC concentrations and its source distribution, thanks to a better synergy between measurements and simulations. For example, with a better estimate of the uncertainty measurement, FAIRMODE (Modelling Quality Objectives and Benchmarking) plots could be calculated in NRT.

RI-URBANS (www.RIURBANS.eu) is supported by the European Commission under the Horizon 2020 – Research and Innovation Framework Programme, H2020-GD-2020, Grant Agreement number: 101036245

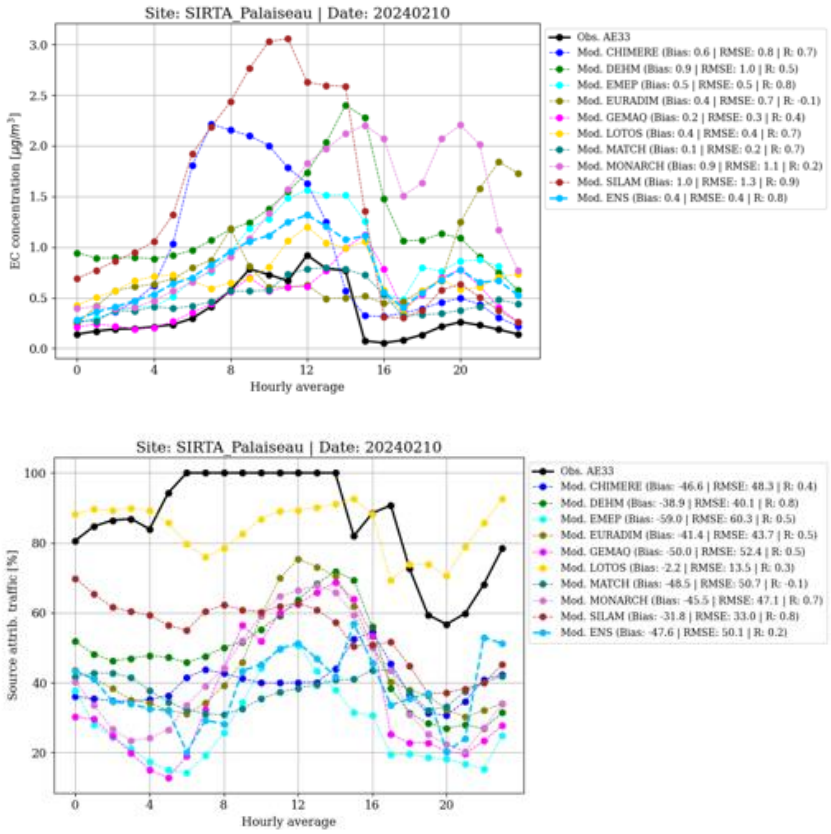

***Figure** 6. Hourly time series of EC concentration in µg/m³ (top panel) and attribution of traffic as source in % (lower panel) simulated by CAMS models and observed from AE33 measurements in a "pseudo-NRT" setup for the date of 10/2/2024 and based on operational models and NRT observations fluxes. Biomass combustion is considered as the complementary source to traffic for a total eBC concentration. Scores of bias (model - observation), RMSE and correlation (Pearson R) per model are given in brackets.*

2.2 Organic Aerosol Model/Observation evaluation (INERIS, TNO, METNO, PSI)

2.2.1 Design of the Model evaluation for the years 2017-2019

An intercomparison between several OA simulation results and ACSM OA PMF has been performed. Results from several CTMs for years 2017 to 2019 have been compiled and compared to PMF results available for those years. Four groups contributed to the intercomparison: CHIMERE (INERIS), CAMx (PSI), EMEP (MET Norway) and LOTOS-EUROS (TNO). All models and configurations are presented in the different factsheets in Annexes 1 to 4. The differences between models are summarized in **Table** 3. One important element of the comparison is that two models considered POA to be semivolatile (CHIMERE, LOTOS-EUROS) while the others considered it non-volatile (CAMx, EMEP). The volatility of primary SVOC is higher within CHIMERE than within LOTOS-EUROS. Indeed, under a temperature of 298K and an organic concentration of 2 ug/m^3, less than 30% of primary SVOC are in the particle with CHIMERE against 56% with LOTOS-EUROS.

RI-URBANS (www.RIURBANS.eu) is supported by the European Commission under the Horizon 2020 – Research and Innovation Framework Programme, H2020-GD-2020, Grant Agreement number: 101036245

***Table** 3. Comparison of the main features of the different models*

	CHIMERE	CAMx	EMEP	LOTOS-EUROS
SOA scheme	Wang et al. (2024) Mechanism reduced from explicit MCM+PRAM mechanism for monoterpenes and sesquiterpenes. H^2O is used for other precursors	VBS-1d (Jiang et al., 2019), which describes the evolution of OA in the 2-D space of oxidation state and volatility.	Standard VBS approach: "NPAS" scheme of Simpson et al. (2012), see also Bergström et al. (2012)	Standard VBS approach: Sturm et al. (2023)
POA treatment	Semivolatile. Distributed over 3 species with different volatilities based on May et al., (2013) for wood burning and Robinson et al. (2007) for other sources. POA distributed for C*<10 000 ug/m^3. According to the distributions, at 298K and 2 µg/m^3, 27% and 17.9% of primary SVOC are in the particle for biomass burning and for other sources, respectively.	Nonvolatile	Nonvolatile	Semivolatile. Custom distribution by volatility. POA distributed for C*<100 ug/m^3. According to the distributions, at 298K and 2 µg/m^3, 56% of primary SVOC are in the particle for all sources.
Aging of SOA	Aging represented explicitly for monoterpenes and sesquiterpenes (following the MCM mechanism). No aging for other precursors	No aging of SOA except for the oxidation of secondary gases from biomass burning with a reaction rate of 4×10^{-11} cm^3 $molec.^{-1}s^{-1}$. Decrease of volatility by a factor 10	Aging reduces volatility by a factor 10 and increase mass of by 7.5%. Aging kinetic of 4×10^{-11} cm^3 $molec.^{-1}s^{-1}$	Aging reduces volatility by a factor 10 and increases mass of by 7.5%. Aging kinetic of 1×10^{-11} cm^3 $molec.^{-1}s^{-1}$ for anthropogenic SOA. No aging for biogenic SOA

RI-URBANS (www.RIURBANS.eu) is supported by the European Commission under the Horizon 2020 – Research and Innovation Framework Programme, H2020-GD-2020, Grant Agreement number: 101036245

Aging of POA	A single oxidation step of aging. Decrease of volatility by a factor 100. Reactions rate of 4×10^{-11} cm^3 $molec.^{-1}s^{-1}$	No aging as POA is nonvolatile	No aging as POA is nonvolatile	As aging of anthropogenic SOA but with a kinetic of 4×10^{-11} cm^3 $molec.^{-1}s^{-1}$
IVOC	No IVOC emissions	No IVOC emissions	No IVOC emissions	IVOC/POA=1.5. IVOC are distributed for C*>100 ug/ m^3.

Due to different constraints within the different groups and to offer possibility to re-use already performed simulations, no common setup was agreed upon and the groups simulated one or two years of the 2017-2019 period. However, all the groups delivered simulations for the year 2019 as shown in **Table 4**. All modelling groups used different inventories. However, based on the information provided in the factsheets, all modelling groups used emission inventories including condensables (CAMS-REG REF2, EMEP with condensable) except for CAMX which used the TNO-MACCII inventory, hence excluding condensables.

Table 4: *Simulated years with the different models*

	2017	2018	2019
CHIMERE	x		x
CAMx	x		x
EMEP		x	x
LOTOS-EUROS			x

To perform comparison to urban stations, simulations with at highest reasonable resolution were asked for. The resolution is 0.1°x0.1° for CHIMERE and EMEP, 0.1°x0.2° for LOTOS-EUROS and 0.125°x0.25° for CAMx. Except for CAMx, which used WRF as a meteorological driver, all models used IFS meteorological data as input.

HOA, BBOA and OOA were directly calculated by the different groups with the same mapping strategy:

- BBOA is the sum of primary particulate organic aerosol (POA) from biomass burning
- HOA is the sum of POA from other sources
- OOA is the sum of all other organic compounds. For the models that considered POA to be semi-volatile, the secondary compounds formed from the oxidation of the primary SVOC are accounted for in OOA. EMEP also considered that some POA emitted by forest fires were directly counted in the OOA fraction.

This strategy results in very different estimations of BBOA and HOA between the models that considered POA as semi-volatile and the other models. Indeed, accounting for volatility may result in around one fifth of the POA to remain in the particle under ambient conditions. The remaining gaseous fraction in those models will react with OH and form less volatile secondary compounds.

RI-URBANS (www.RIURBANS.eu) is supported by the European Commission under the Horizon 2020 – Research and Innovation Framework Programme, H2020-GD-2020, Grant Agreement number: 101036245

2.2.2 Description of the PMF dataset

The data collected for this study are predominantly from the sites studied in Chen et al. (2022), with extended PMF analyses covering a longer time period for Athens-Demokritos, Barcelona, Bucharest, Carnsore Point, Dublin, Hyytiala, Marseille, ATOLL, and SIRTA. An additional site in London (Marylebone Road) and a site in Cyprus (Nicosia) were also included, as well as 10 French sites. In total, we collected data for 31 European sites, most of which are urban. In this study, we focused on the period 2017-2019. **Table 5** presents these sites and their information.

These datasets were processed using the same method, employing a harmonized protocol to resolve the sources of organic aerosols (OA) through rolling PMF analysis. This method involves dividing the dataset into shorter time periods referred to as windows, which move across the entire dataset. This approach offers the advantage of capturing temporal variability in source profiles across multi-year datasets. Primary and secondary organic aerosol factors were resolved for these datasets. The well-known primary factors include HOA (Hydrocarbon-like OA) and BBOA (Biomass Burning OA), identified at all sites except the rural site Hyytiala. Other primary factors were resolved at such sites, including COA (Cooking OA), CCOA (Coal Combustion OA), SFOA (Solid Fuel OA), etc. The secondary factors were distinguished between less and more oxidized oxygenated OA (LO-OOA and MO-OOA).

RI-URBANS (www.RIURBANS.eu) is supported by the European Commission under the Horizon 2020 – Research and Innovation Framework Programme, H2020-GD-2020, Grant Agreement number: 101036245

Table 5. *Description of station used in this study.*

Station Name	Station ID	Country	Latitude	Longitude	Station Type
Athens-Demokritos	DEM	Greece	37.995	23.816	Urban Background
Athens-Thissio	NOA	Greece	37.98	23.7	Urban Background
Barcelona	BCN-PR	Spain	41.3875	2.118	Urban Background
Birkenes	BIR	Norway	58.383	8.25	Regional Background
Magurele-Bucharest	INO	Romania	44.348	26.029	Suburban
Carnsore Point	CRP	Ireland	52.19	-6.34	Regional Background
Dublin	DUB	Ireland	53.3083611	-6.2235555	Urban Background
Helsinki	HEL	Finland	60.1964389	24.9519805	Traffic
Hohenpeißenberg	HPB	Germany	47.8013889	11.009722	Regional Background
Hyytiala	SMR	Finland	61.85	24.28333	Rural
Kosetice	KOS	Czech Republic	49.6	15.12	Regional Background
Krakow	KRK	Poland	50.0666667	19.91666	Suburban
ATOLL-Lille	ATOLL	France	50.611	3.1403	Suburban
London-Marylebone	LON-MR	United Kingdom	51.52	-0.15	Traffic
London-North Kensington	LON-NK	United Kingdom	51.5	-0.2	Urban Background
Marseille Longchamps	MAR-LCP	France	43.3052333	5.39469	Urban Background
Melpitz	MEL	Germany	51.9	13.55	Rural
Nicosia	CAO-NIC	Cyprus	35.1407755	33.3805388	Urban Background
SIRTA-Paris	SIRTA	France	48.71	2.15	Suburban
Tartu	TAR	Estonia	58.3705556	26.7347222	Urban Background
Zurich	ZUR	Switzerland	47.3775556	8.5305	Urban Background
Gennevilliers	GEN	France	48.9298083	2.2946194	Urban Background
Paris Les Halles	HALL	France	48.8627083	2.3446972	Urban Background
Paris BPEst	BPEst	France	48.8385167	2.4126242	Trafic
Rennes	REN	France	48.08965	-1.65911	Urban Background
Metz	MET	France	49.1102806	6.2233361	Urban Background
Strasbourg	STR	France	48.5062222	7.7511806	Urban Background
Creil	CRL	France	49.2597222	2.4744444	Urban Background
Lyon	LYN	France	45.75779	4.85422	Urban Background
Poitiers	POI	France	46.5839885	0.3455967	Urban Background
Talence	TAL	France	44.800442	-0.5893941	Urban Background

RI-URBANS (www.RIURBANS.eu) is supported by the European Commission under the Horizon 2020 – Research and Innovation Framework Programme, H2020-GD-2020, Grant Agreement number: 101036245

2.2.3 Results of the CTM Model evaluation

Here, we compare the PMF results with the CTM simulation results for different European sites. Specifically, we compared HOA, BBOA and OOA resolved from PMF with their estimations in four air quality models (LOTOS-EUROS, CHIMERE, CAMx and EMEP) for the common year 2019 where all simulation results are available. The CHIMERE species were specifically used from models output in the PM_1 fraction, but for EMEP and LOTOS-EUROS they were provided in the $PM_{2.5}$ fraction and assumed to be PM_1 without further correction. This assumption remains to be approved in the future.

Considering the availability of observation data, results from the 19 sites available for year 2019 have been compared. Mean concentrations, scores and diurnal profiles are shown in Figure 7, Figure 8, and Figure 9. Concentrations from boundary conditions of OOA simulated with CHIMERE and the fixed background concentrations of HOA from EMEP (0.2 µg m^{-3} for each) have been placed in OOA instead. At Hyytiala, only the OOA factor has been resolved by PMF, so here the modelled OOA presents the sum of HOA, BBOA, and OOA.

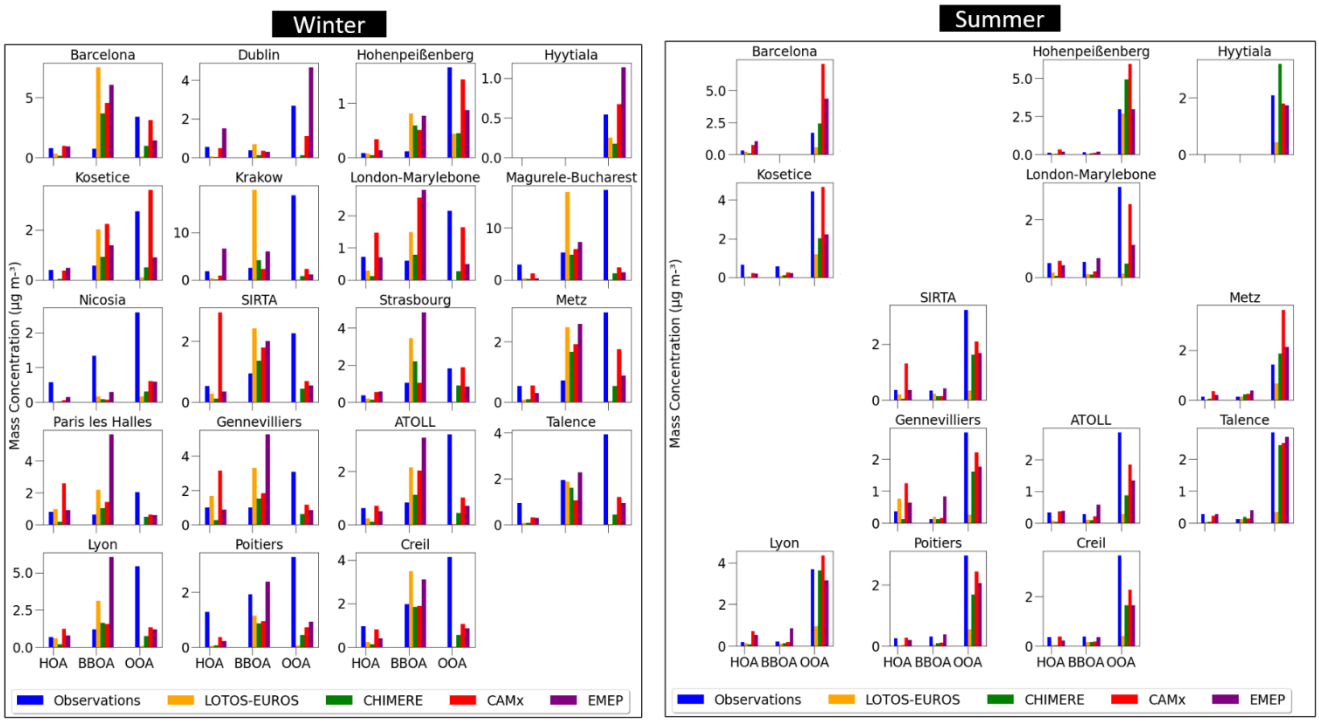

***Figure** 7. Mean mass concentration (in µg m^{-3}) of HOA, BBOA and OOA for observations (in blue) and simulations (in orange, LOTOS-EUROS; in green, CHIMERE; in red, CAMx; in purple, EMEP) at 19 European sites in winter (January-February-March) and summer (June-July-August) 2019.*

RI-URBANS (www.RIURBANS.eu) is supported by the European Commission under the Horizon 2020 – Research and Innovation Framework Programme, H2020-GD-2020, Grant Agreement number: 101036245

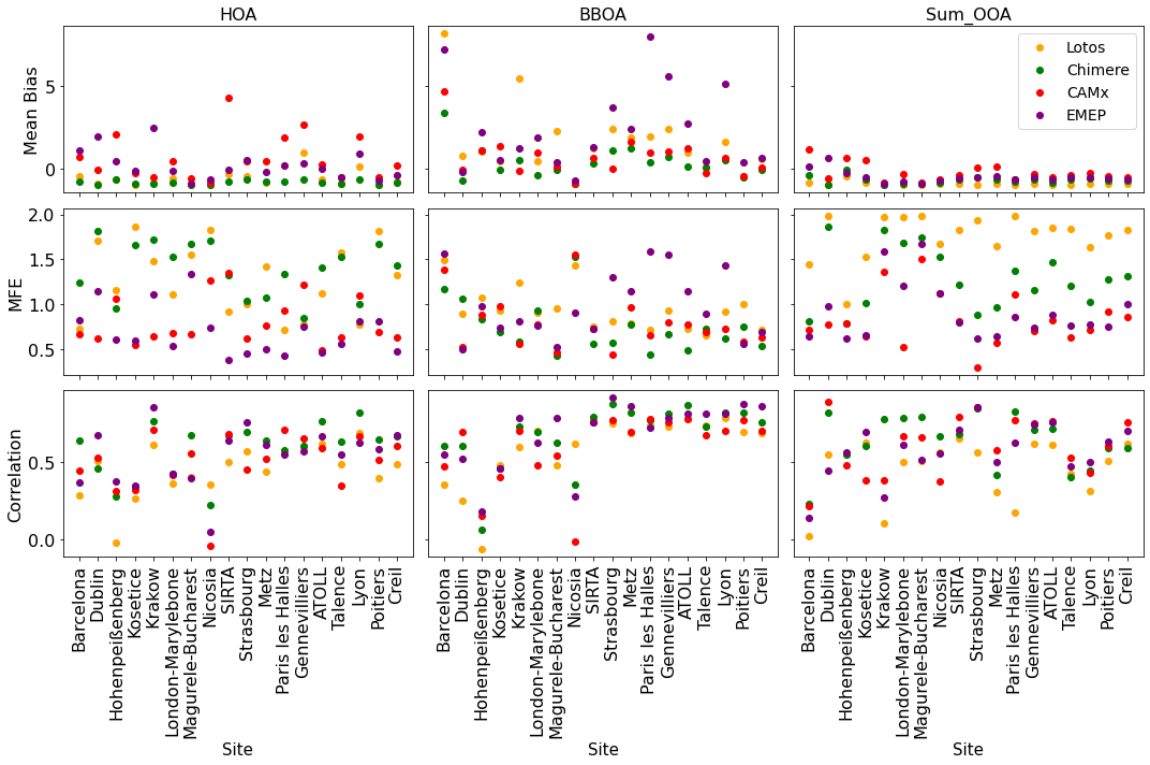

Figure 8. *Statistic scores (from top to bottom: mean bias, mean fractional error MFE, and correlation coefficient r) for OA factors (HOA, BOA and OOA) at each site, using daily averages.*

RI-URBANS (www.RIURBANS.eu) is supported by the European Commission under the Horizon 2020 – Research and Innovation Framework Programme, H2020-GD-2020, Grant Agreement number: 101036245

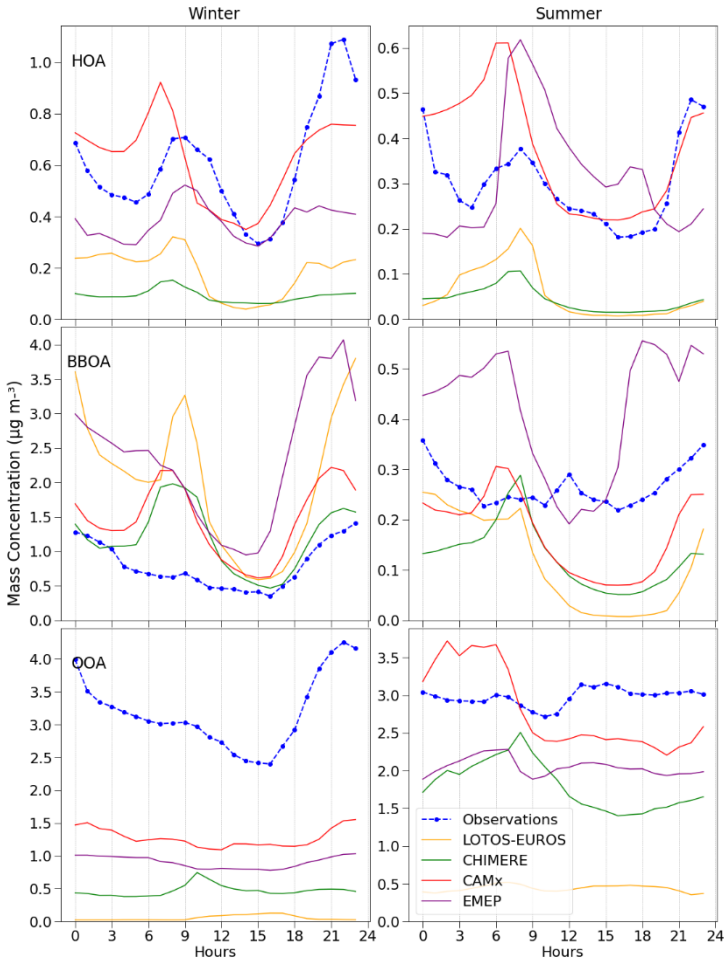

Figure 9. *Observed (in blue) and modelled (in orange, LOTOS-EUROS; in green, CHIMERE; in red, CAMx and in purple, EMEP) diurnal OA profiles (from top to bottom: HOA, BBOA and OOA; median) during winter and summer of 2019 across 18 European urban sites.*

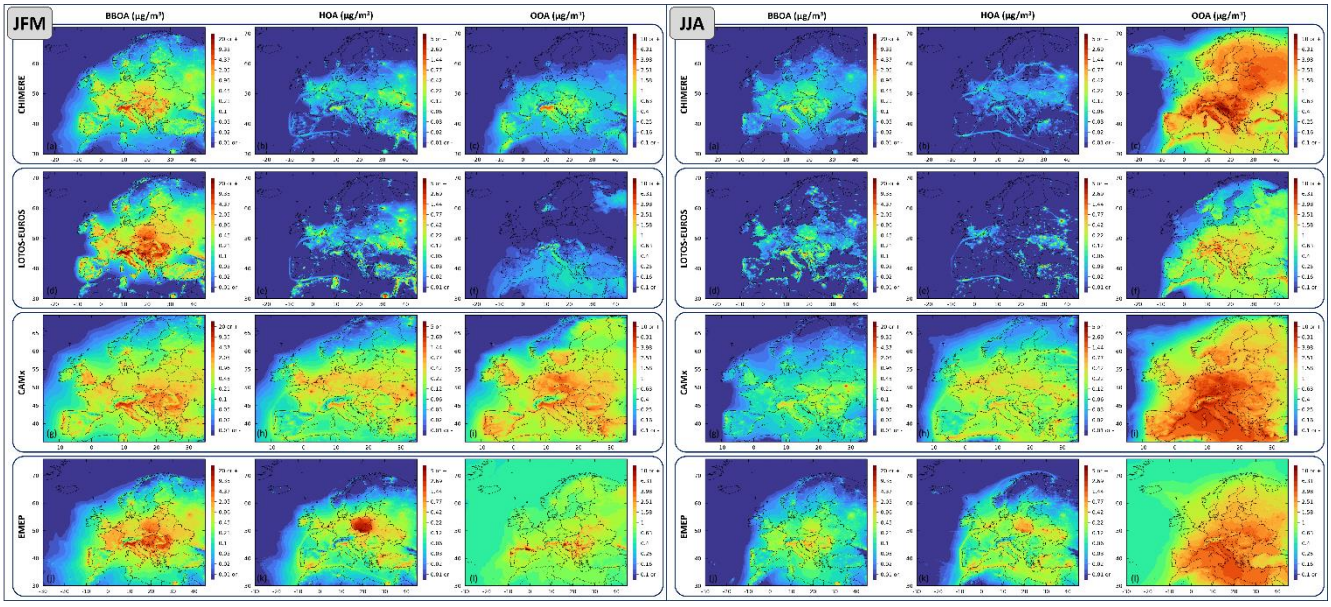

Figure 10. *Maps of simulated concentrations of HOA, BBOA and OOA for winter (left, January to March) and summer (right, June to August).*

RI-URBANS (www.RIURBANS.eu) is supported by the European Commission under the Horizon 2020 – Research and Innovation Framework Programme, H2020-GD-2020, Grant Agreement number: 101036245

2.2.4 Discussion on the results by season

In JFM (January to March), there is good spatial consistency between the different models for BBOA, with high concentrations in northern Italy and eastern Europe. Concentrations simulated by LOTOS-EUROS are locally higher, but also show greater spatial variability, which may be explained by higher local emissions and/or less advection/diffusion. The other three models give similar distributions of BBOA concentration which are overall higher with EMEP and lower with CHIMERE. For HOAs, two types of results can be observed: CHIMERE and LOTOS-EUROS (with POA treated as semi-volatile) simulate overall low concentrations except locally near sources (with some differences, LOTOS-EUROS simulating high concentrations in Tunisia, the Middle East, Moscow and the Nile delta and CHIMERE probably not due to different emission inventories). With CAMx and EMEP (which both treated POA treated as non-volatile), overall concentrations are similar and are higher far from sources throughout Europe. However, CAMx has a similar spatial distribution to LOTOS-EUROS with high concentrations near local sources. A particularity is observed with EMEP, which simulates high concentrations of HOA over the whole of Poland (which is probably due to the emission inventory used). For the OOA, the estimates are quite different depending on the model: low overall concentrations centered on the Mediterranean and Adriatic seas are modelled in LOTOS-EUROS. These low concentrations could partly be explained by the current distribution of the biomass burning emission over the volatility bins (most of the emissions are put into the lowest volatility bins leading to high BBOA and low OOA concentrations). This distribution is currently under review and may be revised. Other possible causes could be an underestimation of the oxidation of the volatile fraction by reaction with OH to form less volatile secondary compounds, and the neglection of background concentrations/inflow through the boundaries ; higher concentrations throughout Europe for CHIMERE with high concentrations in northern Italy; even higher concentrations throughout Europe for EMEP with localized areas of very high concentrations (southwestern France, northern Portugal, Galicia, Croatia, etc.); and concentrations about 3 to 10 times higher for CAMx on the domain compared to other models, with maximum concentration levels close to CHIMERE in northern Italy. The higher background OOA with EMEP is mainly due to the consideration of an additional, constant and homogeneous background concentration of 0.4 µg m^{-3}.

During summer (June to August), BBOA concentrations are logically lower than in winter due to lower emissions. The general spatial distribution is similar in all models with some noticeable differences. LOTOS-EUROS is simulating very localized high concentrations (Crete, Stromboli) which can be attributed to the fact that the LOTOS-EUROS BBOA also includes the OA from fire emissions. Concentrations simulated by CHIMERE are of the same order of magnitude but are more widely distributed, with less marked maxima. Simulated summer BBOA concentrations are higher with CAMx and especially with EMEP (about a factor of 5 to 10). Strong local sources of BBOA are simulated in Ukraine only with CAMx. For summer HOA, results are similar to winter ones, with lower overall concentrations (divided by a factor of 5 approximately). There is considerable variability between models on the OOA in summer. LOTOS-EUROS simulates lower overall concentrations which are higher over land than sea with localized maximum (around the Adriatic, Austria, Maghreb coast, Catalonia, etc.). With EMEP, simulated maximums are lower but overall concentrations are higher by a factor of around 3 on average than those with LOTOS-EUROS. Areas of high concentrations are located over the southern Adriatic, northern Italy and Catalonia in particular. Overall OOA simulated concentrations are much higher with CAMx and CHIMERE (up to x10 compared to LOTOS-EUROS or upon the Genoa's gulf, Germany or Poland for example with CAMx) localized mainly upon Mediterranean Sea, northern Italy and central Europe for CAMx and upon Balkans, Italy and north-east Europe for CHIMERE. CHIMERE simulates the highest maximums in Slovenia, Croatia and Bosnia (> 10 µg m^{-3}).

RI-URBANS (www.RIURBANS.eu) is supported by the European Commission under the Horizon 2020 – Research and Innovation Framework Programme, H2020-GD-2020, Grant Agreement number: 101036245

2.2.5 Discussion on the results by contribution

HOA: The comparison shows a tendency to strongly underestimate HOA for CHIMERE and LOTOS-EUROS. This is because those models considered POA to be semivolatile. On the other side, CAMx and EMEP tend to overestimate HOA at some stations. While the semivolatility assumption is more realistic physically, it may not improve the comparison to the HOA measurements. One possibility is that part of aged POA compounds that are assumed to be in OOA should perhaps be considered in HOA. This could be possible if the aging products are slightly oxidized molecules. Indeed, HOA profile in the PMF is supposed to display a low O/C ratio. Compounds with a O/C<0.1 should probably be considered as HOA compounds. This could mean that SOA compounds formed by aging within one or two oxidation steps should perhaps be classified as HOA compounds (this could be done by tagging species from the first and second oxidation steps but it could prove to be CPU time consuming). Moreover, none of the models is able to represent the observed diurnal profile with maximum at the end of the day. Since it is a primary PM factor, the HOA diurnal cycle results from the interplay between emission timing and vertical mixing (boundary layer development), which may both not be well represented in the models.

BBOA: Except for Barcelona Hohenpeißenberg, Metz, Poitiers and Strasbourg for which all models tend to overestimate or underestimate concentrations, CHIMERE managed to reproduce the good order of magnitude of BBOA concentrations. The other models tend to overestimate the BBOA contribution. However, the BBOA factor retrieved from PMF may not capture all the biomass burning POA emissions, due to their diversity and complexity (Petit et al., 2014, Chebaicheb et al., 2023). This factor strongly relies on the variability of f60 (corresponding to levoglucosan). CHIMERE, EMEP and CAMx manage to reproduce the peak of the concentrations in the evening. LOTOS-EUROS also manages to reproduce this peak, but it seems to persist over the first hours of the morning. All models simulate a peak of concentration between 6 am and 12 am which does not appear in the measurements. This may indicate that the models considered temporal profile for emissions that may include two peaks (one in the morning and in the evening) and should use temporal profile with one strong peak during the night. Although the TEMPO profiles do only have one peak in the evening for residential combustion PM emissions, for this sector LOTOS-EUROS is not using the TEMPO profiles but the heating degree approach with the old standard two peaks for diurnal variation. This will be adapted for future model applications.

OOA: The models behave differently between summer and winter. In summer, LOTOS-EUROS underestimate concentrations at all stations except for the high-altitude site Hohenpeißenberg. The three models (CHIMERE, EMEP and CAMx) have similar results over France, with good results on some stations (Talence, Lyon) and underestimation on others (SIRTA, Gennevilliers, ATOLL, Creil and Poitiers). CAMX has a good order of magnitude for Kosetcie and London, but the other models underestimate OOA. For Barcelona, the models overestimate but to different degrees. For Hyytiala and Hohenpeißenberg, EMEP has a good performance, CHIMERE overestimates at both stations while CAMx overestimates at Hohenpeißenberg but reproduces the order of magnitude of concentrations at Hyytiala. None of the models reproduce exactly the diurnal profile which is stable throughout the day with a small increase between 11 am and 13 am. The diurnal profile in CAMx is particularly different from observations with strong concentrations during the night. In winter, all models consistently underestimate concentrations at almost all the stations. However, CAMx manages to reproduce the high winter OOA concentrations at a few stations (Barcelona, Hyytiala, Hohenpeißenberg, Kosetice, London-Marylebone and Strasbourg). EMEP overestimates OOA at two stations (Hyytiala and Dublin). The model simulates a fairly stable diurnal profile, while in the observations the concentrations decrease during the day and increase strongly during the evening. All the models fail to capture the evening peak. This could be indicative that part of the observed OOA is related to biomass burning emissions and aging processes, while the models were allocated the majority of those in BBOA. This could be consistent with the underestimation of OOA and overestimation of BBOA at 6 of the 11 stations with EMEP, LOTOS-EUROS and CAMx. Further refinement of the semi-volatility of POA (accounted for only for CHIMERE and LOTOS-EUROS) and of the aging processes might help improving this comparison. This peak could

RI-URBANS (www.RIURBANS.eu) is supported by the European Commission under the Horizon 2020 – Research and Innovation Framework Programme, H2020-GD-2020, Grant Agreement number: 101036245

also be due to the condensation of secondary SVOC onto POA from biomass burning (as the absorption of secondary compounds may be favoured by an increase of POA concentrations).

No comparison was performed to LO-OOA and MO-OOA concentrations as it would be necessary to separate appropriately SOA as a function of the oxidation degree (which may not be explicitly simulated by all models). Preliminary tests performed with CHIMERE seem to indicate that using a O/C threshold of 0.7 could be used to separate LO-OOA from MO-OOA and that most of underestimation with CHIMERE could be explained by an underestimation of the very oxidized fraction (and therefore could be related to aging processes).

2.2.6 Can we extend this setup to NRT comparison between CAMS models and PMF?

In practice, we demonstrated in RI-Urbans Task 3.3 the feasibility of a near-real-time comparison between Regional CTMs (such as those used in Operational production in CAMS) models and ACSM PMF for OA at pilot sites. We show that the maturity and operationality of both models and observation is reaching a stage where it can provide useful information on OA formation, the evaluation of models and Source Apportionment. However, two challenges remain to be addressed:

- Matching between organic aerosol chemical composition in CTMs and ACSM/PMF: while the comparison seems to provide useful information, the main challenge for the comparison come from difficulties to have an exact matching between the CTM results and the PMF. Part of the primary aerosol from biomass burning may theoretically be allocated in the OOA by the PMF. Also, the comparison for HOA seems to indicate better results when the semi-volatility of primary PM is not accounted for. However, this could be explained by the fact that part of the HOA is also constituted by aged primary compounds with a very low oxidation degree. Finding a methodology to separate OOA into LO-OOA and MO-OOA in the models could provide very useful information on the capacity of models to simulate highly oxidized molecules. This could be done by separating compounds based on an O/C threshold.
- The simulations presented here rely on high to moderate complexity OA models. Performing simulations of HOA, BBOA, OOA with operational models (such as those implemented on a daily basis in CAMS) is another challenge. Some operational modelling groups are presently using very simplified scheme in the forecast and may not tag HOA, BBOA and OOA. It may be necessary to launch simulations with more complex SOA scheme which may impact significantly the CPU time. One possibility could be to perform daily simulations but with a forecast limited to D-1.

To conclude, the first objective regarded reaching the stage of feasibility for such recurring evaluation. We can consider that this objective is achieved. We already identified two bottlenecks which prevent going further at this stage (need for refinement of LO-OOA/MO-OOA definition, and applicability in Operational setup). But we confirm the overarching ambition to be able to produce recurring evaluation. We consider it will be an important step to demonstrate the performance of the models used in forecast mode in NRT (i.e. during the air pollution episode themselves). This demonstration is critical to build confidence from the user that the models are drawing the right diagnostics (i.e. attributing a given episode either to traffic or residential activities).

RI-URBANS (www.RIURBANS.eu) is supported by the European Commission under the Horizon 2020 – Research and Innovation Framework Programme, H2020-GD-2020, Grant Agreement number: 101036245

Particulate Matter Oxidative Potential Modelling (CNRS/LISA, TNO, MET Norway)

2.2.7 Context

Particle's oxidative potential (OP) measures the ability of particles to induce oxidative stress in the human body by favouring the formation of exogenous reactive oxygen species (ROS) such like OH, HONO or superoxide ions (Ayres et al., 2008; Sauvain et al., 2008). In excess, ROS may lead to imbalance between oxidants and antioxidants in the lung and possibly oxidative stress, that can provoke damages to cell material and inflammation at the origin of biological health endpoints (Costabile et al., 2019; Weichenthal et al., 2016).

The inhalation exposure can be mimicked by following the antioxidant (like ascorbic acid) consumption within surrogate epithelial fluids after exposing PM into a simulated lung fluid according to different protocols. The kinetic depletion rate (in $nmol.min^{-1}.m^{-3}$) is then taken as the volumetric OP (denoted OP^v). Most commonly assays used to measure OP^v are ascorbic acid (AA) and dithiothreitol (DTT) (Calas et al., 2017).

Since measuring OP^v by chemical species is complicated and not necessarily representative of complex chemical cocktails of the real atmosphere, it has been chosen to attribute OP^v to the particle's sources by combining PMF made on aerosol composition and linear regression (MLR) between this PMF results (e.g sources' factors) and OP^v measurements. As a result, Weber et al. (2018) shows how to extract OP per mass unit (OP^m) of PM attributed to a given source. The recent study of Weber et al. (2021) and Daellenbach et al. (2020) propose two differents sets of OP^m for common European PM sources by applying such a method.

MLR was separately performed at each European site, where the results from two different assays (DTT and AA) were the outcomes of interest, and the contributions from different sources of particulate matter (PMF) were the explanatory factors. This was done using a linear equation (Eq. 1), similar to a previous study (Weber et al., 2018), expressed as follows:

$$OP_{obs} = G \times \beta + \varepsilon \qquad \text{(Eq. 1)}$$

Here, OPobs represents the observed oxidative potential (OP) measured by DTT or AA assays in nanomoles per minute per cubic meter ($nmol.min^{-1}.m^{-3}$). G is a matrix representing the mass contributions of PM sources derived from PMF analysis in micrograms per cubic meter ($\mu g.m^{-3}$), including a constant term for the intercept. β denotes the coefficients, which represent the intrinsic OP of each PM source and the intercept, expressed in nanomoles per minute per microgram ($nmol.min^{-1}.\mu g^{-1}$) for the intrinsic OP and in $nmol.min^{-1}.m^{-3}$ for the intercept.

To address the uncertainties associated with the OP measurements, a weighted least-square regression (WLS) was employed. The uncertainties of the coefficients (β) obtained from the multiple linear regression (MLR) were assessed by bootstrapping the solutions 500 times. This involved randomly selecting 70% of the samples each time to capture potential extreme events or seasonal variations that may influence the results.

These datasets give us the opportunity to model the OP and to provide maps and even forecasts of such indicator in the near future. In the following, we describe the methodology that we propose to do so and we show some results of the modelling of PM sources and OP.

RI-URBANS (www.RIURBANS.eu) is supported by the European Commission under the Horizon 2020 – Research and Innovation Framework Programme, H2020-GD-2020, Grant Agreement number: 101036245

Methodology

Description of the common general strategy to model OP

As already shown in Daellenbach et al (2020), the modelling of oxidative potential (OP) can be achieved by assigning a mass-normalized, also defined as intrinsic OP to each CTM source, the OP^m. As already mentioned, the OP^m values are obtained by performing source apportionment (SA) via PMF to the PM mass, after which a weighted least squares multiple linear regression (MLR) analysis assigns OP to each of the receptor sources (S. Weber 2019; 2021). The assumption that receptor sources are equal to CTM sources allows us to assign the identical OP^m value to CTM sources, thereby simulating volume-normalized OP (See Eq. 2), OP^v, within regional CTM. OP^v (nmol.min^{-1}.m^{-3}) represents the OP normalized for air volume for source 's' at timepoint 't'. OP^m (nmol.min^{-1}.µg^{-1}) is the intrinsic OP, derived from the PMF source 's' and C^{mod} is the simulated mass (µg.m^{-3}) of the CTM matched source 's' at timepoint 't'.

$$OP_{t,s}^{v} = \sum_{t,s} \quad (OP_{s}^{m} \times C_{t,s}^{mod}) \qquad \text{(Eq. 2)}$$

One important challenge of the method is to determine proper combinations of the model's source to simulate PMF sources. This can be different from one model to another since models do not necessarily have the same emission inventories, the same formulation of physical and chemical processes, the same method to achieve SA. Moreover, we must consider the representativeness of PMF between each other as well as compared to model's SA.

Description of the various implementation within RCTMs with their specificity

LOTOS-EUROS

Within LOTOS-EUROS the source contributions are determined by using a tagging method. This method is computationally efficient and well suited for establishing the source contributions to the air pollution concentration at a specific location and time. After emission different components are followed through the model system, while keeping track of its source sector or region, allowing the assessment of many contributions within one model simulation. The routine is implemented for primary, inert aerosol tracers as well as chemically active tracers containing a C, N (reduced and oxidized) or S atom, as these are conserved and traceable. The source attribution is valid for current atmospheric conditions as all chemical conversions occur under the same oxidant levels. For secondary aerosols consisting of two components (e.g. ammonium nitrate (NH4NO3)), the contribution is calculated by accounting half of the mass to each component source. For further details on the LOTOS-EUROS model and its tagging source attribution method, the reader is referred to Manders et al. (2017) and Kranenburg et al. (2013).

CHIMERE

Within the CHIMERE version used to simulate OP, we use the Particulate Source Apportionment Technology (PSAT) developed by Wagstrom et al. (2008) that allows tracking the contribution to PM concentration following both primary emissions and secondary formation processes. The sources used for the PSAT are the sectors of activity in the Selected Nomenclature for Air Pollution (SNAP) obtained through a correspondence matrix between Nomenclature For Reporting (NFR) and SNAP. For each species represented in the model, the contribution of different activity sectors represented in the emission inventories is obtained. The model explicitly also accounts for natural such as mineral dust, marine emissions, biogenic emissions, but also boundary conditions, and resuspension of primary particulate matter (PPM).

For CHIMERE we use the version (v2020r3, Menut et al., 2021) of CHIMERE coupled with the Weather Research Forecast (WRF, v3.7.1) meteorological model (Skamarock et al., 2007). For organic aerosol formation and

RI-URBANS (www.RIURBANS.eu) is supported by the European Commission under the Horizon 2020 – Research and Innovation Framework Programme, H2020-GD-2020, Grant Agreement number: 101036245

gas/particle partitioning of primary organic aerosol, the volatility basis set (VBS) for the organic species as described in Cholakian et al. (2018) was activated. Resuspension is considered by the model only in urban meshes and attributed to primary mineral particles (Loosmore, 2003). The EMEP anthropogenic emission database with a resolution of 10 km² provided input data for anthropogenic emissions (Vestreng et al., 2003). Biogenic emissions come from the MEGAN model (Guenther et al., 2012).

EMEP

The EMEP MSC-W chemistry-transport model (hereafter 'EMEP model') has been prepared to calculate the intrinsic OP source categories following the methodologies described in Daellenbach et al. (2020) and Weber et al. (2021). In the EMEP model, the contribution of primary traffic PM to total PPM is tracked using the so-called local fractions (LFs) methodology (Wind et al., 2020). The LFs track the fraction of traffic PPM to the total PPM for each country within the modelling domain, based on traffic emissions within each country. The tracked total traffic country-contributions are then combined with EMEP reported country emission statistics for road traffic exhaust (hydrocarbon-like organic aerosol, HOA), brake and tyre wear (vehicular wear), and road dust emissions, to calculate their respective contributions to total traffic PPM (and corollary total PPM).

For other modelled species, specific source categories are not tracked, with instead their total values contributing towards OP. For biogenic and anthropogenic secondary organic aerosol (BSOA and ASOA), the EMEP model employs a volatility basis set (VBS) approach, partitioning semi-volatile species into their respective gas and particle phases. Secondary inorganic aerosol (SIA) is here calculated using the ISORROPIA-lite thermodynamic equilibrium model, while natural dust and sea salt aerosol are generated internally in the model based on meteorological parameters. Biomass burning aerosol is calculated based on the contributions of residential heating combustion and forest fires. However, as discussed in section 4.3.1, residential combustion emissions are also tracked with LFs, but only for the purpose of downscaling their emissions using uEMEP. The source apportionment model species and methodology are also summarized in Table 2 for the OP approach from Weber et al. (2021). The calculated OP source categories are post-processed using their intrinsic OP values (e.g. for DTT^m in nmol min^{-1} μg^{-1}) to calculate their contributions towards total OP. In addition to the Weber approach, total OP is also calculated using the values and sources described in Daellenbach et al. (2020), as shown in Table 3.

A number of simulation results are presented below. **Table** 6 gives some additional information about the set-ups used by the models for these specific simulations in relation to the OP.

***Table** 6. CTM model main settings for OP modelling*

Model	Source apportionment method	Emissions	Meteorology	Spatial resolution
CHIMERE	Tagging (PSAT)	EMEP	WRF	10 km
LOTOS-EUROS	Tagging	CAMS REF2v1.1	IFS	7 km
EMEP	Local fractions	EMEP	IFS	10 km

RI-URBANS (www.RIURBANS.eu) is supported by the European Commission under the Horizon 2020 – Research and Innovation Framework Programme, H2020-GD-2020, Grant Agreement number: 101036245

Matching strategies between PMF sources and models SA

As we have already mentioned, the correspondence between PMF sources and model sources in terms of the mass contribution required to attribute intrinsic OP (OP^m) from PMF sources, are currently the main challenges to correctly simulating OP with CTM models. Although significant work exists to compare PMF and the attribution of modelled sources (Belis et al, 2020), this is not an exercise that is carried out very often by teams modelling atmospheric composition. However, given the method targeted for modelling the OP, it is becoming necessary to take a serious look at this exercise. Consequently, one of the objectives of WP3.3 was to start thinking about and comparing the mass contribution of PMF sources in France with the contribution of sources in three regional CTM models (CHIMERE, EMEP and LOTOS-EUROS) (**Table** 6).

By their very nature, PMF sources and model sources are different. Model sources derive mainly from the definition of inventories, which is based on the consideration of emissions by species and socio-economic sector (bottom-up method), whereas PMF sources are obtained by a statistical approach (inversion) combining the chemical profiles of the initial sources to reproduce the observations (inverse, top-down method).

In the first approaches we propose in **Table** 7, we first try to associate, using our geophysical expertise, sources that appear to represent similar emission processes. This is the case, for example, for the PMF source "Biomass", which in the model seems to correspond to sectors producing energy from biomass (whether for domestic or industrial use, or even from natural sources).

This is illustrated in our table, but we can see that slightly different choices may be made by different modeling teams. This may be due to the different formulation of emissions in the models. Furthermore, it is important to systematically compare the chemical source profiles of the PMF and the modeled chemical source profiles, i.e. the species that contribute to the sources in both cases. For example, in the CHIMERE model, this comparison led to the choice to exclude biomass-associated sulfate concentrations from this source, as there was little or no sulfate in the "biomass" PMF source chemical profile of Weber et al. (2021). It is then possible to compare the model time series for the combination of sources with that of PMF. Adjustments or new choices can then be made to achieve a better fit. These time series comparisons are presented in the results section. For this process, we need to bear in mind that the models use different formulations of processes or inventories. We must also bear in mind that there may be ambiguity in the formation of the source apportionment itself. This is particularly the case with the marking of nitrates, which may be associated with combustion sources or agricultural sources.

In **Table** 7, without going into detail, we can see that the "traffic" source of PMF is very primary (chemical profile not shown) and so the models have excluded the contribution of nitrate from the combination. The chemical profile of this source is constructed from measurements of metals (mainly from brakes, tires and road abrasion), whereas the models do not explicitly represent these species and instead use the PPM (Primary particulate matter) species. Similarly, at the spatial resolution proposed here for the models, there may be discrepancies with the PMF source if this has been constructed using measurements at traffic stations that are not necessarily representative of the models (or vice versa). To finish commenting on this table, we can see that some PMF sources are by definition more difficult to process, such as nitrate- and sulfate-rich sources, which have very complex chemical profiles often associated with secondary species, with little information on the sectoral sources associated with them. For the result's analysis, based on the work of Weber et al (2021), we mainly focus on two major OP contributors among PMF sources following their OP^m (Table 2); 'Road traffic' and 'Biomass Burning'.

RI-URBANS (www.RIURBANS.eu) is supported by the European Commission under the Horizon 2020 – Research and Innovation Framework Programme, H2020-GD-2020, Grant Agreement number: 101036245

***Table** 7. Overview of matching choices between PMF sources and CTM sources. Moreover, the mass-normalized (intrinsic) OP (measured with DTT assay) associated to the PMF sources are provided (derived from S. Weber 2021).*

	LOTOS-EUROS (TNO)	CHIMERE (LISA)	EMEP (Metno)	**OP^m** (nmol/min/ug) DTT / AA assays
Biomass	Biomass Burning (Res Comb + Energy)	Primary & Secondary species for residential combustion (no SO4)	Prim. Residential + Natural Biomass burning	0,13/0,17
Traffic	Road traffic (no NO3)	Prim. + Sec. Road transport (no NO3)	Prim. Road traffic (exhaust , non-exhaust , dust)	0,23/0,14
Nitrate rich	All SIA components from Agri, Industry, non-biomass Res. Comb & Energy, non-road transport + NO3 road traffic	Sec. agriculture (50%), Sec. Res Comb (SO4), Sec. road Trans (NO3)	All SIA components	0,04/0,01
Sulfate-rich		Sec. Industries , Sec. Agri (50%), Sec. Biogenic		0,08/0,01
Dust	All Dust	Prim. Industry, Prim. Agri, Mineral Dust , Resuspension	All natural dust	0,12/0,01
Aged/Fresh sea salt	All Seasalt	Sea salt	All seasalt	0,04/0,02
MSA Rich	Not modelled	Not modelled	Not modelled	0,13/0,00
Primary biogenic	Not modelled	Prim biogenic, other transport	Not modelled	0,11/0,02

Another matching of the PM components had to be defined for the study of Daellenbach et al (2020). The "vehicular wear" factors represent particles coming from abrasion of roads, tyres and brakes and that are mainly made of different metals. Other factors represent organic factors with HOA for Hydrocarbon-like organic aerosol, BBOA for Biomass Burning Organic aerosol, ASOA for Anthropogenic secondary organic aerosol and BSOA for biogenic secondary organic aerosol.

RI-URBANS (www.RIURBANS.eu) is supported by the European Commission under the Horizon 2020 – Research and Innovation Framework Programme, H2020-GD-2020, Grant Agreement number: 101036245

***Table** 8. Correspondence between PMF and CHIMERE or EMEP sources for the reduced set method and OPi values for DDT and AA tests obtained in Daellenbach et al. (2020) and their intrinsic oxidative potential (OPi) in nmol min-1 µg-1. SNAP number are indicated with S numbers (SNAP sector: 7 traffic, 8 offroad…)*

PMF	PSAT CHIMERE	EMEP	OP_i^{DTT}	OP_i^{AA}
Vehicular wear	**PPM** (only inorganic, exc. EC) road transport (S7) + resuspension	**PPM** non-exhaust from fine and coarse mode traffic emissions	3.51	3.16
HOA	**POA** energy production (S1) + industrial combustion (S3) + road transport (S7) + other transports (S8)	**OA** fraction (⅓) of **PPM** exhaust traffic emissions	0.94	0.00
BBOA	**POA** residential combustion (S2) + waste treatment (S9)	**POA** from residential combustion and forest fires, treated as non-volatile	0.08	0.06
ASOA	**ASOA** all anthropogenic sources (S1 to S10)	**ASOA** from all anthropogenic sources	0.44	0.42
BSOA	**BSOA**	BSOA	0.15	0.00

Results

Modelling PMF factor time series

Here, we present an analysis of the comparisons between LOTOS-EUROS, EMEP and CHIMERE to simulate two specific sources of Weber et al (2021) PMF. For the biomass burning contributions the seasonal cycle with the PMF contributions is well represented as can be seen in the time series for Lens (**Figure** 11). The LOTOS-EUROS and EMEP models are showing high temporal correlations (**Figure** 12) with the PMF biomass combustion contribution. The CHIMERE residential combustion contribution is showing lower correlations. The difference between the CTM models is sometimes larger than between the models and PMF. This could be attributed to the different emission inputs used by the models (**Table** 6). LOTOS-EUROS and EMEP are using CAMS REF2 emission inventories which include condensables for residential wood burning (Denier van der Gon, 2015), and have been shown to lead to better representation of PM concentrations. We do see that the LOTOS-EUROS model has higher biomass burning contributions than the PMF data at all stations. The REF2 emission dataset has since been revised and the updated REF2_v2.1. emission inventory (Simpson et al, 2022) contains lower emissions for wood burning in France. The EMEP model simulation has used the Ref2_v2.1 data set, and indeed the biomass burning contributions from EMEP are lower and in better agreement with the PMF data.

For the road traffic source, the correspondence between the CTMs and PMF is worse (see **Figure** 11). Again, the difference between the CTM models is sometimes larger than between the models and PMF which can be related to the use of different emission and meteorological input data. In general, the CTMs tend to provide lower contributions to road traffic than the PMF results (**Figure** 11). This may be related to the spatial resolution of the models (7-9 km) which is representative for background concentrations and will not represent high concentrations due to local traffic contributions. The models have difficulty in representing the source category traffic in a time consistent manner, as has been seen before for LOTOS-EUROS over Germany (Timmermans et al, 2022), and developments are needed to improve the temporal distribution of the traffic emissions. Interestingly, removing the NO_3 specie from the total PM_{10} road traffic label for LOTOS-EUROS noticeably increased the fit between CTM and PMF. Indeed, the PMF traffic profiles (not shown here) show no or only minimal NO_3 contributions, so it seems that

RI-URBANS (www.RIURBANS.eu) is supported by the European Commission under the Horizon 2020 – Research and Innovation Framework Programme, H2020-GD-2020, Grant Agreement number: 101036245

NO_3 attributed to road traffic emissions in CTM models are largely captured in the SIA-rich PMF sources instead of the more primary PMF road traffic source.

The different contributions shown here from the three CTM models will lead to a difference in modelled OP distributions and contributions. Even if this work of evaluating the simulation of PMF needs to be carried out in greater depth, and if we also evaluate the ability to reproduce PM_{10}, its chemical speciation and OP, we can already produce maps of OP and analyse the results.

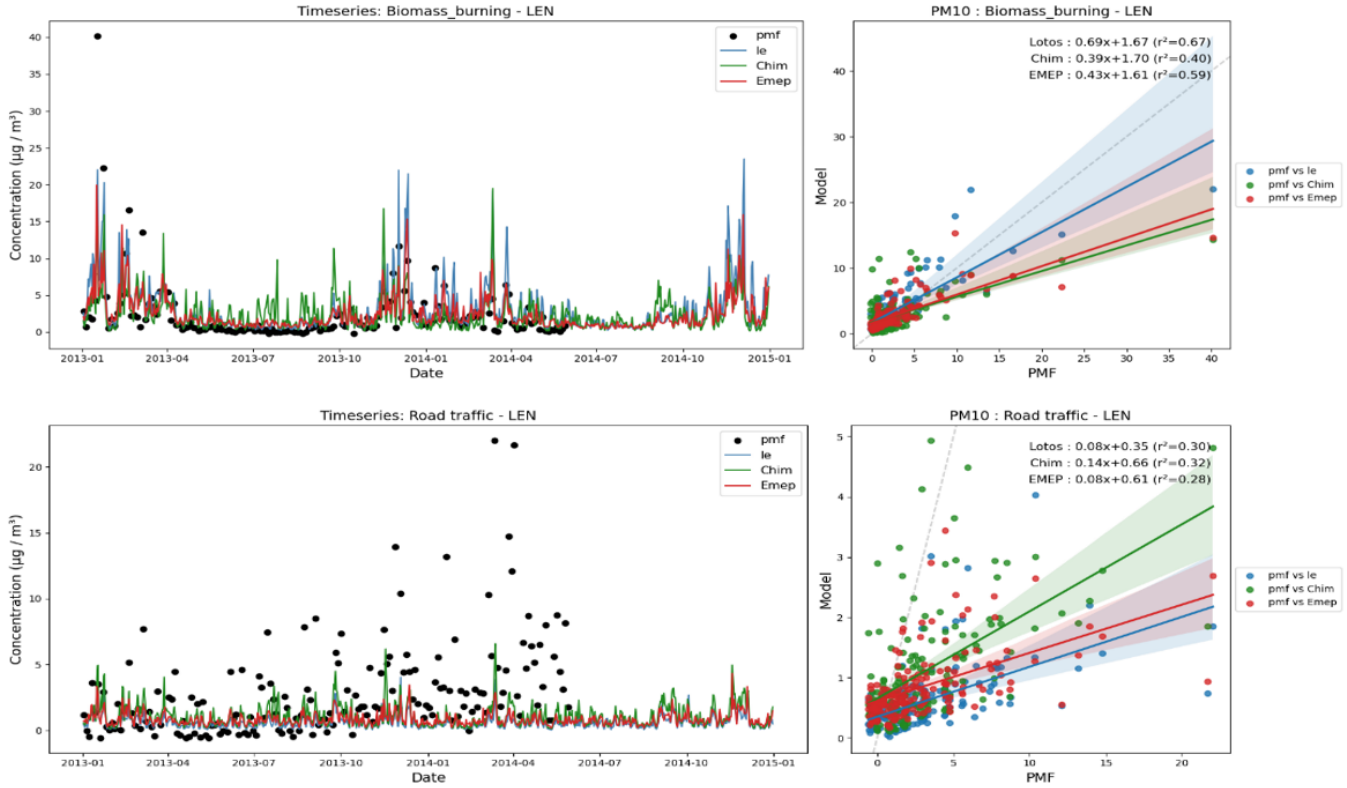

***Figure** 11. Timeseries and Scatterplot between modelled Road traffic & Biomass Burning PM10 and PMF profile PM10 for the station LEN (Lens). Note, each model contains different emission sources to match the PMF biomass burning which are presented in **Table** 7.*

RI-URBANS (www.RIURBANS.eu) is supported by the European Commission under the Horizon 2020 – Research and Innovation Framework Programme, H2020-GD-2020, Grant Agreement number: 101036245

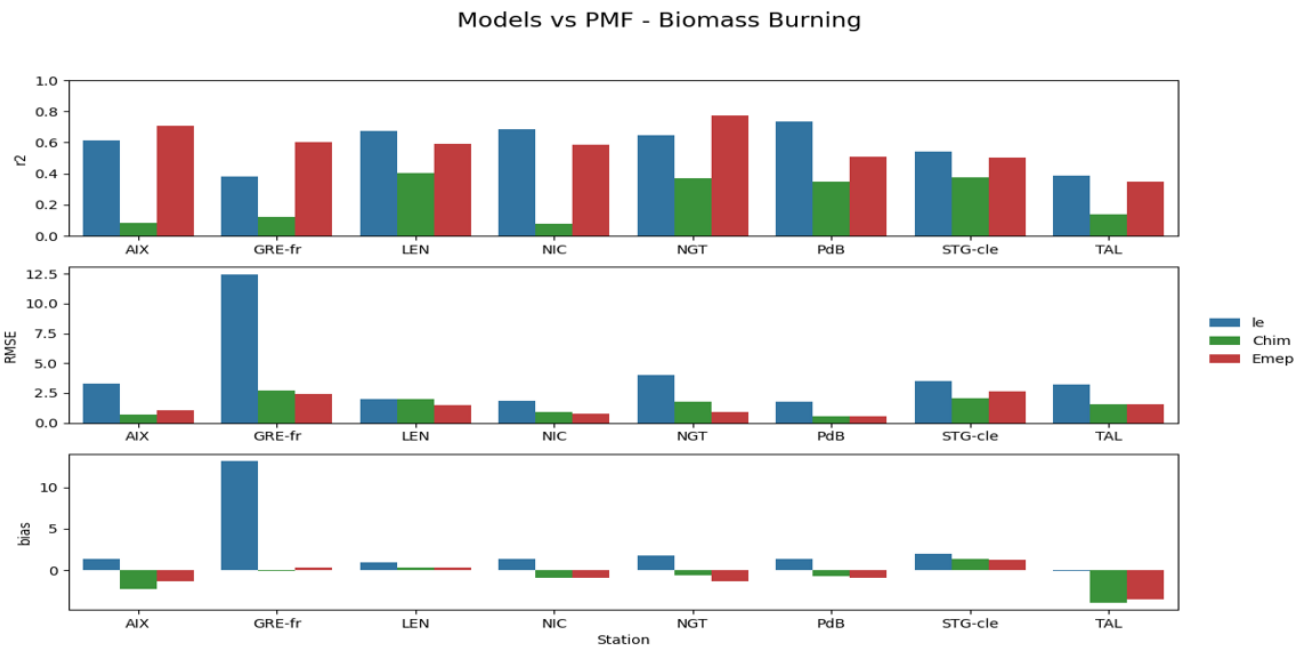

***Figure** 12. R-squared, RMSE and bias for between CTM and PMF source 'Biomass Burning' for all stations. Included stations are LOTOS-EUROS (le – blue) and CHIMERE (Chim – green), EMEP (red)*

2.2.7.1 Regional scale mapping of OP

Using these correspondence matrices between PMF and model tagging, we are able to simulate OP of atmospheric particles. It should, of course, be remembered that the process of evaluating these simulations needs to be completed and that the methods used themselves, as mentioned above, are still under development. It should be noted that for the moment, the different models do not consider all sources proposed by the PMF. Therefore, one should interpret the simulated OP exposure in such maps with caution but use it as an expected direction to where OP modelling is headed.

Figure 3 shows the OP (OP^V) simulated for a full year over France with the LOTOS-EUROS model for two different tests, AA and DTT using the correspondence **Table** 7 based on the work of Weber et al (2021). Note, not all model sectors are included in the current mapping of **Figure** 13 because no trustworthy intrinsic OP value could be assigned to the non-SIA components of such sectors. These sectors are the agriculture, industry non-biomass residential heating and energy production for LOTOS-EUROS. The simulated structures are consistent with what we would expect in terms of concentrations, with urban areas and roads standing out. There are also differences between the two tests, as **Table** 7 suggests, with different intrinsic OPs depending on the sources for these 2 tests. In particular, the DTT test shows higher OP^m for SIA-rich sources, i.e. those which generally contain the secondary fraction of the aerosol. This seems to translate into less pronounced gradients and higher OP values linked to transport, as over oceanic areas.

RI-URBANS (www.RIURBANS.eu) is supported by the European Commission under the Horizon 2020 – Research and Innovation Framework Programme, H2020-GD-2020, Grant Agreement number: 101036245

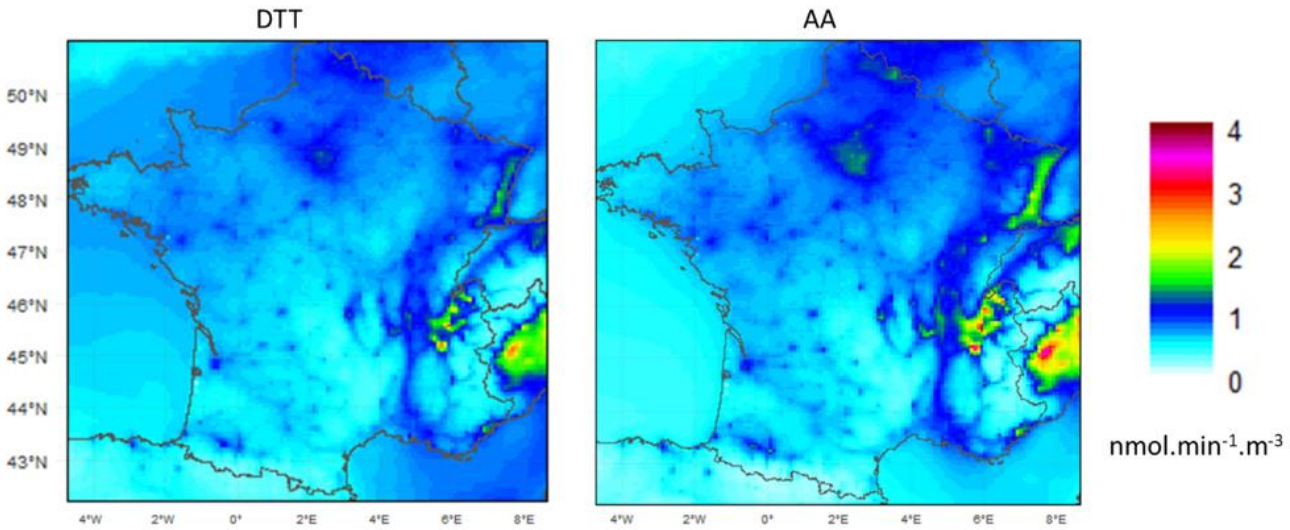

***Figure** 13. OP^{v} calculations over France from the LOTOS-EUROS model. Left panel displays OP^{v} for DTT assay when right panels display OP^{v} for AA. Note: NO OP^{m} was assigned to the mass of EC, OC and ppm components for the model sectors: agriculture, industry and non-biomass residential combustion.*

Figure 14 a and b show annual mean total OP^{v} maps for the DTT assay calculated using the EMEP model over European land areas using the non-traffic intrinsic OP source categories described in Daellenbach et al. (2020) (**Table** 8) and Weber et al. (2021), employing EMEP emissions reported for 2020. These panels show that for the non-traffic OP categories, the two methodologies produce quite similar results. In **Figure** 14 c and d the OP calculated from the Daellenbach HOA OP factor is compared against that calculated from the Weber total traffic PM10 factor. While difficult to distinguish because of their relatively small values relative to total non-traffic OP, the two methodologies produce comparable results also for these categories (as highlighted in **Figure** 15). **Figure** 14 e shows the additional Daellenbach non-exhaust OP factor, calculated from total PM10 non-exhaust (i.e., the total mass contribution of road dust, tire wear and break wear), thereby being an upper estimate of the non-exhaust OP. In reality, the intrinsic OP associated with this factor results primarily from the metal content of the non-exhaust PM. The vehicle non-exhaust OP calculated here is unrealistically high and represents by far the largest contributor to OP, highlighting that modelling the non-exhaust OP contribution requires detailed emission inventories of metals from break wear. The impact of urban scale simulations on OP is discussed in more detail in section 3.3 using the Weber approach.

RI-URBANS (www.RIURBANS.eu) is supported by the European Commission under the Horizon 2020 – Research and Innovation Framework Programme, H2020-GD-2020, Grant Agreement number: 101036245

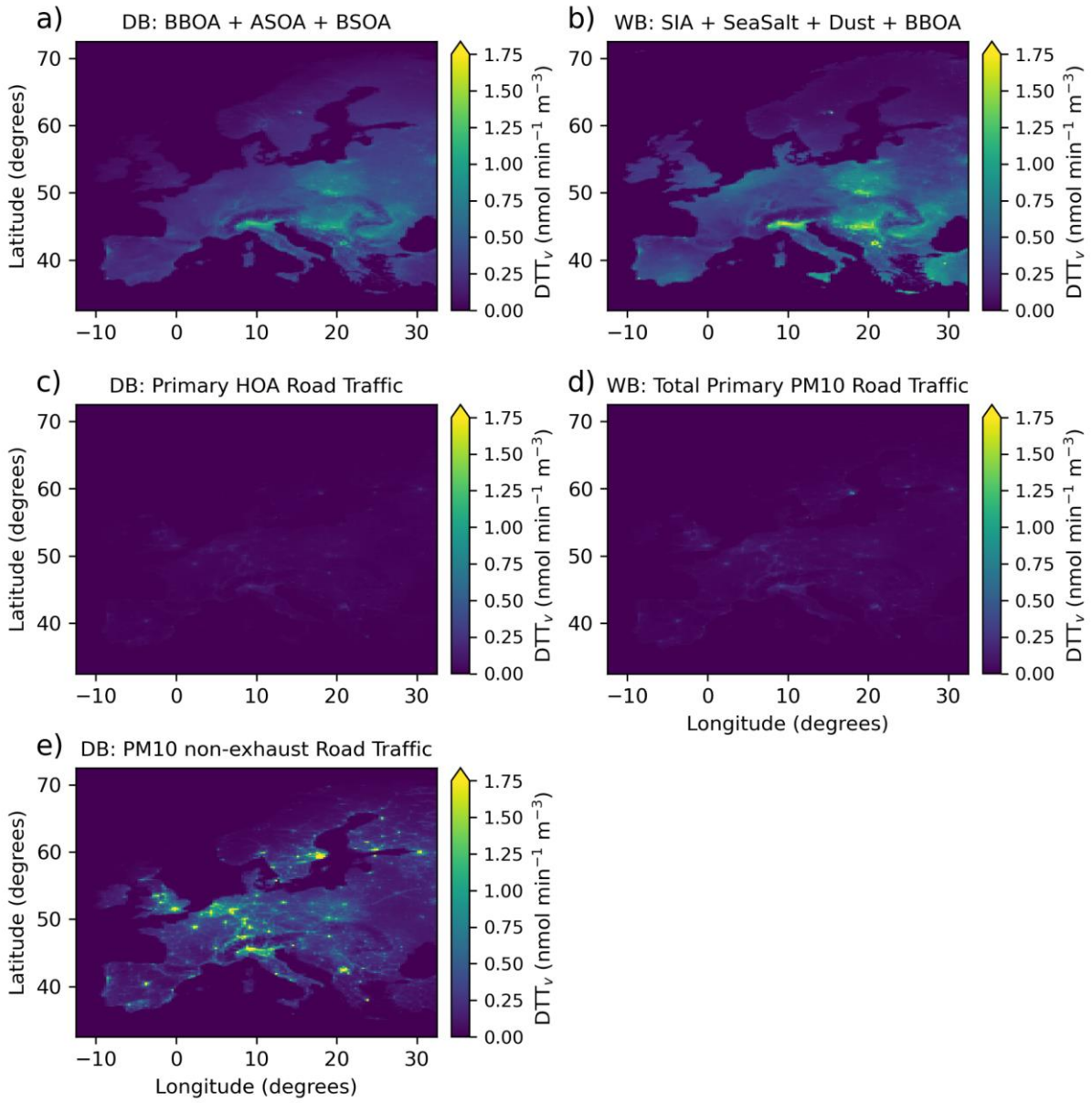

***Figure** 14. OPv DTT calculations over Europe from the EMEP model. Panel (a) shows the sum of OP calculated for the Daellenbach et al. (2020) (DB) BBOA, ASOA, and BSOA categories, while panel (b) show the sum of OP calculated using the Weber et al. (2021) (WB) SIA, sea salt, Dust, and BBOA categories. Panel (c) shows the DB HOA traffic OP calculated from primary traffic HOA, while panel (d) shows WB traffic OP calculated from total primary traffic PM10. Panel (e) shows the DB non-exhaust OP calculated from total PM_{10} non-exhaust traffic emissions.*

RI-URBANS (www.RIURBANS.eu) is supported by the European Commission under the Horizon 2020 – Research and Innovation Framework Programme, H2020-GD-2020, Grant Agreement number: 101036245

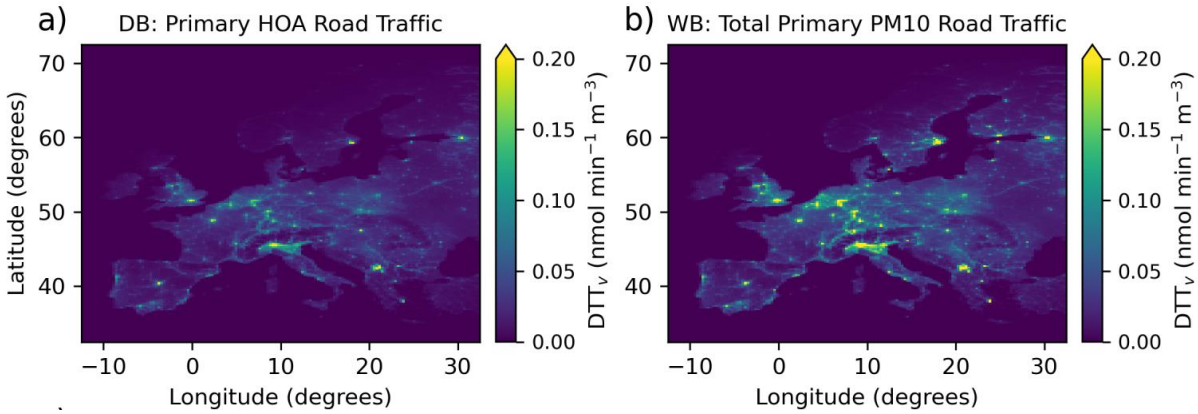

***Figure** 15. OP^{v} DTT calculations over Europe for the Daellenbach et al. (2020) HOA category (a) and Weber et al. (2021) total traffic PM10 category (b).*

RI-URBANS (www.RIURBANS.eu) is supported by the European Commission under the Horizon 2020 – Research and Innovation Framework Programme, H2020-GD-2020, Grant Agreement number: 101036245

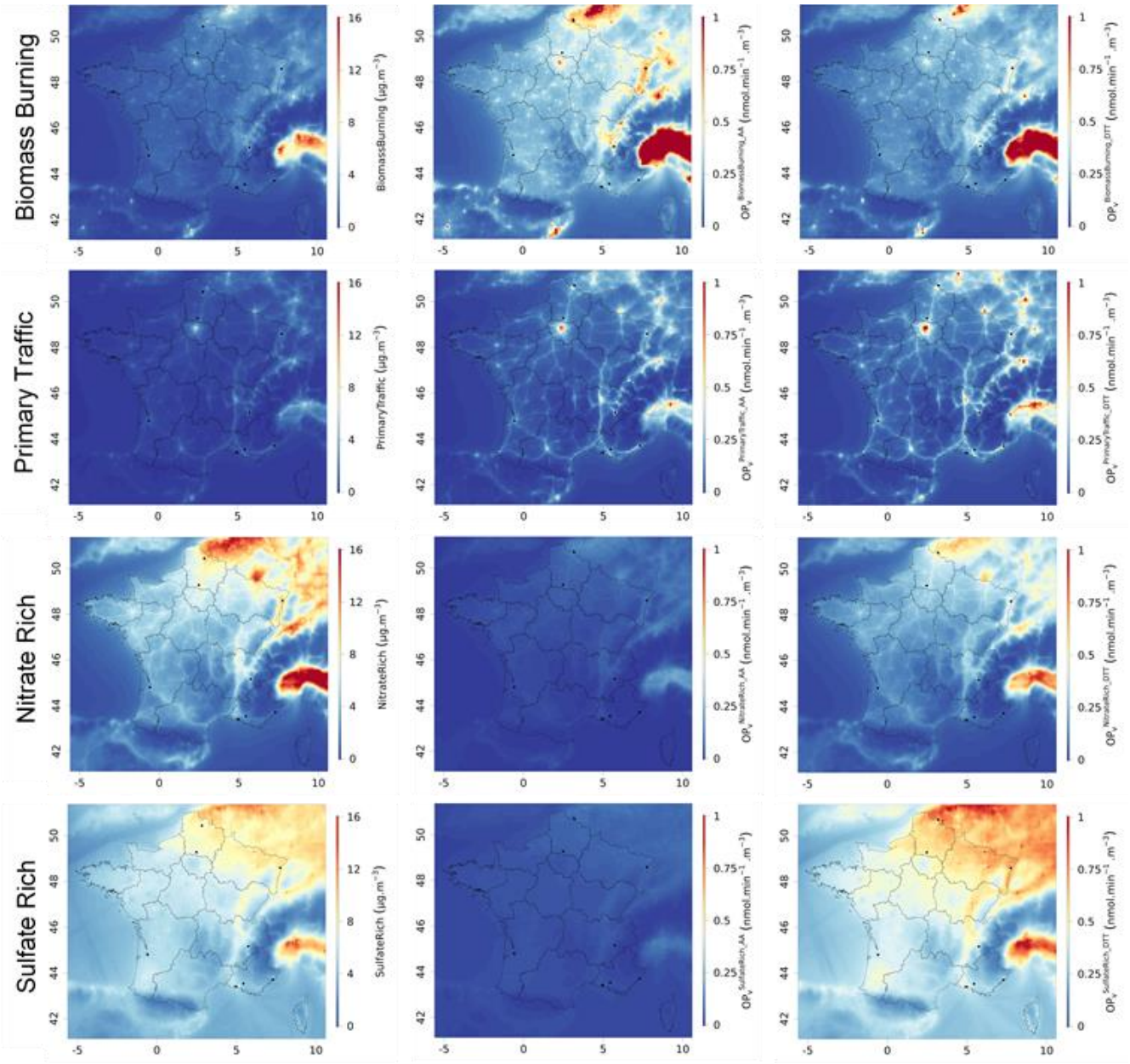

***Figure** 16. Contribution of major sources to PM_{10} (left column), to OP_v^{AA} (middle column) and OP_v^{DTT} (right column) oxidative potential spatialized over France as a two-year average (2013-2014) for the Weber approach. Only the first vertical level of the CHIMERE model is shown.*

The simulation of OP^v values also makes it possible to carry out analyses by source, for example by comparing modelled OP^v by source and simulated concentrations by source. ***Figure** 16* shows the concentrations modelled by the CHIMERE model for 4 factors, Biomass burning, Primary traffic, Nitrate-rich, Sulphate-rich. We have used the Weber approach here. In parallel, we can see the OP^v simulated by this same model for the same sources and for the AA and DTT tests. We can clearly see, as was shown in Daellenbach et al (2020), that the sources that dominate PM_{10} concentrations are not necessarily those that dominate OP. For example, the Nitrate-rich source of the OPv AA is weak whereas it dominates PM_{10} concentrations. We can also see the differences that may exist between the 2 simulated OP tests in relation to the differences observed in the PMF (**Table** 7).

RI-URBANS (www.RIURBANS.eu) is supported by the European Commission under the Horizon 2020 – Research and Innovation Framework Programme, H2020-GD-2020, Grant Agreement number: 101036245

Discussion

As shown above, developments to model the OP are underway and it is already possible to produce maps of this indicator. However, it is clear that we still need to improve the methods used, and this will involve exchanges between the different scientific teams (modellers, experimenters). A number of improvements are needed before adequate PM mass-derived and source specific OP modelling can be achieved:

- Using intrinsic OP values for non-traffic source categories as described in Daellenbach et al. (2020) or Weber et al. (2021) leads to similar OP maps. Including the traffic source from Daellenbach (for exhaust) and Weber (total traffic) only increase total OP values slightly. Daellenbach et al. also defines intrinsic OP values for the non-exhaust source (in practice this source is representing break wear and the OP values are normalized to metals). This source is difficult to model, as it requires emissions of metals from break wear, which is not readily available and has not been used in this study. As an upper estimate, the OP values for this source has been combined with PM_{10} from non-exhaust emissions, resulting in high modelled OP values and an apparent large difference to the results using intrinsic OP values from Weber et al. Clearly, the modelled source representing non-exhaust metals is important, and indeed a topic where further work is being pursued at present.
- Both studies do not rely on the same number of observations and OP^m is also known to be site dependent. A way to define homogeneous OP/µg among European sources would be essential in order to arrive at a more mature stage of OP modelling. This could be achieved by performing a multi-site PMF along EU sites.
- Large as possible database of chemical speciation, PMF temporal series and OP observations are needed. This should include various geographical areas as well as different site typologies.
- Matching of PMF and CTM sources needs to be optimised which can be achieved by adding/removing PM constituents (e.g. NO_3^-) from CTM sources. Comparisons of chemical profiles of sources are needed to do that and then tight relationship with scientist producing the data.
- Not all PMF sources are modelled in the CTMs (e.g. MSA-rich) and vice versa not all CTM sources are identified as a PMF source (e.g. Agriculture) and can therefore not be assigned a clear (PMF-derived) OP value. Source specific OP measurements are required for all relevant sources and extension of models with most relevant OP sources (e.g. metals from break wear in traffic source which have high OP). The latter requires availability of accurate emission inventories for all relevant sources.
- Intrinsic OP for identical sources is quite variable between locations (S. Weber et al. 2021, C. Daellenbach et al. 2020) which is partly due to the regional differences in chemical composition of such sources. Moreover, due to expected changes in chemical compositions of sources (e.g. increase in electric vehicles in road traffic) the temporal differences should also be considered.

From this list we can conclude that bringing OP modelling further requires strong cooperation between modelling teams and observational experts, both to optimize the model-to-measurement comparisons and to harmonize the intrinsic OP categories and values. The RI-urbans project serves as an excellent platform to initialize this discussion and bring communities together.

RI-URBANS (www.RIURBANS.eu) is supported by the European Commission under the Horizon 2020 – Research and Innovation Framework Programme, H2020-GD-2020, Grant Agreement number: 101036245

2.3 Ultra Fine Particles Modelling at European Scale (FORTH)

2.3.1 PMCAMx-UF

The three-dimensional chemical transport model PMCAMx-UF simulates both chemically resolved mass concentrations and size-dependent particle number down to the nanometer size range (Fountoukis et al., 2012; Jung et al., 2010; Patoulias & Pandis, 2022; Patoulias et al., 2018). PMCAMx-UF is based on the PMCAMx (Gaydos et al., 2007; Karydis et al., 2007) air quality model that describes the processes of horizontal and vertical dispersion and advection, emissions, dry and wet deposition, aerosol dynamics and thermodynamics, aqueous and aerosol phase chemistry. The simulation of the aerosol microphysics, is handled by the updated version of the Dynamic Model for Aerosol Nucleation (DMANx), which includes the processes of condensation, evaporation, new particle formation (NPF), and coagulation assuming an internally mixed aerosol (Patoulias et al., 2015). DMANx includes the Two-Moment Aerosol Sectional (TOMAS) algorithm which tracks independently both the aerosol number and mass distributions for each of the 41 logarithmically-spaced size bins between 0.8 nm and 10 μm (Adams and Seinfeld, 2002). In the current study, the nucleation rate was computed using a scaled ternary sulfuric acid-ammonia-water parameterization and assuming a scaling factor of 10^{-7} (Fountoukis et al., 2012; Napari et al., 2002). During the last years, PMCAMx-UF has been extended to include chemical aging of semi-volatile anthropogenic organic vapors, intermediate-volatility organic compounds (IVOCs), and the production of extremely low-volatility organic compounds (ELVOCs) by monoterpenes (Patoulias and Pandis, 2022). Additional information describing the evolution and evaluation of PMCAMx-UF model can be found in previous publications (Fountoukis et al., 2012; Jung et al., 2010; Patoulias et al., 2018; Patoulias and Pandis, 2022).

2.3.2 Continued Development of PMCAMx-UF in RI-URBANS

During the RI-URBANS project PMCAMx-UF has been extended to treat the fresh primary organic particles emitted by transportation as sem-ivolatile. This allows these particles to partially evaporate after emission, a process that reduces their size, accelerates their coagulation with larger particles and thus reduces their lifetime and concentration levels.

A second major development is that PMCAMx-UF is now using the RI-URBANS number emission inventory developed by TNO. The emissions are downscaled to 1x1 km resolution using the NOA downscaling algorithm developed also in the same project.

2.3.3 Number source apportionment

Performing number source apportionment in a chemical transport model is challenging. Zeroing all but one source's number emissions results in changes of the condensation and coagulation sinks, to which the model responds non-linearly for particle number concentrations. In this work we use the approach of Posner and Pandis (2015) for number source apportionment.

In a mass-based zero-out technique, all particle emissions of a source are assumed to be zero. Here we zero the number emissions of the specific source up to a threshold diameter, keeping the larger particles mostly intact. This modification to the zero-out method is designed to preserve most of the surface area and mass of emitted particles while capturing the source's contribution to number emissions. The source-specific zero-out threshold diameters are determined by the point at which approximately 90% of the source's number emissions are eliminated. The removal of more than 90% of the corresponding number emissions suggests that the error in our approach is of the order of 10% or less. This has been confirmed by a number balance of the corresponding source contributions.

RI-URBANS (www.RIURBANS.eu) is supported by the European Commission under the Horizon 2020 – Research and Innovation Framework Programme, H2020-GD-2020, Grant Agreement number: 101036245

The contribution of each source to ultrafine particle number concentrations was determined by subtracting the predicted number concentrations of the source's zero-out simulation from the respective predicted number concentration of the base simulation with the nucleation routine turned off. Zero-out simulations were performed with the nucleation routine turned off in order to avoid additional particles nucleating in the zero-out cases due to the decrease in the condensation sink from unavoidable removal of some emitted particle surface area in the zero-out inventories. The source contribution of nucleation to all size ranges was determined by a separate simulation including non-zero emissions from all sources and the nucleation routine turned on.

2.3.4 Effect of treating fresh primary organic particles as semi-volatile

The PEGASOS intensive period was used for the evaluation of the new version of PMCAMx-UF developed in RI-URBANS. The updated PMCAMx-UF predicted lower concentrations of N_{10} (number concentrations of particles smaller than 10 nm) over most of Europe (**Figure** 17). The reductions were up to 30% in large areas.

This reduction in predicted concentrations led to a significant improvement in the ability of the model to reproduce the N_{10} observations in 27 stations all across Europe (**Figure 18**). The overall N_{10} normalized mean bias was reduced from 21% to 12%.

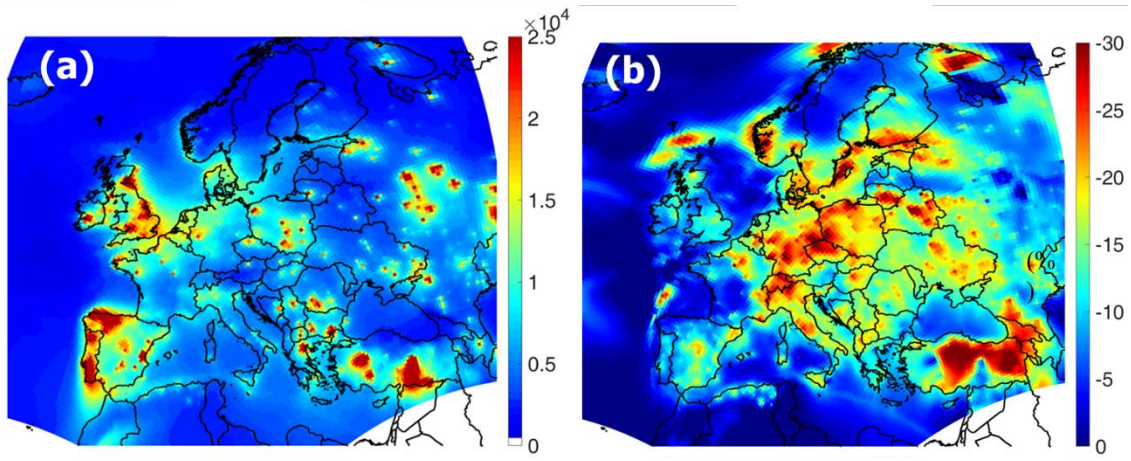

***Figure** 17. (a) Predicted average N_{10} (particles larger than 10 nm) number concentrations for the ground level for Europe during the July 2012 PEGASOS intensive and (b) change in the predicted N_{10} levels due to the treatment of fresh combustion nanoparticles as semi-volatile.*

RI-URBANS (www.RIURBANS.eu) is supported by the European Commission under the Horizon 2020 – Research and Innovation Framework Programme, H2020-GD-2020, Grant Agreement number: 101036245

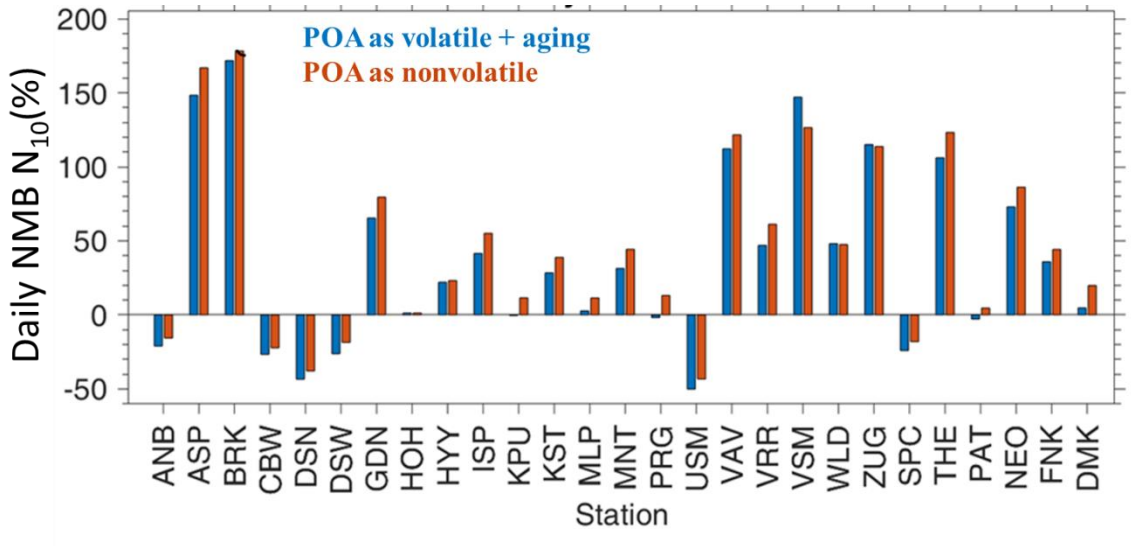

Figure 18. *Normalized mean free bias of updated PMCAMx-UF N10 predictions in 27 stations in Europe. With red the results when primary organic particles are treated as nonvolatile and with blue the performance of the model simulating the evaporation of the primary particles and the subsequent aging chemistry.*

2.3.5 Effect of nucleation rate parameterization

PMCAMx-UF is able to use a variety of nucleation parameterizations. These were tested using the TNO number inventory for 2012 against the PEGASOS intensive data for 27 stations in Europe. The results of the evaluation for N_{10} and N_{100} are summarized in **Figure** 19 and ***Figure*** *20*. If nucleation is neglected the model clearly underpredicts the observed concentrations. The base case sulfuric acid-ammonia- water nucleation parameterization (using a nucleation tuner of 10^{-6}) performs better but tends to overpredict N_{10}. The model performance improves if a slightly lower nucleation tuner equal to 10^{-7} is used. This value will be used in the rest of the PMCAMx-UF simulations. The sulfuric acid-organic-water nucleation parameterizations have good performance that can be improved if the fresh nucleus size is set equal to 1 nm.

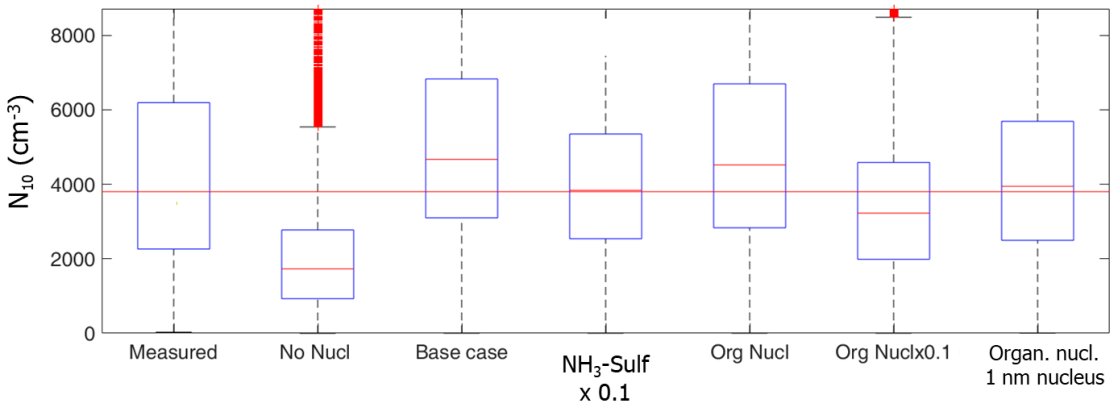

Figure *19. Comparison of PMCAMx-UF predictions for N_{10} against observations in 27 sites for five nucleation parameterizations, a simulation without nucleation for the 2012 PEGASOS intensive in Europe.*

RI-URBANS (www.RIURBANS.eu) is supported by the European Commission under the Horizon 2020 – Research and Innovation Framework Programme, H2020-GD-2020, Grant Agreement number: 101036245

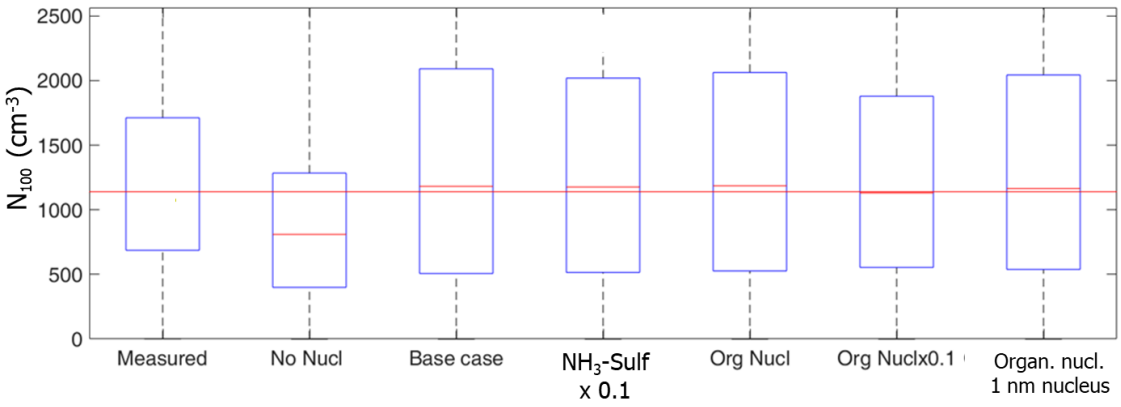

***Figure** 20. Comparison of PMCAMx-UF predictions for N_{100} against observations in 27 sites for five nucleation parameterizations, a simulation without nucleation for the 2012 PEGASOS intensive in Europe.*

For N_{100} all nucleation parameterizations have good performance as these larger particles are less sensitive to the details of the formation of 1 nm particles (***Figure** 20*).

2.3.6 Source contributions in the European Scale

The contributions of each source to the particle number (with high size resolution) have been estimated first at the European scale using 36x36 km grid size simulations for the summer and winter of 2019. The sources included are the following: nucleation, industry including power generation, small combustion, gasoline road transport, diesel road transport, shipping, off-road vehicles, other sources (fugitives, LPG road transport, non-exhaust road transport, waste, agricultural sources), long-range transport (sources outside the modeling domain), and biomass burning.

The predicted concentrations of total particle number (N_{tot}), particles above 10 nm (N_{10}) and above 50 nm (N_{50}) during the summer of 2019 are shown in ***Figure** 21*. Different size classes have different spatial distributions as different processes and sources dominate.

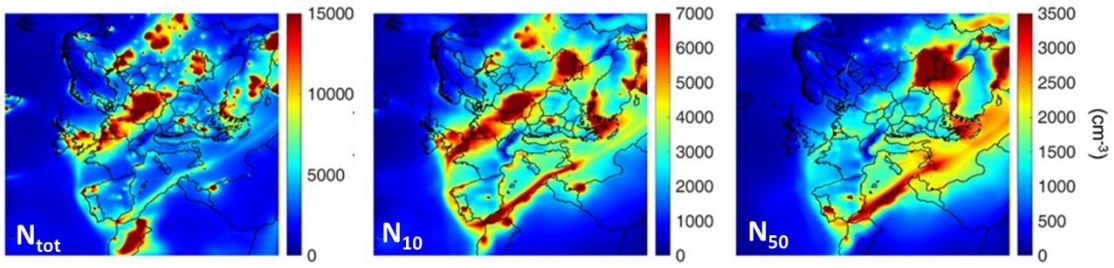

***Figure** 21. Predicted ground level concentrations of total particle number (N_{tot}), particles above 10 nm (N_{10}) and above 50 nm (N_{50}) during the summer of 2019.*

The corresponding concentrations during the winter of 2019 are shown in ***Figure** 22*. The spatial patterns are quite different as, for example, nucleation takes place mainly in Northern Africa and the Middle East during this cold period. There are also different sources (e.g. residential heating) that are important in parts of Europe.

RI-URBANS (www.RIURBANS.eu) is supported by the European Commission under the Horizon 2020 – Research and Innovation Framework Programme, H2020-GD-2020, Grant Agreement number: 101036245

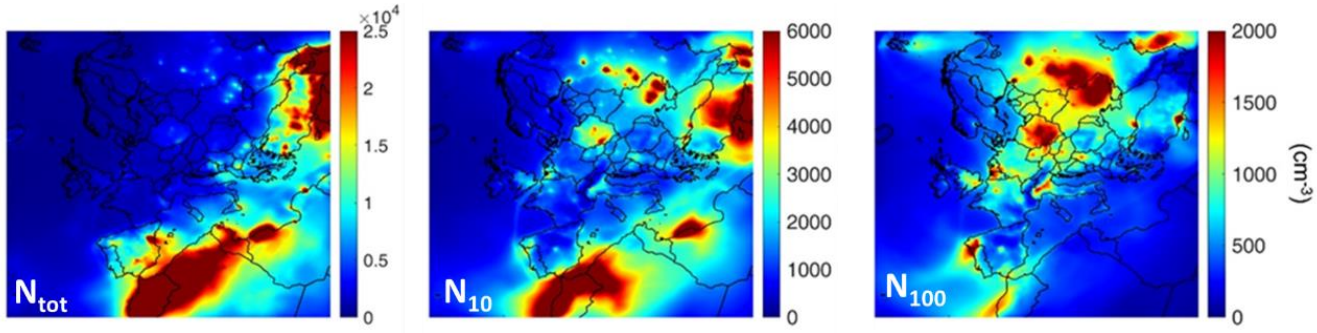

***Figure** 22. Predicted ground level concentrations of total particle number (N_{tot}), particles above 10 nm (N_{10}) and above 50 nm (N_{50}) during the summer of 2019.*

The source contributions to all size ranges have been calculated. The contributions to N_{10} for the summer are shown as an example in Figure 23. Nucleation is the major source over most of continental Europe, while shipping is important for the marine areas. On-road diesel emissions are the dominant primary source of N_{10} over most of continental Europe, with fires being important in the Iberian Peninsula, Ukraine, and other areas where major wildfires were present during the simulated period.

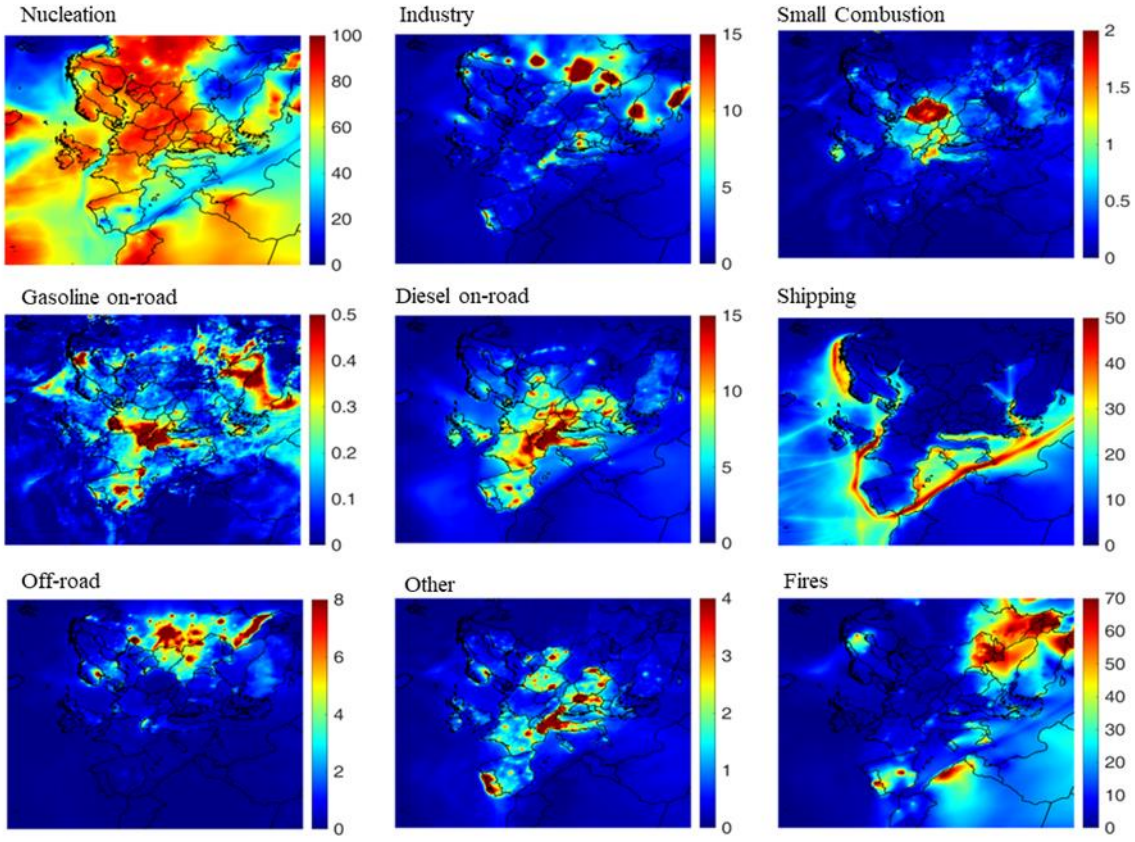

Figure 23. Predicted source contributions as percentage of the total N_{10} over Europe for the summer of 2019 using PMCAMx-UF.

RI-URBANS (www.RIURBANS.eu) is supported by the European Commission under the Horizon 2020 – Research and Innovation Framework Programme, H2020-GD-2020, Grant Agreement number: 101036245

The situation is quite different in the winter (***Figure** 24*). During this period nucleation is important only in parts of southern Europe. It is still the dominant process over northern Africa. Small combustion due to residential heating contributes significantly to N_{10} in eastern Europe but also parts of central Europe. On-road diesel emissions are predicted to contribute 40% or even more of the N_{10} in most of central Europe and the UK. Wildfires are an important source for parts of the Iberian Peninsula even during winter. Industrial sources are dominant contributors to particle number in Russia and other eastern European countries outside the EU. On-road gasoline vehicles are predicted to contribute only a few percent to N_{10} in most areas at this scale. Shipping is more important in the northern marine areas than in the Mediterranean during this season. Finally, the other sources are responsible for up to 10% of particle number above 10 nm in several countries mostly in southern Europe.

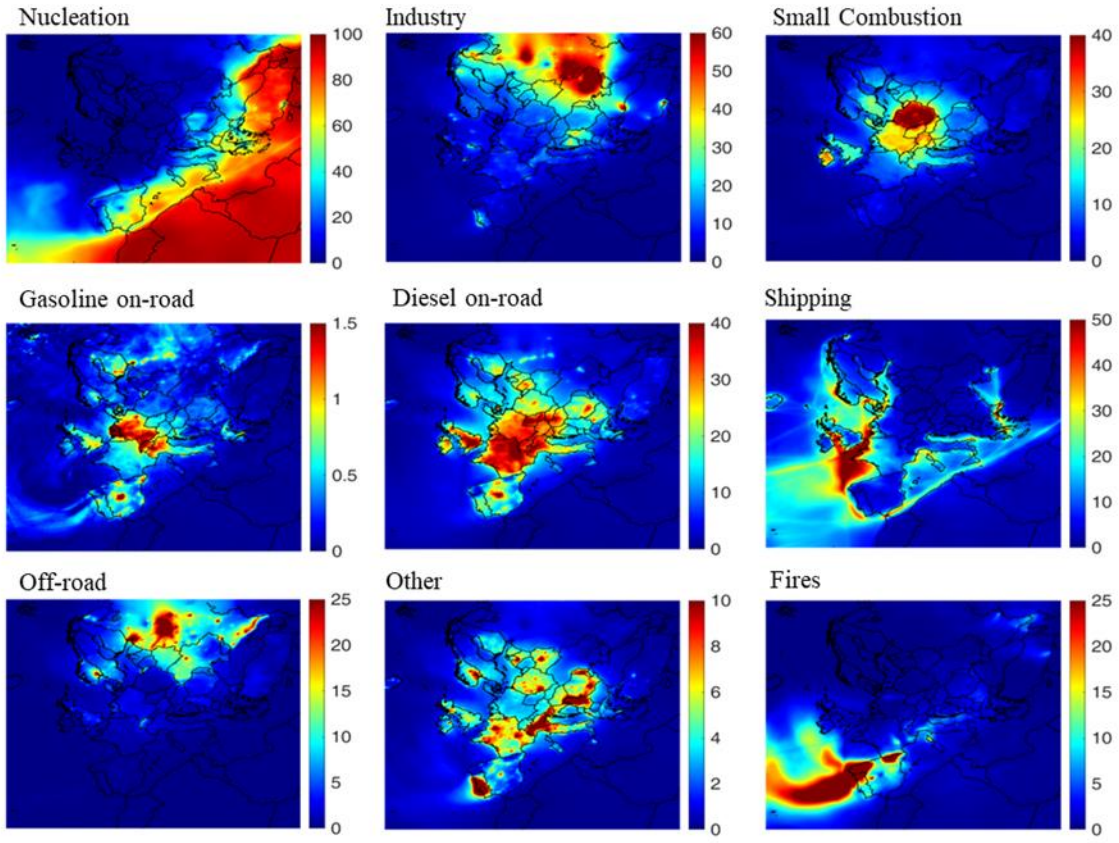

***Figure** 24. Predicted source contributions as percentage of the total N_{10} over Europe for the winter of 2019 using PMCAMx-UF.*

RI-URBANS (www.RIURBANS.eu) is supported by the European Commission under the Horizon 2020 – Research and Innovation Framework Programme, H2020-GD-2020, Grant Agreement number: 101036245

3 Mapping high resolution urban air quality

3.1 BC modelling at city scale (CNRS/CEREA)

High resolution concentrations are simulated with the CHIMERE model (Menut et al. 2021) coupled to the street network MUNICH (Lugon et al. 2021, Kim et al. 2022) for NO_2, PM2.5, PM10, Number, BC and other particle compounds (e.g. organic aerosols). The chain CHIMERE/MUNICH uses the same aerosol module (SSH-aerosol, Sartelet et al. 2020) at both the regional and local scales, allowing to consider the dynamic of particles (coagulation, condensation/evaporation, nucleation) at all scales when computing the number concentrations. At the regional scale, nested domains are considered using CAMS boundary conditions over Europe. The smallest domain of simulation is discretized with a 1 km x 1 km resolution over Greater Paris, with a zoom in the streets of Paris. Simulations are performed for a winter and a summer period: December 2020/January 2021, and June/July 2022.

As BC and PPNC are strongly influenced by traffic, a bottom-up approach is used for emissions. The road traffic emissions data were produced by Airparif with the Heaven system (see more details in deliverable of T3.1). The strength of this system is to use a traffic model that is corrected from the count data received in near-real time. In the chain CHIMERE/MUNICH, the regional-scale traffic emissions were estimated by aggregating the local-scale emissions corrected from the local traffic counts. For other activity sectors, the Airparif inventory of 2019 was used, and biogenic emissions were modelled using MEGAN, as implemented in CHIMERE. Number emissions were estimated from the Airparif inventory using the methodology detailed in Sartelet et al. (2022).

For comparisons to observations, as the model simulates EC, the BC observed concentrations are normalized using a harmonization factor, following Savadkoohi et al. (2023). A harmonization factor of 1.76 and 1.7 was determined for Paris in the summer 2022 and the winter 2020/2021 respectively using EC and BC collocated measurements at Les Halles station, which is a urban background station operated by Airparif in the centre of Paris.

The measured and simulated concentrations are compared in **Table** 9 at urban background stations and traffic stations. Urban background EC is under-estimated during wintertime, linked to uncertainties in the speciation of emissions from the residential sector. However, the mean concentrations compare well to the observations satisfying the model performance criteria (MFE < 75%, MFB < ±50%) and in the summer and a traffic stations, the model performance goal (MFE< 50% and MFB < ±30%) of Boylan and Russell (2006). Note that, as shown in the deliverable of T3.1, the BC concentrations are better modelled using the bottom-up inventory with correction from traffic loop counts than using the top-down inventory.

Maps of EC for the winter and summer simulations are shown in **Figure** 25Figure 15. A more detailed analysis on the variability of BC is presented in the deliverable D4.6 of T4.3.

***Table** 9. EC model to measurement comparisons at background and traffic stations for summer and winter over Greater Paris*

EC	Station Type	Nb Stattions	Obs. ($\mu g\ m^{-3}$)	Sim. ($\mu g\ m^{-3}$)	MFE (%)	MFB (%)	RMSE ($\mu g\ m^{-3}$)
Summer	Urban	4	0.4	0.4	50	0	0.28
	Traffic	3	1.3	1.1	37	4	0.58
Winter	Urban	5	0.7	0.4	56	-46	0.35
	Traffic	2	1.8	1.7	46	10	0.99

RI-URBANS (www.RIURBANS.eu) is supported by the European Commission under the Horizon 2020 – Research and Innovation Framework Programme, H2020-GD-2020, Grant Agreement number: 101036245

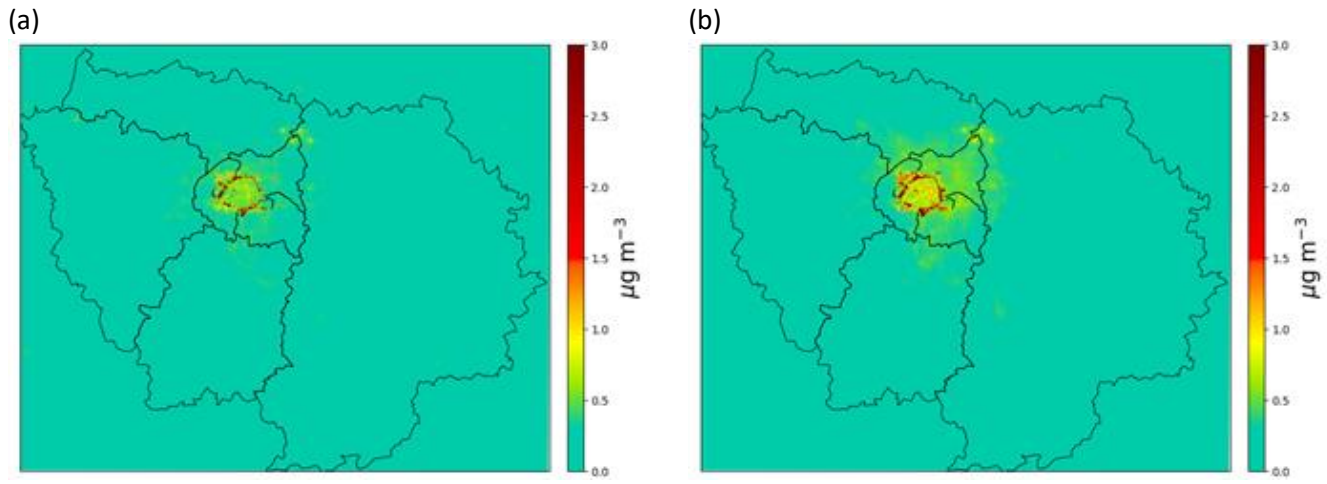

***Figure** 25. Map of EC for the (a) summer 2022 and (b) winter 2020/2021 using CHIMERE/MUNICH*

3.2 3.2. UFP modelling at city scale (FORTH, CNRS/CEREA, TNO, FMI)

Focus over the Greater Paris with the multi-scale CHIMERE/MUNICH model

Using the set-up detailed in the previous section for BC, the measured and simulated concentrations of PN for particles of diameters larger than 10 nm are compared in Table 10at urban background stations and traffic stations. The model evaluation for other pollutants may be found in the Deliverable D26 (D4.6).

No measurement is available at traffic station for the winter simulation. However, at background sites in winter, and at background and traffic sites in summer, the mean concentrations compare well to the observations satisfying the model performance criteria (MFE < 75%, MFB < ±50%) and the model performance goal (MFE< 50% and MFB < ±30%) of Boylan and Russell (2006). Although the statistical comparison is good, the PN concentrations are under-estimated in summer at urban background sites, because nucleation is not considered in the simulations presented here. Performing simulations over Greater Paris in the summer 2009 with the chemistry transport model Polair3D coupled to the aerosol module SSH-aerosol, Sartelet et al. (2022) showed that statistics satisfies model evaluation criteria when not considering nucleation, similarly to the results obtained here for the summer 2022. However, Sartelet et al. (2022) showed that model/measurement comparisons of PNC are improved at all measurement sites when considering the heteromolecular nucleation, which involves sulfuric acid and extremely low volatile organic compounds from monoterpene autoxidation.

***Table 10.** PNC model to measurement comparisons at background and traffic stations for summer and winter*

PNC	station	Stat. Type	Obs. (# m^{-3})	Sim. (# m^{-3})	MFE (%)	MFB (%)	RMSE (# m^{-3})
summer	Urban	3	8145	5843	41	-34	3562
	Traffic	1	9141	7713	23	-13	2521
winter	Urban	4	7396	7342	32	0	3057
	Traffic	-	-	-	-	-	-

RI-URBANS (www.RIURBANS.eu) is supported by the European Commission under the Horizon 2020 – Research and Innovation Framework Programme, H2020-GD-2020, Grant Agreement number: 101036245

Maps of PNC for the winter and summer simulations are shown in **Figure** 26. A more detailed analysis on the variability of PNC is presented in the deliverable D26 (D4.6) of T4.3.

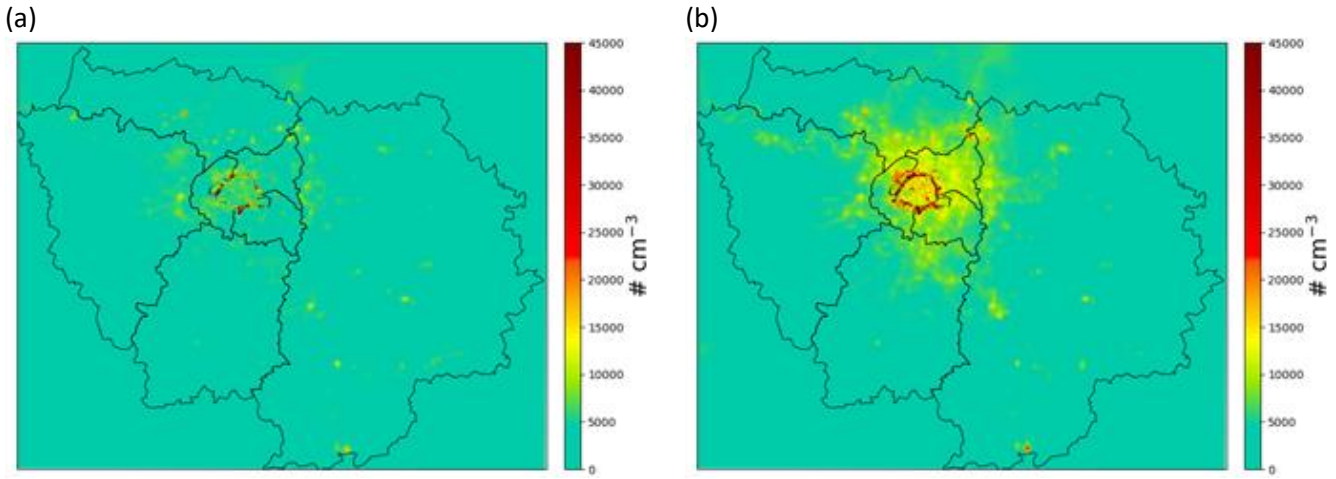

***Figure** 26. Map of UFP for the (a) summer 2022 and (b) winter 2020/2021 using CHIMERE/MUNICH*

PMCAMx-UFP

The ability of PMCAMx-UF to use multiple grids has been used to allow it to focus on specific RI-URBANS pilot cities. The particle number distribution over three cities (Athens, Barcelona, and Paris) has been simulated for the summer and winter of 2019. In all simulations the full European domain is simulated at 36x36 km, and the city is simulated at 1x1 km. For numerical purposes the grid size is reduced gradually, so there is an area in which 12x12 km grid cells are used and another with 3x3 km. The corresponding areas for Athens are shown in ***Figure** 27*.

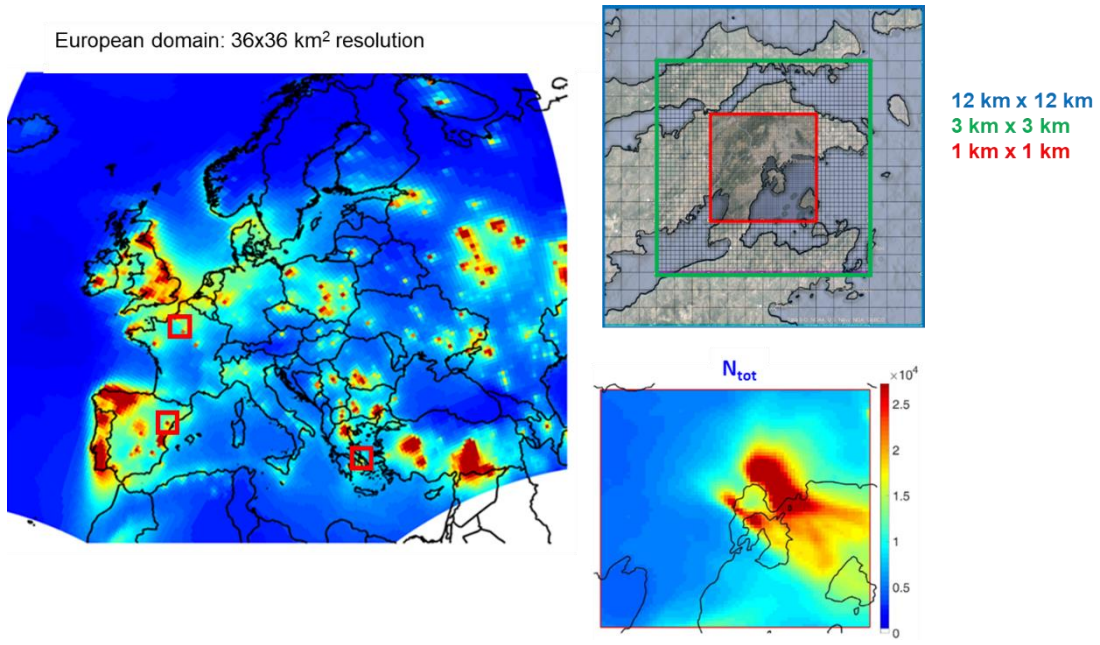

***Figure** 27. Example of the multiple modeling scales used in PMCAMx-UF for the pilot city of Athens. Europe is the outer domain (36x36 km) and there are two intermediate domains plus the inner domain, the city itself which is simulated at high resolution.*

RI-URBANS (www.RIURBANS.eu) is supported by the European Commission under the Horizon 2020 – Research and Innovation Framework Programme, H2020-GD-2020, Grant Agreement number: 101036245

Similar grid systems have been used for Paris and Barcelona.

Athens

During the summer the higher N_{10} concentrations are predicted for the port of Piraeus and the Saronic Gulf while during the winter there are high concentrations also over most of Athens (**Figure** 28).

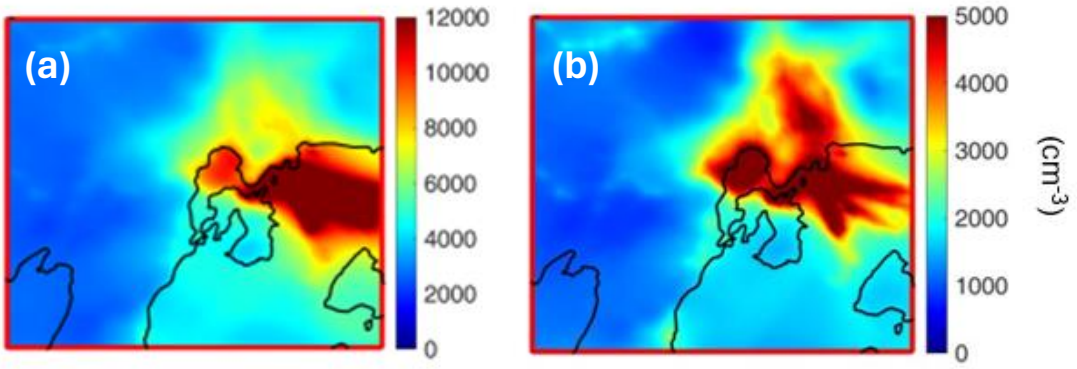

***Figure** 28. Predicted ground-level N_{10} concentrations for the city of Athens for (a) summer of 2019 and (b) winter of 2019.*

The predictions of PMCAMx-UF have been evaluated against the measurements in the two RI-URBAN sites in Athens. The comparison of the predictions with the measured concentrations of N_{25} are shown in **Figure** 29.

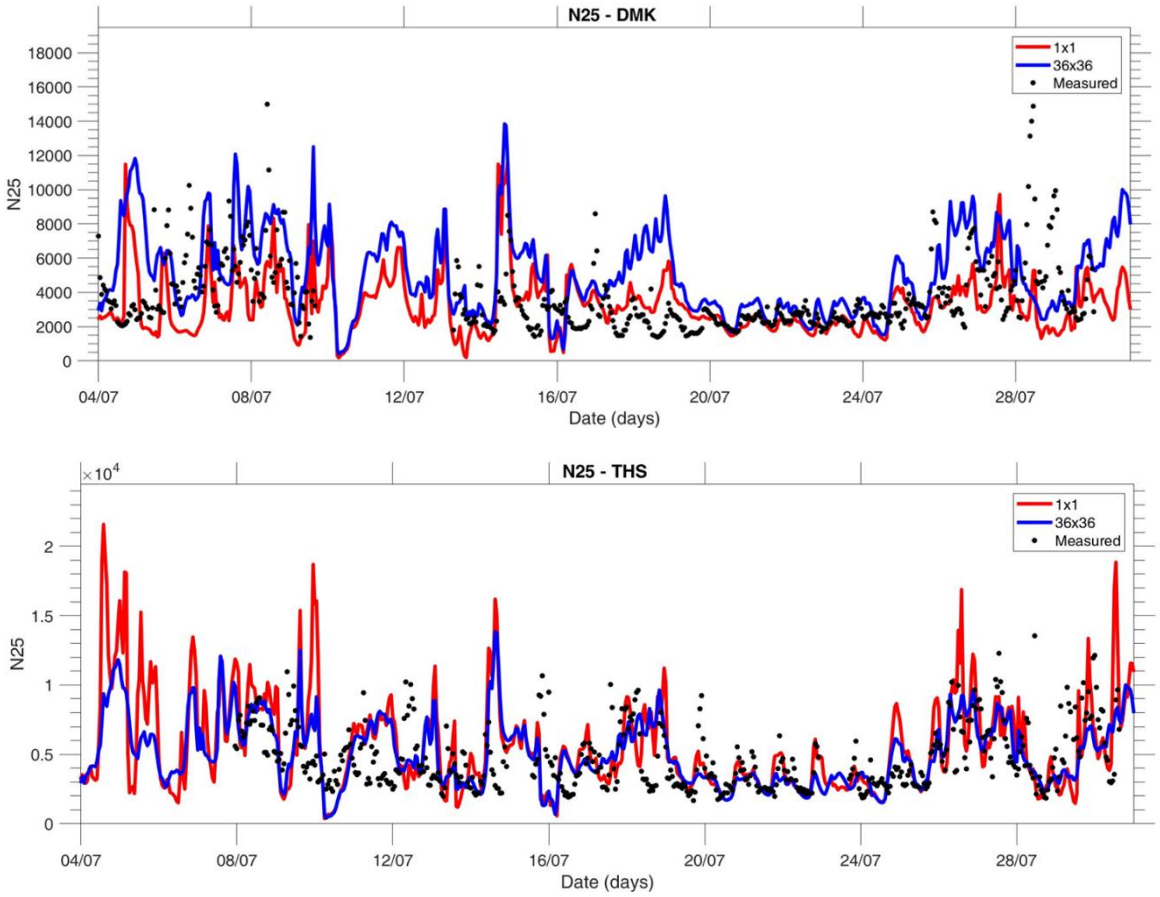

***Figure** 29. Comparison of the measured N_{25} concentrations in Demokritos (DMK, top) and Thision (THS, bottom) shown with symbols against the predictions of PMCAMx-UF at low (in blue) and high (in red) grid resolution for July 2019)*

RI-URBANS (www.RIURBANS.eu) is supported by the European Commission under the Horizon 2020 – Research and Innovation Framework Programme, H2020-GD-2020, Grant Agreement number: 101036245

Nucleation is predicted to be the major source of N_{10} in Athens and the surrounding areas over land, while shipping is a major source in Piraeus with its major port and the norther Saronic Gulf. On road diesel emissions contribute 20-30% to N_{10} in the urban core of the city while gasoline emissions contribute less than 5%. In the major industrial areas to the west and to the north of the city the corresponding sources are responsible for 10-15% of the particles. Significant industrial contributions are also predicted locally. A major fire to the north of the city contributed locally 15-20% to the average of the particle number in the nearby areas during the whole modeling period (it was obviously the dominant source during the few days that it lasted).

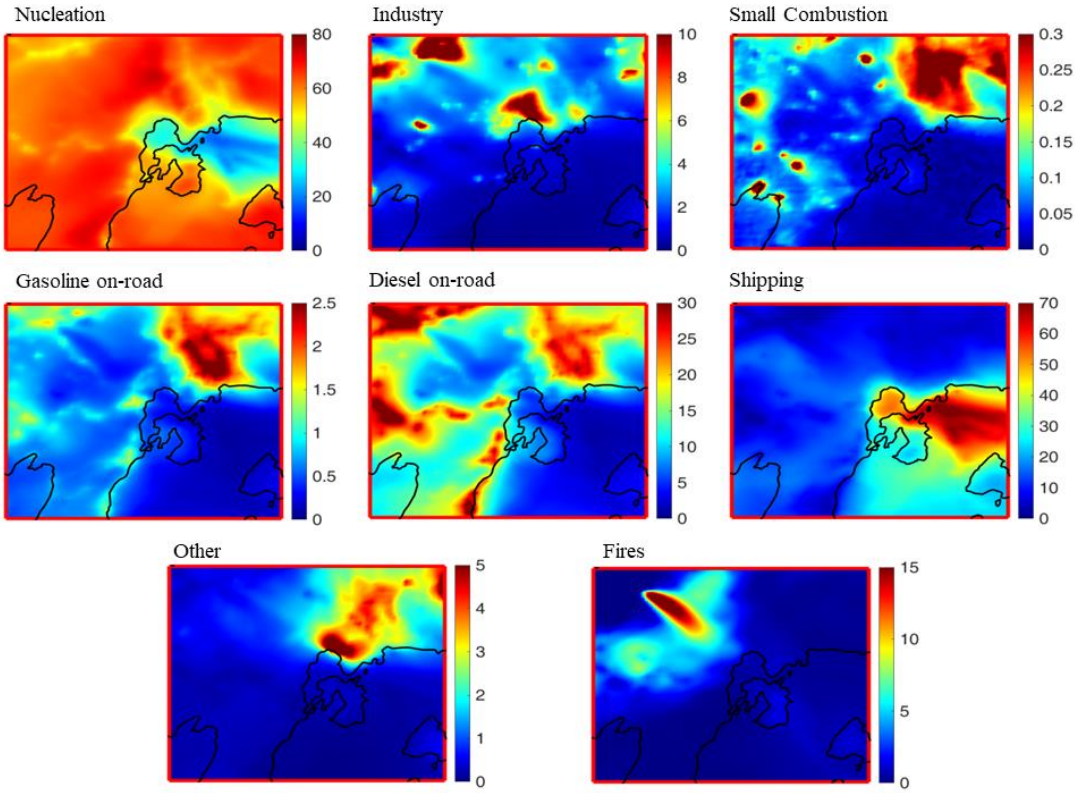

***Figure** 30. Predicted source contributions as percentage of the total N_{10} over Athens for the summer of 2019 using PMCAMx-UF.*

During the winter nucleation becomes less frequent, but still contributes around 20% to the N_{10} over the city and above 40% outside the urban area (**Figure** 31). The importance of all primary sources increases as a result, with on-road diesel contributing almost half the particles in the city of Athens. Shipping is still a major source of particle number in Piraeus and other coastal areas. The relative importance of industry and other sources increases. Small scale combustion due to residential heating is important locally. However, there is evidence that the emissions of this source are seriously underestimated in Athens.

RI-URBANS (www.RIURBANS.eu) is supported by the European Commission under the Horizon 2020 – Research and Innovation Framework Programme, H2020-GD-2020, Grant Agreement number: 101036245

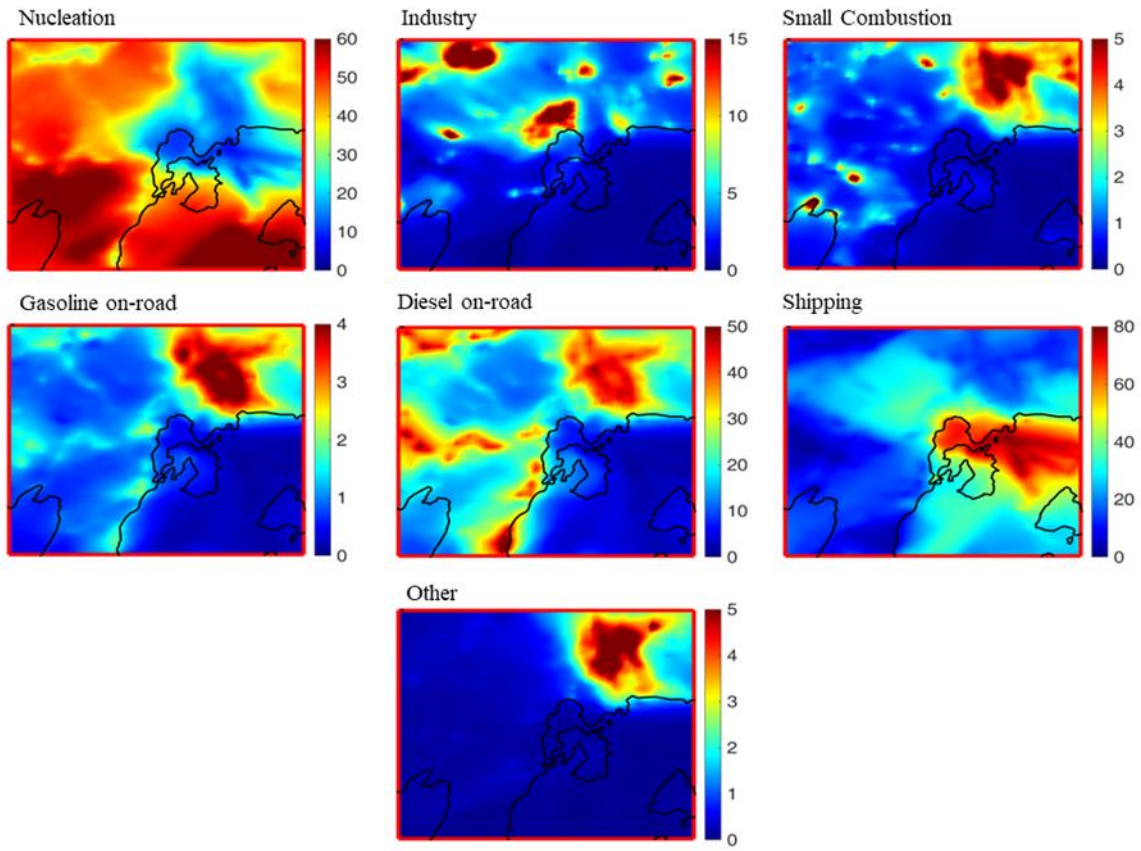

***Figure** 31. Predicted source contributions as percentage of the total N_{10} over Athens for the winter of 2019 using PMCAMx-UF.*

Barcelona

During the summer the higher N_{10} concentrations are predicted for the port of Barcelona and the nearby marine area while during the winter there are high concentrations also over most of the urban area (**Figure** 32).

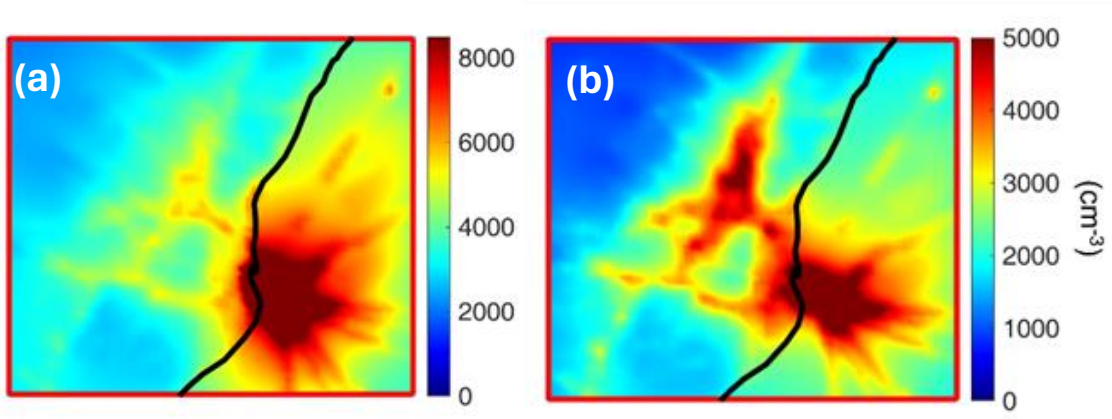

***Figure** 32. Predicted ground-level N_{10} concentrations for the city of Barcelona for: (a) summer of 2019 and (b) winter of 2019.*

RI-URBANS (www.RIURBANS.eu) is supported by the European Commission under the Horizon 2020 – Research and Innovation Framework Programme, H2020-GD-2020, Grant Agreement number: 101036245

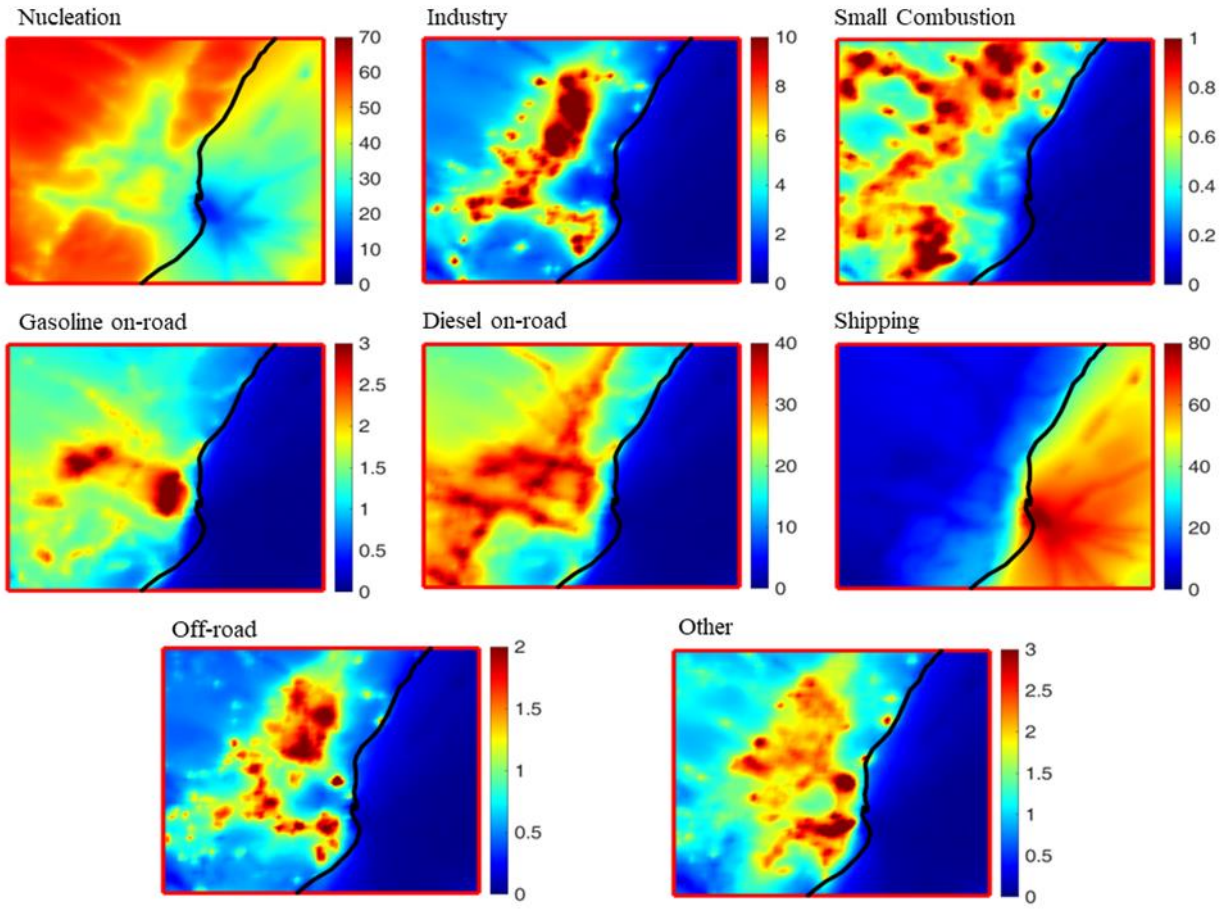

***Figure** 33. Predicted source contributions as percentage of the total N_{10} over Barcelona for the summer of 2019 using PMCAMx-UF.*

Nucleation was an important source of particle number outside the urban area, but primary sources dominated inside the city (**Figure** 33). On road diesel emissions were responsible for most of the particles inland. Shipping was the dominant source near the port but also in some coastal areas. Industrial emissions were important further inland. The average contributions of small-scale combustion, on-road gasoline, off-road, and other sources were less than 5% each.

During the winter as expected, the importance of nucleation decreases and the primary sources become more important (***Figure** 34*). The small scale combustion due to the residential heating increases in importance more than the other sources. Based on the estimated emissions it still contributes less than 10% inside the city, with higher contributions outside.

RI-URBANS (www.RIURBANS.eu) is supported by the European Commission under the Horizon 2020 – Research and Innovation Framework Programme, H2020-GD-2020, Grant Agreement number: 101036245

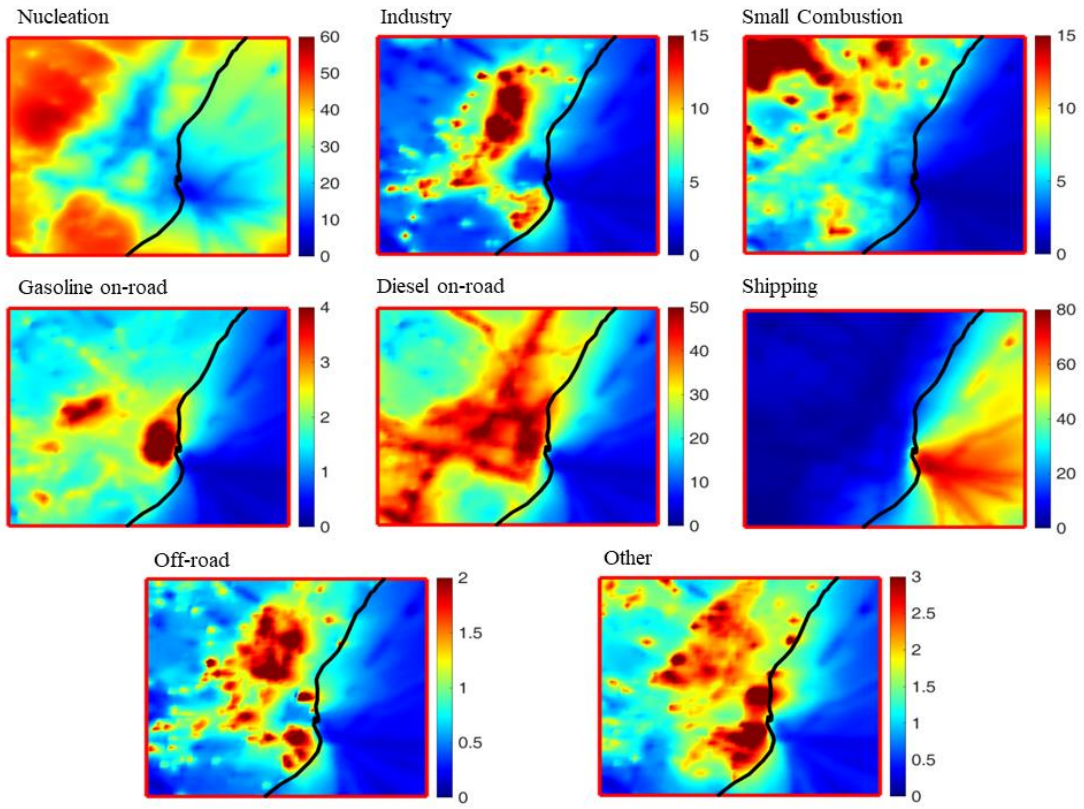

***Figure** 34. Predicted source contributions as percentage of the total N_{10} over Barcelona for the winter of 2019 using PMCAMx-UF.*

Paris

During the summer relatively uniform N_{10} concentrations are predicted for Paris with some local hot spots while during the winter there are high concentrations over most of the urban area (**Figure** 35).

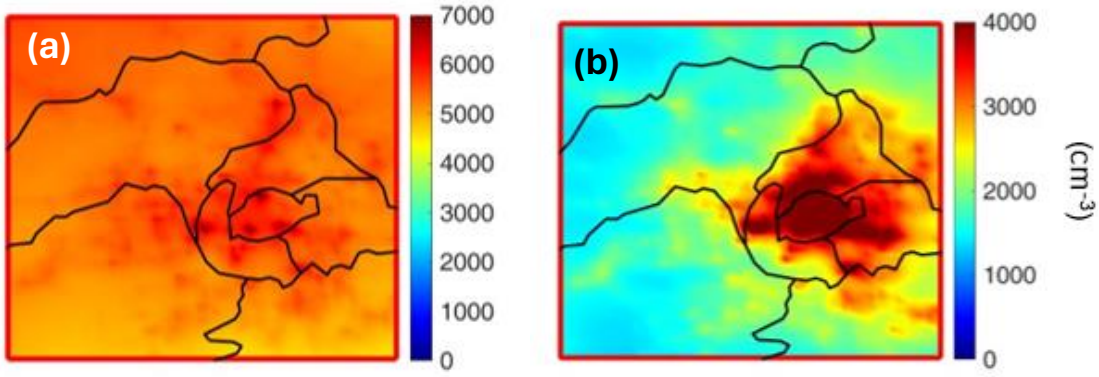

***Figure** 35. Predicted ground-level N_{10} concentrations for the city of Paris for (a) summer of 2019 and (b) winter of 2019.*

RI-URBANS (www.RIURBANS.eu) is supported by the European Commission under the Horizon 2020 – Research and Innovation Framework Programme, H2020-GD-2020, Grant Agreement number: 101036245

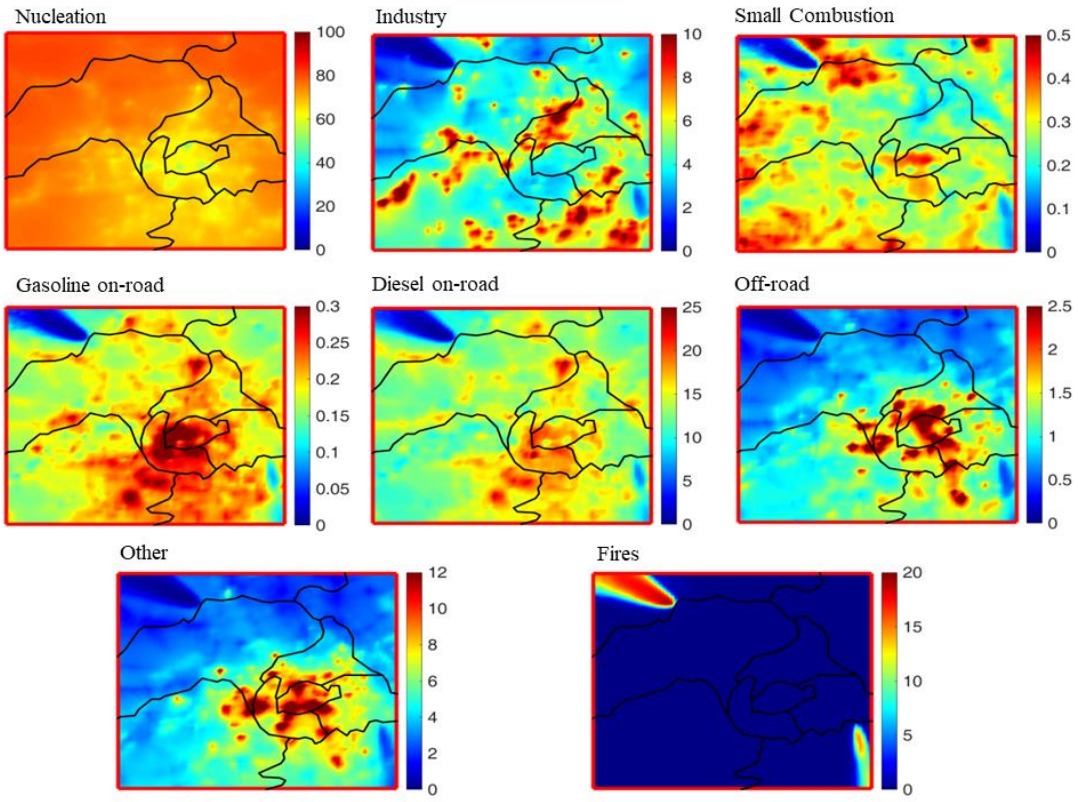

***Figure** 36. Predicted source contributions as percentage of the total N_{10} over Paris for the summer of 2019 using PMCAMx-UF.*

The relatively uniform concentration levels are due to the predicted dominance of nucleation as a source of particle number (**Figure** 36). On road diesel is the dominant primary source, with industry and other sources following.

During the winter nucleation is predicted to a have a negligible contribution and diesel on road emissions to be a major source (**Figure** 37).

RI-URBANS (www.RIURBANS.eu) is supported by the European Commission under the Horizon 2020 – Research and Innovation Framework Programme, H2020-GD-2020, Grant Agreement number: 101036245

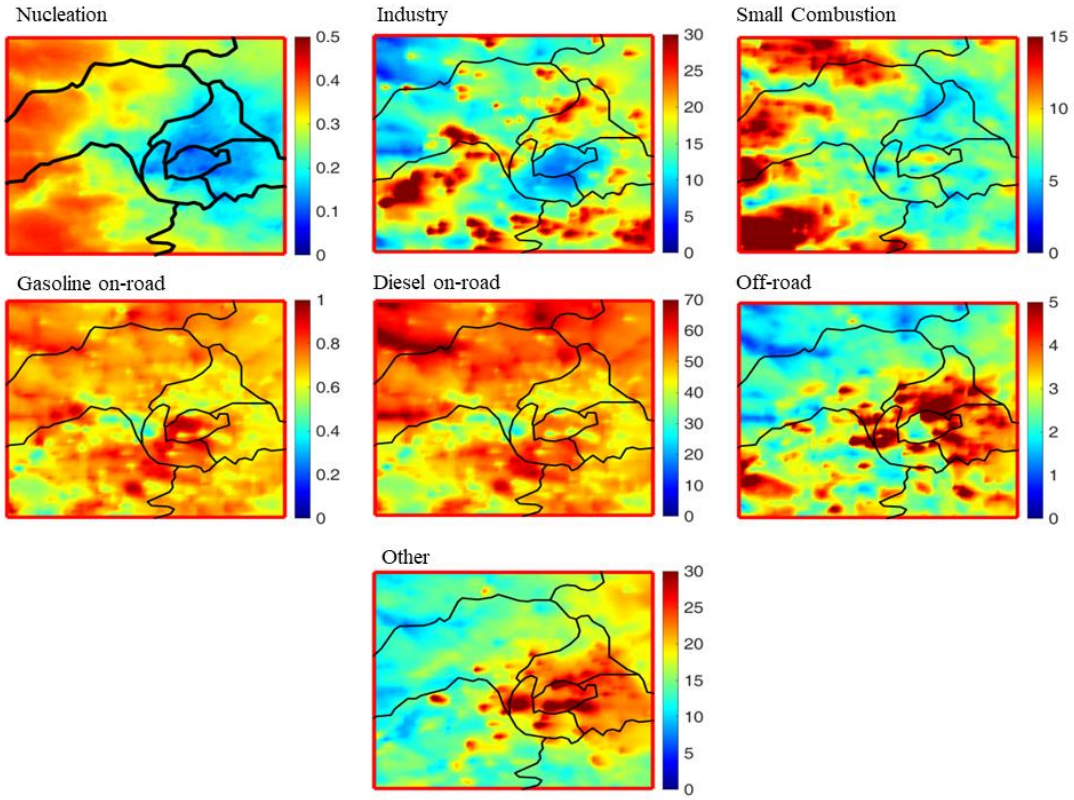

***Figure** 37. Predicted source contributions as percentage of the total N_{10} over Paris for the winter of 2019 using PMCAMx-UF.*

The other sources are predicted to be the second most important local source. Industrial emissions and small scale combustion are important sources outside the urban area in selected areas.

Focus over the Rotterdam area with LOTOS-EUROS

Within LOTOS-EUROS the modelling of UFP has also been developed. Initial developments and implementation focused on Berlin. Further developments and application focused on the city of Rotterdam. For Rotterdam a bottom-up inventory was made by TNO for the Rijnmond area for 2019. This emission inventory was combined with the RI-URBANS' PNC inventory, with a downscaling of PNC from country totals per sector to 1x1km resolution using $PM_{2.5}$ sector-wise spatial gridding for the Netherlands as used by RIVM. As boundary conditions, SMPS observation data from Cabauw for 2022 were used with gap-filling using a daily mean cycle for that month to preserve typical behaviour per season. A simulation was done for the year 2022 on a 1x1 km grid. Figure 17**Figure** 38 shows the annual mean modelled UFP and PNC concentrations. UFP and PNC concentrations are clearly highest for the shipping lanes. The airports stand out due to very high UFP emissions. Note that the aviation emissions are with a fixed height distribution, not mimicking the actual landing-and take-off height distribution and are quite uncertain due to the large contribution of volatile particles and coagulation processes close to the source. Highways do not stand out so clearly at the scale used.

RI-URBANS (www.RIURBANS.eu) is supported by the European Commission under the Horizon 2020 – Research and Innovation Framework Programme, H2020-GD-2020, Grant Agreement number: 101036245

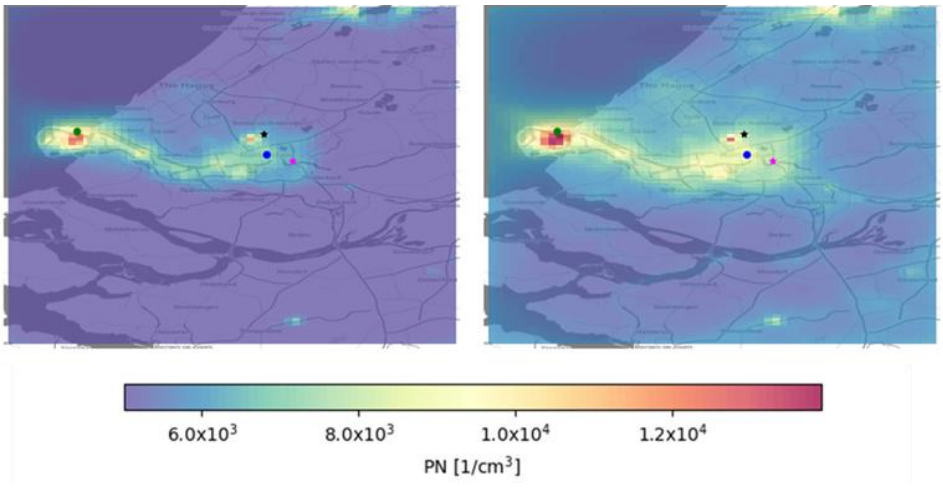

***Figure** 38. Annual mean concentrations for UFP (left) and PN (right) for 2022 in the Rijnmond area around Rotterdam. Blue dot = centre of Rotterdam, pink star = Ruisdael measurement location close to Nieuwe Maas, and black star = DCMR measurement location close to Rotterdam airport (Veldkersweg)*

The modelled results have been compared to observations at two locations (Figure 18) **Figure** 39. For Veldkersweg, a background station with some expected influences of the Rotterdam airport the modelled background concentrations are in good agreement with the observations, but there is a general underestimation of elevated UFP concentrations. For the Nieuwe Maas site the modelled background values are also reasonable but there is a strong general underestimation. Here we suspect the influence of shipping, which already has high UFP emissions, but further formation of particles due to generally elevated SO_2 concentrations in the Rotterdam region can be expected and is as yet not implemented. Furthermore, some days had fairly high temperatures (>25 C in period from 22 Aug. to 6 Sept.) which enhance particle formation events, currently not yet implemented. In theory, this is included in taking Cabauw values as background. However, by putting the values at the boundaries, the required time to arrive at the middle of the domain already allows for coagulation and loss of the smallest particles with the highest number concentrations. Cabauw values at the boundaries thus do not make up for the large-scale events that could take place close to or downwind of the source areas.

RI-URBANS (www.RIURBANS.eu) is supported by the European Commission under the Horizon 2020 – Research and Innovation Framework Programme, H2020-GD-2020, Grant Agreement number: 101036245

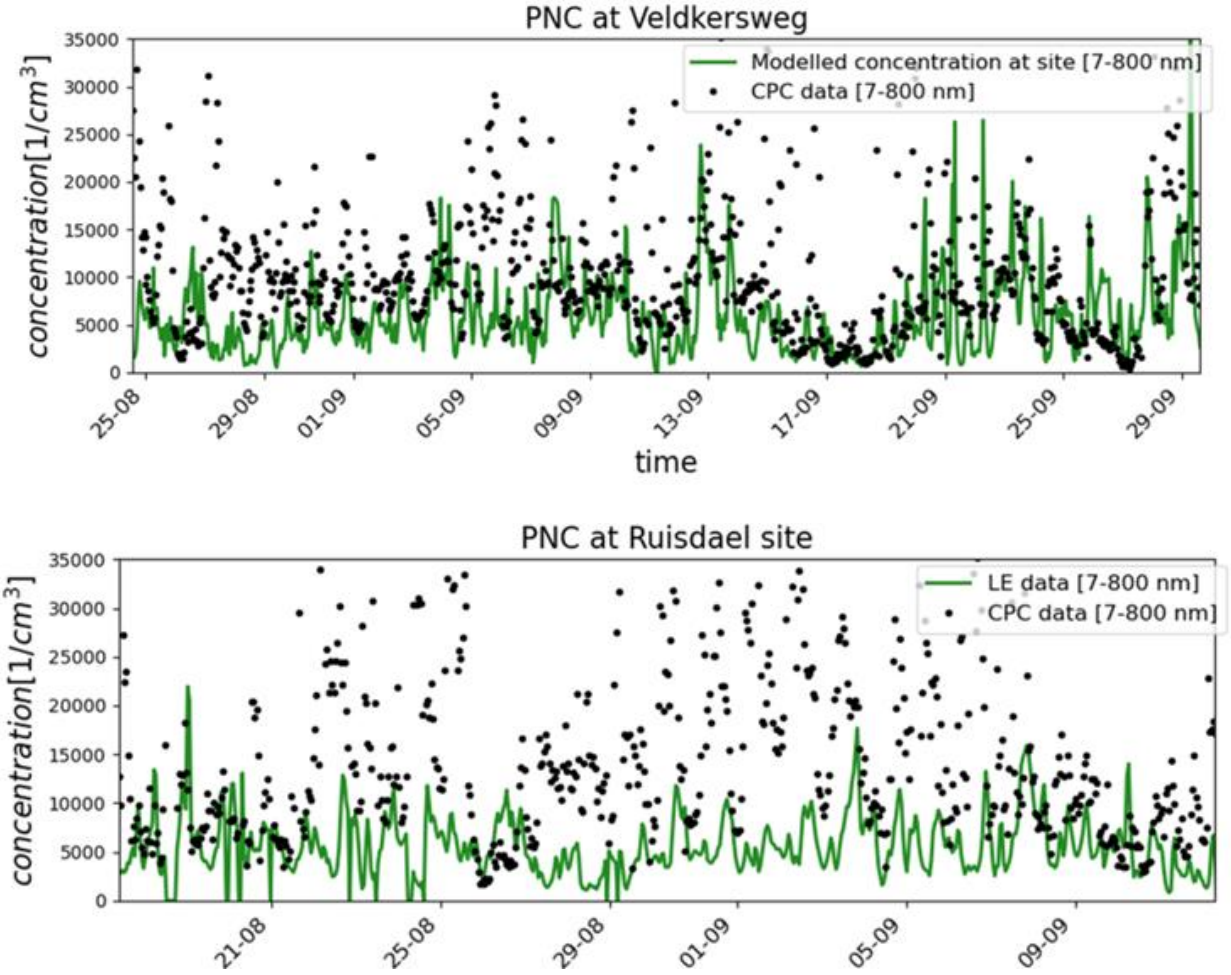

***Figure** 39. Observed and modelled total number concentration up to 800 nm for two measurement campaigns.*

The RI-URBANS' UFP emission inventory has also been used for a European model test run. This run showed relatively low concentrations when compared to other studies and the Rotterdam application. The difference in resolution only explains a small part of the discrepancy. The Rotterdam simulation has Cabauw as background conditions, naturally implementing a minimum concentration from measurements to account for nucleation events. For such a European-scale simulation it is essential to have the process of nucleation included, which is taken as the next development step.

Accounting for UFPs in parametrisation of PM coagulations on bioaerosols

SILAM has been employed to evaluate the effect of coagulation of small diesel particles on bioaerosols (pollen allergen). The simulations showed a comparatively fast removal of small particles due to coagulation on the surface of larger allergen aerosol. The experiment was repeated at several atmospheric humidities to account for a high solubility of the allergen particles. FIGURE 19**Figure** 40 depicts the effect for the dry atmosphere.

RI-URBANS (www.RIURBANS.eu) is supported by the European Commission under the Horizon 2020 – Research and Innovation Framework Programme, H2020-GD-2020, Grant Agreement number: 101036245

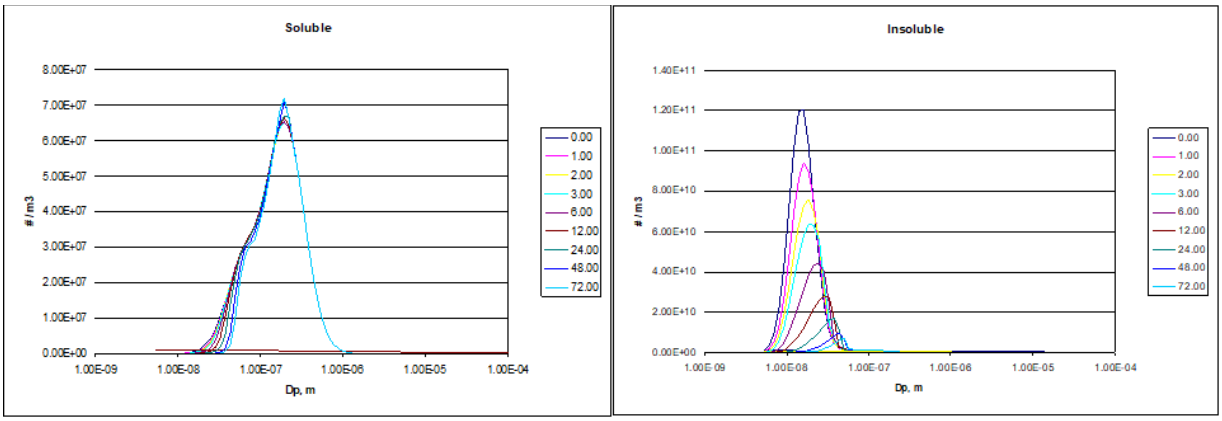

***Figure** 40. Temporal evolution and size distribution of allergen from birch (soluble particles, left) and that of diesel exhaust particles (insoluble particles, right). Dry atmosphere.*

3.3 PM Oxidative Potential Modelling at city scale (METNO, CNRS/LISA, TNO)

Here we present the feasibility of producing very high-resolution OP simulations. The OP data are just becoming available for a focus using specific measurement in Paris and Rotterdam, so that city-specific OP maps for those pilots will only become available at a later stage.

Instead, we present here how the generic European methodology can be applied in a high-resolution model such as uEMEP to provide OP maps over any European city but using default OP values.

Calculations of annual mean OP for the 10 target cities have been made at 250 m resolution using the combined EMEP/uEMEP modelling system, Figure 20**Figure** 41. In general, the procedure is the same as described in Section 0 for the EMEP MSC-W model implementation except that the contributions from road transport and residential combustion primary emissions have been downscaled using methodologies described in Mu et al. (2022). All other contributions are provided by the EMEP MSC-W model at 0.1° resolution. From these downscaled source contributions OP has been calculated using the methodology prescribed by Weber et al. (2021).

Exposure, population weighted concentration (PWC), is calculated for each city within the city administrative borders. There is a large variation between the pilot cities, from 0.7 nmol min^{-1} m^{-3} for Helsinki to 2.1 nmol min^{-1} m^{-3} for Milan. Traffic emissions clearly plays a significant part in the higher OP contributions.

RI-URBANS (www.RIURBANS.eu) is supported by the European Commission under the Horizon 2020 – Research and Innovation Framework Programme, H2020-GD-2020, Grant Agreement number: 101036245

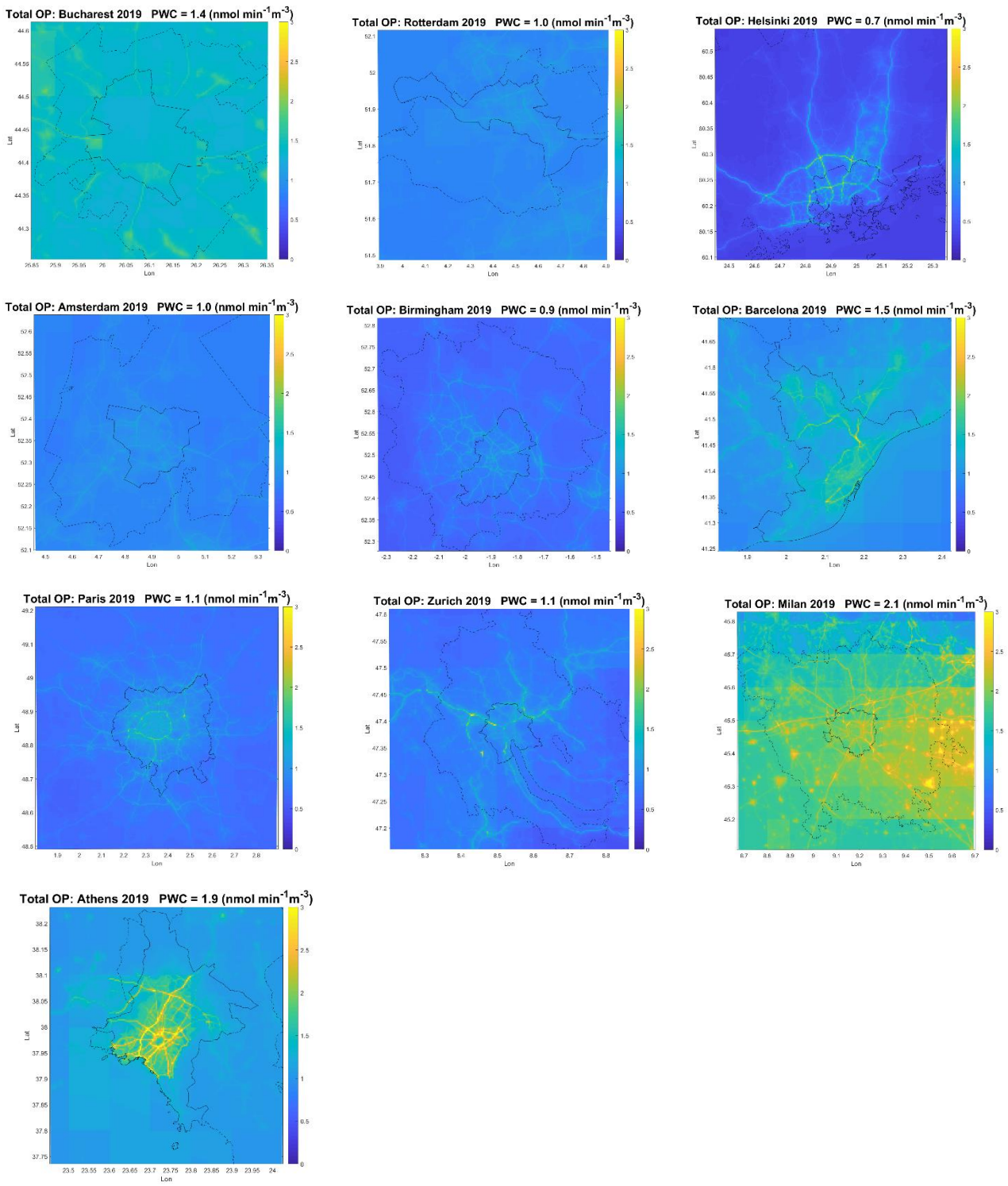

***Figure** 41. Maps of annual mean OP at 250 m resolution using the Weber et al. (2021) methodology, calculated with EMEP/uEMEP for 2019. Cities are ordered in the calculated exposure, population weighted concentration (PWC), from top to bottom. Exposure is calculated within the administrative borders of each city, shown as a solid black line. The functional urban area is also shown as a dashed black line.*

RI-URBANS (www.RIURBANS.eu) is supported by the European Commission under the Horizon 2020 – Research and Innovation Framework Programme, H2020-GD-2020, Grant Agreement number: 101036245

In **Figure** 42 a comparison between the EMEP and uEMEP results is shown for the city of Athens. These maps are distinctly different. One of the largest differences between the two methods is that the contribution to OP from road transport is considerably more centred on roads. The downscaling furthermore causes the population weighted exposure to increase from 1.7 to 1.9 nmol min^{-1} m^{-3}.

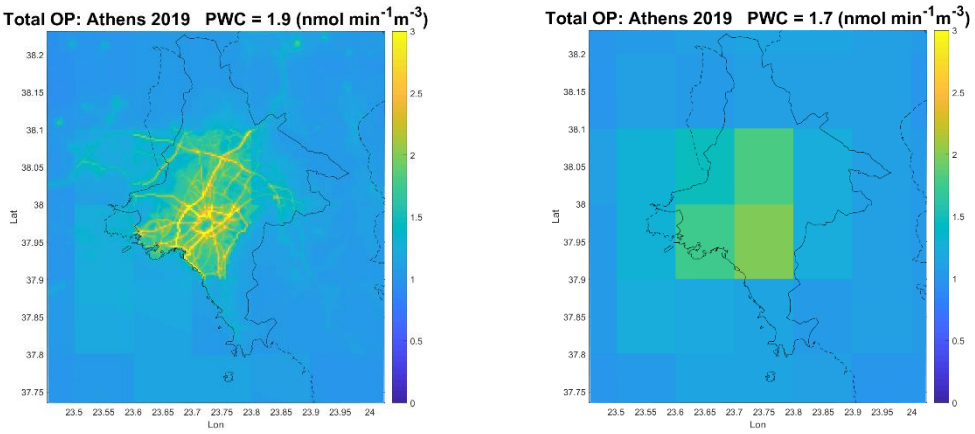

***Figure** 42. Comparison of uEMEP (left) and regular 0.1 x 0.1 degree EMEP (right) calculations for the city of Athens.*

The following conclusions are made concerning these calculations:

- The population weighted exposure was always higher, from +1 to +30% when using uEMEP compared to just EMEP, except for Paris that was 10% higher when using just EMEP.
- Additional calculations using higher resolution downscaling at 100 m did not affect the exposure calculations.
- There appears to be some inconsistencies in the road transport emissions in Bucharest, as the two EMEP grids within the city centre region are significantly lower than the surrounding grids.
- The downscaling methodology applied for the pilot cities can also be applied to all of Europe, if required.

RI-URBANS (www.RIURBANS.eu) is supported by the European Commission under the Horizon 2020 – Research and Innovation Framework Programme, H2020-GD-2020, Grant Agreement number: 101036245

4 References

Adams, P.J., Seinfeld, J.H., 2002. Predicting global aerosol size distributions in general circulation models. J. Geophys. Res. 107, 4370. https://doi.org/10.1029/2001JD001010

Ayres, J. G., Borm, P., Cassee, F. R., Castranova, V., Donaldson, K., Ghio, A., Harrison, R. M., Hider, R., Kelly, F., Kooter, I. M., Marano, F., Maynard, R. L., Mudway, I., Nel, A., Sioutas, C., Smith, S., Baeza-Squiban, A., Cho, A., Duggan, S., and Froines, J.: Evaluating the Toxicity of Airborne Particulate Matter and Nanoparticles by Measuring Oxidative Stress Potential– A Workshop Report and Consensus Statement, Inhal. Toxicol., 20, 75–99, https://doi.org/10.1080/08958370701665517, 2008.

Belis, C. A., Pernigotti, D., Pirovano, G., Favez, O., Jaffrezo, J. L., Kuenen, J., Denier Van Der Gon, H., Reizer, M., Riffault, V., Alleman, L. Y., Almeida, M., Amato, F., Angyal, A., Argyropoulos, G., Bande, S., Beslic, I., Besombes, J.-L., Bove, M. C., Brotto, P., Calori, G., Cesari, D., Colombi, C., Contini, D., De Gennaro, G., Di Gilio, A., Diapouli, E., El Haddad, I., Elbern, H., Eleftheriadis, K., Ferreira, J., Vivanco, M. G., Gilardoni, S., Golly, B., Hellebust, S., Hopke, P. K., Izadmanesh, Y., Jorquera, H., Krajsek, K., Kranenburg, R., Lazzeri, P., Lenartz, F., Lucarelli, F., Maciejewska, K., Manders, A., Manousakas, M., Masiol, M., Mircea, M., Mooibroek, D., Nava, S., Oliveira, D., Paglione, M., Pandolfi, M., Perrone, M., Petralia, E., Pietrodangelo, A., Pillon, S., Pokorna, P., Prati, P., Salameh, D., Samara, C., Samek, L., Saraga, D., Sauvage, S., Schaap, M., Scotto, F., Sega, K., Siour, G., Tauler, R., Valli, G., Vecchi, R., Venturini, E., Vestenius, M., Waked, A., and Yubero, E.: Evaluation of receptor and chemical transport models for PM10 source apportionment, Atmospheric Environ. X, 5, 100053, https://doi.org/10.1016/j.aeaoa.2019.100053, 2020.

Bergström, R., Denier van der Gon, H. A. C., Prévôt, A. S. H., Yttri, K. E., and n, D.: Modelling of organic aerosols over Europe (2002–2007) using a volatility basis set (VBS) framework: application of different assumptions regarding the formation of secondary organic aerosol, Atmos. Chem. Physics, 12, 8499–8527, https://doi.org/10.5194/acp-12-8499-2012, 2012.

Brown, R. J., Beccaceci, S., Butterfield, D. M., Quincey, P. G., Harris, P. M., Maggos, T., Panteliadis, P., John, A., Jedynska, A., Kuhlbusch, T., Puteau, J.-P., & Karanasiou, A. Standardisation of a European measurement method for organic carbon and elemental carbon in ambient air: results of the field trial campaign and the determination of a measurement uncertainty and working range. Environmental Science: Processes & Impacts, 19(10), 1249-1259., 2017.

Chebaicheb, H., F. de Brito, J., Chen, G., Tison, E., Marchand, C., Prévôt, A. S. H., Favez, O., and Riffault, V.: Investigation of four-year chemical composition and organic aerosol sources of submicron particles at the ATOLL site in northern France, Environ. Pollut., 330, 121805, https://doi.org/10.1016/j.envpol.2023.121805, 2023.

Chen, G., Canonaco, F., Tobler, A., Aas, W., Alastuey, A., Allan, J., Atabakhsh, S., Aurela, M., Baltensperger, U., Bougiatioti, A., De Brito, J. F., Ceburnis, D., Chazeau, B., Chebaicheb, H., Daellenbach, K. R., Ehn, M., El Haddad, I., Eleftheriadis, K., Favez, O., Flentje, H., Font, A., Fossum, K., Freney, E., Gini, M., Green, D. C., Heikkinen, L., Herrmann, H., Kalogridis, A.-C., Keernik, H., Lhotka, R., Lin, C., Lunder, C., Maasikmets, M., Manousakas, M. I., Marchand, N., Marin, C., Marmureanu, L., Mihalopoulos, N., Močnik, G., Nęcki, J., O'Dowd, C., Ovadnevaite, J., Peter, T., Petit, J.-E., Pikridas, M., Matthew Platt, S., Pokorná, P., Poulain, L., Priestman, M., Riffault, V., Rinaldi, M., Różański, K., Schwarz, J., Sciare, J., Simon, L., Skiba, A., Slowik, J. G., Sosedova, Y., Stavroulas, I., Styszko, K., Teinemaa, E., Timonen, H., Tremper, A., Vasilescu, J., Via, M., Vodička, P., Wiedensohler, A., Zografou, O., Cruz Minguillón, M., and Prévôt, A. S. H.: European aerosol phenomenology − 8: Harmonised source apportionment of organic aerosol using 22 Year-long ACSM/AMS datasets, Environ. Int., 166, 107325, https://doi.org/10.1016/j.envint.2022.107325, 2022.

RI-URBANS (www.RIURBANS.eu) is supported by the European Commission under the Horizon 2020 – Research and Innovation Framework Programme, H2020-GD-2020, Grant Agreement number: 101036245

Cholakian, A., Beekmann, M., Colette, A., Coll, I., Siour, G., Sciare, J., Marchand, N., Couvidat, F., Pey, J., Gros, V., Sauvage, S., Michoud, V., Sellegri, K., Colomb, A., Sartelet, K., Langley DeWitt, H., Elser, M., Prévot, A. S. H., Szidat, S., and Dulac, F.: Simulation of fine organic aerosols in the western Mediterranean area during the ChArMEx 2013 summer campaign, Atmospheric Chem. Phys., 18, 7287–7312, https://doi.org/10.5194/acp-18-7287-2018, 2018.

Costabile, F., Gualtieri, M., Canepari, S., Tranfo, G., Consales, C., Grollino, M. G., Paci, E., Petralia, E., Pigini, D., and Simonetti, G.: Evidence of Association between Aerosol Properties and In-Vitro Cellular Oxidative Response to PM1, Oxidative Potential of PM2.5, a Biomarker of RNA Oxidation, and Its Dependency on Combustion Sources, Atmos. Environ., 213, 444–455, https://doi.org/10.1016/j.atmosenv.2019.06.023, 2019.

Daellenbach, K.R., Uzu, G., Jiang, J. et al. Sources of particulate-matter air pollution and its oxidative potential in Europe. Nature 587, 414–419 (2020). https://doi.org/10.1038/s41586-020-2902-8

Denier van der Gon, H., Hendriks, C., Kuenen, J., Segers, A., & Visschedijk, A. Description of current temporal emission patterns and sensitivity of predicted AQ for temporal emission patterns (EU FP7 MACC deliverable report D_D-EMIS_1.3). TNO. https://atmosphere.copernicus.eu/sites/default/files/2019-07/MACC_TNO_del_1_3_v2.pdf, 2011.

Denier van der Gon, H. A. C., Bergström, R., Fountoukis, C., Johansson, C., Pandis, S. N., Simpson, D., and Visschedijk, A. J. H.: Particulate emissions from residential wood combustion in Europe - revised estimates and an evaluation, Atmos. Chem. Physics, 15, 6503–6519, doi:10.5194/acp-15-6503-2015, URL http: //www.atmos-chem-phys.net/15/6503/2015/, 2015.

Ebel, A., Friedrich, R., & Rodhe, H. GENEMIS: Assessment, Improvement, and Temporal and Spatial Disaggregation of European Emission Data. In A. Ebel, R. Friedrich, & H. Rodhe (Éds.), Tropospheric Modelling and Emission Estimation (p. 181-214). Springer Berlin Heidelberg. https://doi.org/10.1007/978-3-662-03470-5_6, 1997.

Fountoukis, C., Riipinen, I., Denier van der Gon, H.A.C., Charalampidis, P.E., Pilinis, C., Wiedensohler, A., O'Dowd, C., Putaud, J.P., Moerman, M., Pandis, S.N., 2012. Simulating ultrafine particle formation in Europe using a regional CTM: contribution of primary emissions versus secondary formation to aerosol number concentrations. Atmos. Chem. Phys. 12, 8663–8677. https://doi.org/10.5194/acp-12-8663-2012

Gaydos, T.M., Pinder, R., Koo, B., Fahey, K.M., Yarwood, G., Pandis, S.N., 2007. Development and application of a three-dimensional aerosol chemical transport model, PMCAMx. Atmos. Environ. 41, 2594–2611. https://doi.org/10.1016/j.atmosenv.2006.11.034

Guenther, A. B., Jiang, X., Heald, C. L., Sakulyanontvittaya, T., Duhl, T., Emmons, L. K., and Wang, X.: The Model of Emissions of Gases and Aerosols from Nature version 2.1 (MEGAN2.1): an extended and updated framework for modeling biogenic emissions, Geosci. Model Dev., 5, 1471–1492, https://doi.org/10.5194/gmd-5-1471-2012, 2012.Kranenburg, R., Segers, A.J.J., Hendriks, C., Schaap, M., 2013. Source apportionment using LOTOS-EUROS: module description and evaluation. Geosci. Model Dev. 6, 721–733. https://doi.org/10.5194/gmd-6-721-2013

Hussein, T., Li, X., Bakri, Z., Alastuey, A., Arar, S., Al-Hunaiti, A., Viana, M. and Petäjä, T. Organic and Elemental Carbon in the Urban Background in an Eastern Mediterranean City. Atmosphere, 13(2), 197, https://doi.org/10.3390/atmos13020197, 2022.

INERIS & Datalystica. Deliverable 1: Report on data workflow, data treatment procedures and proof of concept for near real-time black carbon source apportionment software package applied to AE33 multi-wavelength Aethalometer datasets., Ineris-Datalystica NRT BC SA deliverable 1_CCAR 0210012, Ref.: 205200-Datalystica-D1, 2022

RI-URBANS (www.RIURBANS.eu) is supported by the European Commission under the Horizon 2020 – Research and Innovation Framework Programme, H2020-GD-2020, Grant Agreement number: 101036245

Janssen, S., Thunis, P., Adani, M., Piersanti, A., Carnevale, C., Cuvelier, C., Durka, P., Georgieva, E., Guerreiro, C., Malherbe, L., Maiheu, B., Meleux, F., Monteiro, A., Miranda, A., Olesen, H., Pfäfflin, F., Stocker, J., Sousa Santos, G., Stidworthy, A., Stortini, M., Trimpeneers, E., Viaene, P., Vitali, L., Vincent, K., Wesseling, J. FAIRMODE Guidance Document on Modelling Quality Objectives and Benchmarking, version 3.3. JRC Technical Report. 2022.

Jiang, J., Aksoyoglu, S., El-Haddad, I., Ciarelli, G., Denier van der Gon, H. A. C., Canonaco, F., Gilardoni, S., Paglione, M., Minguillón, M. C., Favez, O., Zhang, Y., Marchand, N., Hao, L., Virtanen, A., Florou, K., O'Dowd, C., Ovadnevaite, J., Baltensperger, U., and Prévôt, A. S. H.: Sources of organic aerosols in Europe: a modeling study using CAMx with modified volatility basis set scheme, Atmos. Chem. Phys., 19, 15247–15270, https://doi.org/10.5194/acp-19-15247-2019, 2019.

Jung, J., Fountoukis, C., Adams, P.J., Pandis, S.N., 2010. Simulation of in situ ultrafine particle formation in the eastern United States using PMCAMx-UF. J. Geophys. Res. 115, D03203. https://doi.org/10.1029/2009JD012313

Karydis, V.A., Tsimpidi, A.P., Pandis, S.N., 2007. Evaluation of a three-dimensional chemical transport model (PMCAMx) in the eastern United States for all four seasons. J. Geophys. Res. 112, D14211. https://doi.org/10.1029/2006JD007890

Kranenburg, R., Segers, A.J.J., Hendriks, C., Schaap, M., 2013. Source apportionment using LOTOS-EUROS: module description and evaluation. Geosci. Model Dev. 6, 721–733. https://doi.org/10.5194/gmd-6-721-2013

Loosmore, G. A.: Evaluation and development of models for resuspension of aerosols at short times after deposition, Atmos. Environ., 37, 639 –647, https://doi.org/10.1016/S1352-2310(02)00902-0, 2003.

Manders, A.M.M., Builtjes, P.J.H., Curier, L., Denier van der Gon, H.A.C., Hendriks, C., Jonkers, S., Kranenburg, R., Kuenen, J., Segers, A.J., Timmermans, R.M.A., Visschedijk, A., Wichink Kruit, R.J., Van Pul, W.A.J., Sauter, F.J., van der Swaluw, E., Swart, D.P.J., Douros, J., Eskes, H., van Meijgaard, E., van Ulft, B., van Velthoven, P., Banzhaf, S., Mues, A., Stern, R., Fu, G., Lu, S., Heemink, A., van Velzen, N., Schaap, M., 2017. Curriculum Vitae of the LOTOS-EUROS (v2.0) chemistry transport model. Geosci. Model Dev. 10, 4145–4173. https://doi.org/10.5194/gmd-10-4145-2017

May, A.A., Levin, E.J.T., Hennigan, C.J., Riipinen, I., Lee, T., Collett Jr., J.L., Jimenez, J. L., Kreidenweis, S.M., Robinson, A.L., 2013. Gas-particle partitioning of primary organic aerosol emissions: 3. biomass burning. J. Geophys. Res. (Atmospheres) 118. https://doi.org/10.1002/jgrd.50828, 11,327–11,338.

Mbengue, S., Serfozo, N., Schwarz, J., Ziková, N., Šmejkalová, A. H., & Holoubek, I. Characterization of Equivalent Black Carbon at a regional background site in Central Europe: Variability and source apportionment. Environmental Pollution, 260, 113771, https://doi.org/10.1016/j.envpol.2019.113771, 2020.

Merico, E., Cesari, D., Dinoi, A. et al. Inter-comparison of carbon content in PM_{10} and $PM_{2.5}$ measured with two thermo-optical protocols on samples collected in a Mediterranean site. Environ Sci Pollut Res 26, 29334–29350. https://doi.org/10.1007/s11356-019-06117-7, 2019.

Menut, L., Bessagnet, B., Briant, R., Cholakian, A., Couvidat, F., Mailler, S., Pennel, R., Siour, G., Tuccella, P., Turquety, S., and Valari, M.: The CHIMERE v2020r1 online chemistry-transport model, Geosci. Model Dev., 14, 6781–6811, https://doi.org/10.5194/gmd-14-6781-2021, 2021.Sauvain et al., 2008

Mu, Q., Denby, B. R., Wærsted, E. G., and Fagerli, H.: Downscaling of air pollutants in Europe using uEMEP_v6, Geosci. Model Dev., 15, 449–465, https://doi.org/10.5194/gmd-15-449-2022, 2022.

RI-URBANS (www.RIURBANS.eu) is supported by the European Commission under the Horizon 2020 – Research and Innovation Framework Programme, H2020-GD-2020, Grant Agreement number: 101036245

Napari, I., Noppel, M., Vehkamäki, H., Kulmala, M., 2002. Parametrization of ternary nucleation rates for H2O-H2SO4-NH3 vapors.

Patoulias, D., Fountoukis, C., Riipinen, I., Asmi, A., Kulmala, M., Pandis, S.N., 2018. Simulation of the size-composition distribution of atmospheric nanoparticles over Europe. Atmos. Chem. Phys. 18, 13639–13654. https://doi.org/10.5194/acp-18-13639-2018

Patoulias, D., Fountoukis, C., Riipinen, I., Pandis, S.N., 2015. The role of organic condensation on ultrafine particle growth during nucleation events. Atmos. Chem. Phys. 15, 6337–6350. https://doi.org/10.5194/acp-15-6337-2015

Patoulias, D., Pandis, S.N., 2022. Simulation of the effects of low-volatility organic compounds on aerosol number concentrations in Europe. Atmos. Chem. Phys. 22, 1689–1706. https://doi.org/10.5194/acp-22-1689-2022.

Pérez, N., Pey, J., Querol, X., Alastuey, A., López, J. M., & Viana, M. Partitioning of major and trace components in PM10–PM2. 5–PM1 at an urban site in Southern Europe. *Atmospheric Environment*, *42*(8), 1677-1691, https://doi.org/10.1016/j.atmosenv.2007.11.034, 2008.

Petit, J.-E., Favez, O., Sciare, J., Canonaco, F., Croteau, P., Močnik, G., Jayne, J., Worsnop, D., Leoz-Garziandia, E., 2014. Submicron aerosol source apportionment of wintertime pollution in Paris, France by double positive matrix factorization (PMF2) using an aerosol chemical speciation monitor (ACSM) and a multi-wavelength Aethalometer. Atmospheric Chem. Phys. 14, 13773–13787. https://doi.org/10.5194/acp-14-13773-2014.

Posner, L. N. and Pandis, S. N., 2015. Sources of ultrafine particles in the Eastern United States. Atmospheric Environment, 111, 103-112.

Robinson, A.L., Donahue, N.M., Shrivastava, M.K., Weitkamp, E.A., Sage, A.M., Grieshop, A.P., Lane, T.E., Pierce, J.R., Pandis, S.N., 2007. Rethinking organic aerosols: semivolatile emissions and photochemical aging. Science 315, 1259–1262. https://doi.org/10.1126/science.1133061.

Sandradewi, J., Prévôt, A. S., Szidat, S., Perron, N., Alfarra, M. R., Lanz, V. A., Weingartner, E. & Baltensperger, U. R. S. Using aerosol light absorption measurements for the quantitative determination of wood burning and traffic emission contributions to particulate matter. Environmental science & technology, 42(9), 3316-3323, https://doi.org/10.1021/es702253m, 2008.

Savadkoohi, M., Pandolfi, M., Reche, C., Niemi, J.V., Mooibroek, D., Titos, G., Green, D. C., Tremper, A.H., Hueglin, C., Liakakou, E., Mihalopoulos, N., Stavroulas, I., Artinano, B., Coz, E., Alados-Arboledas, L., Beddows, D., Riffault, V., De Brito, J.F., Bastian, S., Baudic, A., Colombi, C., Costabile, F., Chazeau, B., Marchand, N., Gomez-Amo, J.L., Estelles, V., Matos, V., van der Gaag, E., Gille, G., Luoma, K., Manninen, H.E., Norman, M., Silvergren, S., Petit, J.-E., Putaud, J.-P., Rattigan, O.V., Timonen, H., Tuch, T., Merkel, M., Weinhold, K., Vratolis, S., Vasilescu, J., Favez, O., Harrison, R.M., Laj, P., Wiedensohler, A., Hopke, P.K., Petaja, T., Alastuey, A., Querol, X. The variability of mass concentrations and source apportionment analysis of equivalent black carbon across urban Europe. Environ. Int. 178, 108081 https://doi.org/10.1016/j.envint.2023.108081,2023.

Simpson, D., Benedictow, A., Berge, H., öm, R., Emberson, L. D., Fagerli, H., Flechard, C. R., Hayman, G. D., Gauss, M., Jonson, J. E., Jenkin, M. E., Nyíri, A., Richter, C., Semeena, V. S., Tsyro, S., Tuovinen, J.-P., Valdebenito, Á., and Wind, P.: The EMEP MSC-W chemical transport model – technical description, Atmos. Chem. Physics, 12, 7825–7865, https://doi.org/10.5194/acp-12-7825-2012, 2012.

Simpson D, Kuenen J, Fagerli H, Heinesen D, Benedictow A, Denier van der Gon H, Visschedijk A, Klimont Z, Aas W, Lin Y, YttriKE, Paunu V (2022) Revising PM2.5 emissions from residential combustion, 2005–2019: implications

RI-URBANS (www.RIURBANS.eu) is supported by the European Commission under the Horizon 2020 – Research and Innovation Framework Programme, H2020-GD-2020, Grant Agreement number: 101036245

for air quality concentrations and trends. Nordic Council of Ministers, available from https://pub.norden.org/temanord2022-540/#108663

Timmermans, R., van Pinxteren, D., Kranenburg, R., Hendriks, C., Fomba, K. W., Herrmann, H., and Schaap, M.: Evaluation of modelled LOTOS-EUROS with observational based PM10 source attribution, Atmospheric Environment: X, 14, 100173, https://doi.org/10.1016/j.aeaoa.2022.100173, 2022.

Vestreng, V.: Review and Revision, Emission Data Reported to CLRTAP, MSC-W Status Report, Norwegian Meteorological Institute, Oslo, Norway, 2003.

Weber, S., Uzu, G., Favez, O., Borlaza, L. J. S., Calas, A., Salameh, D., Chevrier, F., Allard, J., Besombes, J.-L., Albinet, A., Pontet, S., Mesbah, B., Gille, G., Zhang, S., Pallares, C., Leoz-Garziandia, E., and Jaffrezo, J.-L.: Source apportionment of atmospheric PM10 oxidative potential: synthesis of 15 year-round urban datasets in France, Atmos. Chem. Phys., 21, 11353–11378, https://doi.org/10.5194/acp-21-11353-2021, 2021.

Wagstrom, K. M., Pandis, S. N., Yarwood, G., Wilson, G. M., & Morris, R. E. (2008). Development and application of a computationally efficient particulate matter apportionment algorithm in a three-dimensional chemical transport model. Atmospheric Environment, 42(22), 5650-5659.

Wang, Z., Couvidat, F. and Sartelet, K. Response of biogenic secondary organic aerosol formation to anthropogenic NOx emission mitigation. Submitted to Science of The Total Environment, 2024.

Weichenthal, S., Crouse, D. L., Pinault, L., Godri-Pollitt, K., Lavigne, E., Evans, G., van Donkelaar, A., Martin, R. V., and Burnett, R. T.: Oxidative Burden of Fine Particulate Air Pollution and Risk of Cause-Specific Mortality in the Canadian Census Health and Environment Cohort (CanCHEC), Environ. Res., 146, 92–99, https://doi.org/10.1016/j.envres.2015.12.013, 2016.

Wind, P., Rolstad Denby, B. and Gauss, M., Local fractions -a method for the calculation of local source contributions to air pollution, illustrated by examples using the EMEP MSC-W model rv4_33, Geoscientific Model Development, 13 (3), 1623-1634, https://doi.org/10.5194/gmd-13-1623-2020, 2020

Yus-Díez, J., Bernardoni, V., Močnik, G., Alastuey, A., Ciniglia, D., Ivančič, M., Querol, X., Perez N., Reche, C., Rigler, M., Vecchi, R., Valentini, S. & Pandolfi, M. Determination of the multiple-scattering correction factor and its cross-sensitivity to scattering and wavelength dependence for different AE33 Aethalometer filter tapes: A multi-instrumental approach. Atmospheric measurement techniques, 14(10), 6335-6355, https://doi.org/10.5194/amt-14-6335-2021, 2021.

Zhao, W., Tan, W., Zhao, G., Shen, C., Yu, Y., and Zhao, C.: Determination of equivalent black carbon mass concentration from aerosol light absorption using variable mass absorption cross section, Atmos. Meas. Tech., 14, 1319–1331, https://doi.org/10.5194/amt-14-1319-2021, 2021.

Zotter, P., Herich, H., Gysel, M., El-Haddad, I., Zhang, Y., Močnik, G., Hüglin, C., Baltensperger, U., Szidat, S., and Prévôt, A. S. H.: Evaluation of the absorption Ångström exponents for traffic and wood burning in the Aethalometer-based source apportionment using radiocarbon measurements of ambient aerosol, Atmos. Chem. Phys., 17, 4229–4249, https://doi.org/10.5194/acp-17-4229-2017, 2017.

RI-URBANS (www.RIURBANS.eu) is supported by the European Commission under the Horizon 2020 – Research and Innovation Framework Programme, H2020-GD-2020, Grant Agreement number: 101036245

5 Annex 1: Factsheet of CHIMERE simulations for the Organic Aerosol Model/Observation evaluation

Years simulated: 2017 and 2019

Emissions: CAMS-REG-AP v4.2 for year 2017 REF2.1 and REG-AP_v5_1_REF2.1 for year 2018

Speciation PM: corresponding split providing with CAMS-REG

Meteo: IFS

Short description of the model

Describe the configuration of the model and all generalities that can be useful for the comprehension of results (including information on the particle physics, biogenic emissions)

3-D simulations are conducted using the CHIMERE model (Menut et al., 2021), which is coupled to the aerosol model SSH-aerosol v1.3 (Sartelet et al., 2020) through a splitting approach: the model first solves processes related to transport, deposition, and emissions. Subsequently, it calculates the evolution of gas-phase concentrations resulting from chemical reactions. As a final step, CHIMERE launches SSH-aerosol to solve processes related to aerosol dynamics, such as condensation/evaporation of semi-volatile compounds and coagulation.

Within SSH-aerosol, gas-particle partitioning is computed using the thermodynamic module ISORROPIA (Nenes et al., 1998) for inorganic aerosols and SOAP (Couvidat and Sartelet, 2015) for organic aerosols. In SOAP, interactions between organic and inorganic compounds are estimated based on the molecular structure of the molecules, considering the non-ideality of aerosols.

In this study, thermodynamic equilibrium is assumed for gas-particle partitioning. For particle size discretization, a sectional approach with ten sections is employed, encompassing diameters ranging from 10 nm to 10 µm.

Biogenic emissions are computed with the MEGAN 2.1 algorithm (Guenther et al., 2012), which is implemented in CHIMERE. It uses meteorological conditions (temperature, solar radiation and soil moisture), the leaf area index and the plant functional type (PFT) to compute biogenic emissions. In this study, the above-canopy model is used. The effects of soil moisture on isoprene emissions are not considered because no wilting point (i.e., the soil moisture level below which plants cannot extract water from soil) database is available over Europe. Therefore, isoprene emissions may be overestimated during dry periods. High spatiotemporal data (30 arcsec every 8 days) generated from MODIS (Yuan et al., 2011) are used for LAI inputs. The 30 arcsec USGS (US Geophysical Survey) land-use database is used to provide information on the plant functional type. The PFT is then combined with the emission factors for each functional type of Guenther et al. (2012) to compute the landscape average emission factors

Description of the SOA mechanism

Provide all necessary information on SOA formation: precursors, inclusion of IVOC, treatment of POA as SVOC, aging mechanism

Accounted biogenic SOA precursor: Isoprene, monoterpenes (alpha-pinene, beta-pinene, limonene) and sesquiterpenes.

Accounted anthropogenic SOA precursor: Aromatics (Toluene, Xylene, Trimethylbenzene), PAH (Naphthalene), phenolic compounds from residential wood burning. IVOC are not considered.

The SOA mechanism of Wang et al. (2024) was used. This mechanism was obtained by using the GENOA v2.0 algorithm (Wang et al., 2022, 2023) reducing the SOA mechanism for monoterpenes and sesquiterpenes of the

RI-URBANS (www.RIURBANS.eu) is supported by the European Commission under the Horizon 2020 – Research and Innovation Framework Programme, H2020-GD-2020, Grant Agreement number: 101036245

Master Chemical Mechanism (Saunders et al., 2003) coupled with PRAM (to account for SOA formation from monoterpenes by auto-oxidation) (Roldin et al., 2019). Following Wang et al. (in prep), the Hydrophilic/Hydrophobic Organics (Chrit et al., 2017) mechanism was used for other precursors.

Following Couvidat et al. (2018), primary organic aerosols are assumed to be semi-volatile compounds: the model assumed that the compounds exist in both the gas and particle phases, the gas-particle partitioning being calculated as a function of their thermodynamic properties. Primary organic aerosols from biomass burning (BOA) and primary organic aerosols from other sources (POA) are split into different compounds.

POA are split as described by Couvidat et al. (2012), three compounds: POAlP (Kp = 1.1 m^3 μg^{-1}), POAmP (Kp = 0.0116 m^3 μg^{-1}) and POAhP (Kp = 0.00031 m^3 μg^{-1}) having respectively a low, medium and high volatility to follow the dilution curve of POA in Robinson et al. (2007).

Similarly, BOA is split into three compounds: BOAlP (Kp = 18.3 m^3 μg^{-1}), BOAmP (Kp = 0.04 m^3 μg^{-1}) and BOAhP (Kp = 0.00023 m^3 μg^{-1}) having respectively a low, medium and high volatility to follow the dilution curve of BOA in May et al. (2013).

The aging of these compounds is also considered with a reaction with OH which leads to less volatile compounds (SOAlP, SOAmP and SOAhP, BSOAlP, BOAmP, BSOAhP) via the following reactions: POAlP + OH→ SOAlP

POAmP + OH→ SOAmP

POAhP + OH→ SOAhP

BOAlP + OH→ BSOAlP

BOAmP + OH→ BSOAmP

BOAhP + OH→ BSOAhP

A kinetic of aging of 2×10^{-11} $molecules^{-1}$ cm^3 s^{-1} is used. The aging step is assumed to lead to a decrease of volatility by a factor 100.

Correspondence to PMF

BBOA: all primary SVOC from biomass burning (not aged)

HOA: all primary SVOC from other sources (not aged)

OOA: all SOA compounds + aged POA species

COA: no emissions included (cannot be match to PMF)

5.1 References

Boylan J.W, Russell A.G., PM and light extinction model performance metrics, goals, and criteria for three-dimensional air quality models, Atmos. Env., 40, 26, 4946-4959, 2006, https://doi.org/10.1016/j.atmosenv.2005.09.087.

Chrit, M., Sartelet, K., Sciare, J., Pey, J., Marchand, N., Couvidat, F., Sellegri, K., and Beekmann, M. (2017). Modelling organic aerosol concentrations and properties during ChArMEx summer campaigns of 2012 and 2013 in the western Mediterranean region. Atmos. Chem. Phys., 17:12509–12531

RI-URBANS (www.RIURBANS.eu) is supported by the European Commission under the Horizon 2020 – Research and Innovation Framework Programme, H2020-GD-2020, Grant Agreement number: 101036245

Couvidat, F., Debry, E., ´ Sartelet, K., Seigneur, C., 2012. A Hydrophilic/Hydrophobic Organic (H2 O) model: model development, evaluation and sensitivity analysis. J. Geophys. Res. 117, D10304. https://doi.org/10.1029/2011JD017214.

Couvidat, F., Sartelet, K., 2015. The Secondary Organic Aerosol Processor (SOAP v1. 0) model: a unified model with different ranges of complexity based on the molecular surrogate approach. Geosci. Model Dev 8, 1111–1138.

Couvidat, F., Bessagnet, B., Garcia-Vivanco, M., Real, E., Menut, L., Colette, A., 2018. Development of an inorganic and organic aerosol model (chimere 2017β v1.0): seasonal and spatial evaluation over europe. Geosci. Model Dev. 11, 165–194. https://doi.org/10.5194/gmd-11-165-2018

Guenther, A. B., Jiang, X., Heald, C. L., Sakulyanontvittaya, T., Duhl, T., Emmons, L. K., and Wang, X.: The Model of Emissions of Gases and Aerosols from Nature version 2.1 (MEGAN2.1): an extended and updated framework for modeling biogenic emissions, Geosci. Model Dev., 5, 1471–1492, https://doi.org/10.5194/gmd-5-1471-2012, 2012.

Kim, Y., Lugon, L., Maison, A., Sarica, T., Roustan, Y., Valari, M., Zhang, Y., André, M., and Sartelet, K.: MUNICH v2.0: a street-network model coupled with SSH-aerosol (v1.2) for multi-pollutant modelling, Geosci. Model Dev., 15, 7371–7396, https://doi.org/10.5194/gmd-15-7371-2022, 2022.

Lugon L, Sartelet K, Kim Y, Vigneron J, Chrétien O: Simulations of primary and secondary particles in the streets of Paris using MUNICH. Faraday Discussions, http://dx.doi.org/10.1039/D0FD00092B, 2021.

May, A.A., Levin, E.J.T., Hennigan, C.J., Riipinen, I., Lee, T., Collett Jr., J.L., Jimenez, J. L., Kreidenweis, S.M., Robinson, A.L., 2013. Gas-particle partitioning of primary organic aerosol emissions: 3. biomass burning. J. Geophys. Res. (Atmospheres) 118. https://doi.org/10.1002/jgrd.50828, 11,327–11,338.

Menut, L., Bessagnet, B., Briant, R., Cholakian, A., Couvidat, F., Mailler, S., Pennel, R., Siour, G., Tuccella, P., Turquety, S., Valari, M., 2021. The CHIMERE v2020r1 online chemistry-transport model. Geoscientific Model Development 14, 6781–6811.

Nenes, A., Pandis, S.N., Pilinis, C., 1998. ISORROPIA: A new thermodynamic equilibrium model for multiphase multicomponent inorganic aerosols. Aquat. Geochem. 4, 123–152.

Robinson, A.L., Donahue, N.M., Shrivastava, M.K., Weitkamp, E.A., Sage, A.M., Grieshop, A.P., Lane, T.E., Pierce, J.R., Pandis, S.N., 2007. Rethinking organic aerosols: semivolatile emissions and photochemical aging. Science 315, 1259–1262. https://doi.org/10.1126/science.1133061.

Sartelet K., Couvidat F., Wang Z., Flageul C., Kim Y. (2020), SSH-Aerosol v1.1: A Modular Box Model to Simulate the Evolution of Primary and Secondary Aerosols. Atmosphere, 2020, 11, 525, https://doi.org/10.3390/atmos11050525.

Sartelet, K., Kim, Y., Couvidat, F., Merkel, M., Petäjä T., Sciare J. and Wiedensohler, A. (2022), Influence of emission size distribution and nucleation on number concentrations over Greater Paris. Atmos. Chem. Phys., 22, 8579-8596, https://doi.org/10.5194/acp-22-8579-2022.

Savadhooki Savadkoohi, M., Pandolfi, M., Reche, C., Niemi, J., Mooibroek, D., Titos, G., Green, D., Tremper, A., Hueglin, C., Liakakou, E., Mihalopoulos, N., Stavroulas, I., Artiñano, B., Coz, E., Alados-Arboledas, L., Beddows, D., Riffault, V., Brito, J., Bastian, S., Baudic, A., Colombi, C., Costabile, F., Chazeau, B., Marchand, N., Gómez-Amo, J., Estellés, V., Matos, V., Gaag, E., Gille, G., Luoma, K., Manninen, H., Norman, M., Silvergren, S., Petit, J., Putaud, J., Rattigan, O., Timonen, H., Tuch, T., Merkel, M., Weinhold, K., Vratolis, S., Vasilescu, J., Favez, O., Harrison, R., Laj, P., Wiedensohler, A., Hopke, P., Petäjä, T., Alastuey, A., and Querol, X. The variability of mass concentrations

RI-URBANS (www.RIURBANS.eu) is supported by the European Commission under the Horizon 2020 – Research and Innovation Framework Programme, H2020-GD-2020, Grant Agreement number: 101036245

and source apportionment analysis of equivalent black carbon across urban europe. Environ. Int., 178:108081, 2023

Saunders, S. M., Jenkin, M. E., Derwent, R. G., and Pilling, M. J.: Protocol for the development of the Master Chemical Mechanism, MCM v3 (Part A): tropospheric degradation of non-aromatic volatile organic compounds, Atmos. Chem. Phys., 3, 161–180, https://doi.org/10.5194/acp-3-161-2003, 2003.

Wang, Z., Couvidat, F., and Sartelet, K.: GENerator of reduced Organic Aerosol mechanism (GENOA v1.0): an automatic generation tool of semi-explicit mechanisms, Geosci. Model Dev., 15, 8957–8982, https://doi.org/10.5194/gmd-15-8957-2022, 2022.

Wang, Zhizhao and Couvidat, Florian and Sartelet, Karine, Implementation of a Parallel Reduction Algorithm in the Generator of Reduced Organic Aerosol Mechanisms (Genoa V2.0): Application to Multiple Monoterpene Aerosol Precursors. Available at SSRN: https://ssrn.com/abstract=4431972 or http://dx.doi.org/10.2139/ssrn.4431972

Wang, Z., Couvidat, F. and Sartelet, K. Response of biogenic secondary organic aerosol formation to anthropogenic NOx emission mitigation. Submitted to Science of The Total Environment, 2024.

Yuan, H., Dai, Y., Xiao, Z., Ji, D., and Shangguan, W.: Reprocessing the MODIS leaf area index products for land surface and climate modelling, Remote Sensing Environ., 155, 1171–1187, https://doi.org/10.1016/j.rse.2011.01.001, 2011.

RI-URBANS (www.RIURBANS.eu) is supported by the European Commission under the Horizon 2020 – Research and Innovation Framework Programme, H2020-GD-2020, Grant Agreement number: 101036245

6 Annex 2: Factsheet of CAMx simulations for the Organic Aerosol Model/Observation evaluation

Years simulated: 2017, 2019

Emissions: TNO-MACC-II for both years

Speciation PM: TNO split/PSI VBS split

Meteo: WRF 3.7

Short description of the model

Describe the configuration of the model and all generalities that can be useful for the comprehension of results (including information on the particle physics, biogenic emissions)

The regional air quality model CAMx version 6.50 with an updated VBS (volatility basis set) scheme based on Jiang et al., 2019 was used. The model domain (15◦ W–35◦ E, 35◦–70◦ N) covered Europe with a horizontal resolution of 0.25◦ × 0.125◦. The meteorological inputs were prepared by the Weather Research and Forecasting Model Advanced Research (WRF-ARW) version 3.7.1 (NCAR, 2016; Skamarock et al., 2008). We used the ECMWF (European Centre for Medium-Range Weather Forecasts) global atmospheric reanalysis ERA-Interim data as initial and boundary conditions for the WRF model, with a spatial resolution of 0.72◦×0.72◦ and a time step of 6 h. The Carbon Bond 6 Revision 2 (CB6r2) mechanism (Hildebrandt Ruiz and Yarwood, 2013) was used for the gas phase chemistry. Aqueous sulfate and nitrate formation in resolved cloud water was simulated by the Regional Acid Deposition Model (RADM) algorithm (Chang et al., 1987). Partitioning of inorganic aerosol components between the gas and particle phases was calculated by the ISORROPIA thermodynamic model (Nenes et al., 1998). The gridded initial concentrations of chemical species in each layer of the model domain as well as at the domain lateral boundaries were obtained from the global model data MOZART-4/GEOS-5 (Horowitz et al., 2003) with a time resolution of 6 h. Anthropogenic emissions of non-methane volatile organic compounds (NMVOCs), SO_2, NO_x, CO, NH_3, PM10, and PM2.5 were obtained from the high-resolution European emission inventory TNO-MACC (The Netherlands Organization for Applied Scientific Research - Monitoring Atmospheric Composition and Climate)-III. As an update to TNO-MACC-II (Kuenen et al., 2014), TNO-MACC-III has a major improvement in spatial distribution proxies, especially for urban areas (van Der Gon, 2015). The NMVOC speciation was conducted following the approach described by Passant (2002). The PM emissions were further split into organic carbon, elemental carbon, sodium, sulphate, and crustal minerals, based on country specific profiles provided by TNO. Biogenic emissions (isoprene, monoterpenes, sesquiterpenes, soil NO) were calculated using the in-house PSI biogenic module (Andreani-Aksoyoglu and Keller, 1995) and further improved by Oderbolz et al. (2013) and Jiang et al. (2019). A comparison study with the widely used biogenic Model of Emissions of Gases and Aerosols from Nature (MEGAN) version 2.1 indicated that the PSI model produces higher monoterpene emissions in Europe than MEGAN and leads to a better performance of CAMx for OA (Jiang et al., 2019).

Description of the SOA mechanism

Provide all necessary information on SOA formation: precursors, inclusion of IVOC, treatment of POA as SVOC, aging mechanism

Organic aerosol formation from anthropogenic (including both land and ships) and biogenic (terrestrial) sources was modelled with a modified 1.5- D VBS organic aerosol chemistry and partitioning module (Jiang et al., 2019), which describes the evolution of OA in the 2-D space of oxidation state and volatility. This is a modified parameterization based on smog chamber experimental studies. Major changes were made for diesel vehicles and biomass burning. Diesel vehicles constitute nearly half of the total passenger car registrations in Europe (ACEA, 2017). While the standard VBS of CAMx disables the aging of SOA for the basis set PBS (biomass burning and

RI-URBANS (www.RIURBANS.eu) is supported by the European Commission under the Horizon 2020 – Research and Innovation Framework Programme, H2020-GD-2020, Grant Agreement number: 101036245

biogenic sources) to avoid overestimation of biogenic SOA, the separated sets for biomass burning (BB) and biogenic (BIO) allow us to implement individual parameterization schemes. Therefore, the default parameterization is kept (without aging of SOA) for BIO sources as a compromise for the lack of gas-phase fragmentation, and enabled the oxidation of secondary gases from biomass burning (see BB in Fig. 1) with a reaction rate of $4\times10-11$ cm^3 $molec.^{-1}$ s^{-1} according to previous studies (Ciarelli et al., 2017a, b). A more detailed description can be found at Jiang et al. 2019.

Correspondance to PMF

BBOA: All POA from biomass burning

HOA: All POA from road traffic and other anthropogenic sources

OOA: Sum of all anthropogenic and biogenic SOA

Total OA: Sum of all the above

6.1 References

Jiang, J., Aksoyoglu, S., El-Haddad, I., Ciarelli, G., Denier van der Gon, H. A. C., Canonaco, F., Gilardoni, S., Paglione, M., Minguillón, M. C., Favez, O., Zhang, Y., Marchand, N., Hao, L., Virtanen, A., Florou, K., O'Dowd, C., Ovadnevaite, J., Baltensperger, U., and Prévôt, A. S. H.: Sources of organic aerosols in Europe: a modeling study using CAMx with modified volatility basis set scheme, Atmos. Chem. Phys., 19, 15247–15270, https://doi.org/10.5194/acp-19-15247-2019, 2019.

Skamarock, W. C., Klemp, J. B., Dudhia, J., Gill, D. O., Barker, D. M., Duda, M. G., Huang, X.-Y., Wang, W., and Powers, J. G.: A Description of the Advanced Research WRF Version 3, Mesoscale and Microscale Meteorology Division, National Center for Atmospheric Research, Boulder, Colorado, USA, 2008.

Hildebrandt Ruiz, L. and Yarwood, G.: Interactions between organic aerosol and NOy: Influence on oxidant production., University of Texas at Austin, and ENVIRON International Corporation, Novato, CA, 2013.

Chang, J. S., Brost, R. A., Isaksen, I. S. A., Madronich, S., Middleton, P., Stockwell, W. R., and Walcek, C. J.: A 3-dimensional Eulerian acid deposition model – physical concepts and formulation, J. Geophys. Res.-Atmos., 92, 14681–14700, https://doi.org/10.1029/JD092iD12p14681, 1987

Nenes, A., Pandis, S. N., and Pilinis, C.: ISORROPIA: A new thermodynamic equilibrium model for multiphase multicomponent inorganic aerosols, Aquat. Geochem., 4, 123–152, https://doi.org/10.1023/a:1009604003981, 1998.

Horowitz, L. W., Walters, S., Mauzerall, D. L., Emmons, L. K., Rasch, P. J., Granier, C., Tie, X. X., Lamarque, J. F., Schultz, M. G., Tyndall, G. S., Orlando, J. J., and Brasseur, G. P.: A global simulation of tropospheric ozone and related tracers: Description and evaluation of MOZART, version 2, J. Geophys. Res.-Atmos, 108, 4784, https://doi.org/10.1029/2002jd002853, 2003.

Kuenen, J. J. P., Visschedijk, A. J. H., Jozwicka, M., and Denier van der Gon, H. A. C.: TNO-MACC_II emission inventory; a multi-year (2003–2009) consistent high-resolution European emission inventory for air quality modelling, Atmos. Chem. Phys., 14, 10963–10976, https://doi.org/10.5194/acp-14-10963-2014, 2014.

Denier van der Gon, H. A. C., Bergström, R., Fountoukis, C., Johansson, C., Pandis, S. N., Simpson, D., and Visschedijk, A. J. H.: Particulate emissions from residential wood combustion in Europe – revised estimates and an evaluation, Atmos. Chem. Phys., 15, 6503–6519, https://doi.org/10.5194/acp-15-6503-2015, 2015.

RI-URBANS (www.RIURBANS.eu) is supported by the European Commission under the Horizon 2020 – Research and Innovation Framework Programme, H2020-GD-2020, Grant Agreement number: 101036245

Passant, N. R.: Speciation of UK emissions of non-methane volatile organic compounds, AEA Technology, Culham, Abingdon, Oxon, UK, 2002.

Andreani-Aksoyoglu, S. and Keller, J.: Estimates of monoterpene and isoprene emissions from the forests in switzerland, J. Atmos. Chem., 20, 71–87, https://doi.org/10.1007/bf01099919, 1995.

Jiang, J., Aksoyoglu, S., Ciarelli, G., Oikonomakis, E., El-Haddad, I., Canonaco, F., O'Dowd, C., Ovadnevaite, J., Minguillón, M. C., Baltensperger, U., and Prévôt, A. S. H.: Effects of two different biogenic emission models on modelled ozone and aerosol concentrations in Europe, Atmos. Chem. Phys., 19, 3747–3768, https://doi.org/10.5194/acp-19-3747-2019, 2019.

Oderbolz, D. C., Aksoyoglu, S., Keller, J., Barmpadimos, I., Steinbrecher, R., Skjøth, C. A., Plaß-Dülmer, C., and Prévôt, A. S. H.: A comprehensive emission inventory of biogenic volatile organic compounds in Europe: improved seasonality and land-cover, Atmos. Chem. Phys., 13, 1689–1712, https://doi.org/10.5194/acp-13-1689-2013, 2013.

RI-URBANS (www.RIURBANS.eu) is supported by the European Commission under the Horizon 2020 – Research and Innovation Framework Programme, H2020-GD-2020, Grant Agreement number: 101036245

7 Annex 3: Factsheet of EMEP simulations for the Organic Aerosol Model/Observation evaluation

Years simulated: 2018, 2019

Emissions: EMEP/CEIP 2023 update for 2018, 2019 (incl. REF2.1 emis for countries without condensables)

Speciation PM: Detailed CAMEO CAMS-REG_v6_1_for_CAMEO_v1 for year 2019

Meteo: IFS (MSC-W version)

Short description of the model

Describe the configuration of the model and all generalities that can be useful for the comprehension of results (including information on the particle physics, biogenic emissions)

3-D simulations are conducted using the EMEP MSC-W model v5.1 (Simpson et al., 2012, 2023 and refs therein, van Caspel et al., 2023), which includes the EmChem19c gas-phase chemical mechanism (Simpson et al., 2020, 2023, Bergström et al., 2020), and a VBS approach for organic aerosols (below). For particle size discretization we assume one fine mode (<2.5μm) and one coarse mode (2.5-10μm). Thermodynamic equilibrium is assumed for gas-particle partitioning for fine-mode particles, calculated here using the default MARS solver (Saxena et al., 1986, Binkowski and Shankar, 1995), though Isorropia-lite (Nenes et al., 2002, Kakavas et al. 2022) and EQSAM4clim (Metzger et al., 2018) are also available (tests show little difference between the schemes). Explicit losses of gases onto coarse aerosol are also considered (Stadtler et al., 2018, Simpson et al., 2018).

Biogenic emissions are computed with the EMEP system, which aggregates emission potentials (EPs) from 115 forest species (Simpson et al., 1999, 2012) into 4 forest plant functional types (PFTs), and assigns EPs to several low-vegetation PFTs. The system uses meteorological conditions (temperature, solar radiation), the PFT-specific leaf area index, and the Guenther et al. (1993, 1995) functions to compute biogenic emissions every model time-step. Emissions are given of isoprene, monoterpenes (aggregated to the surrogate compound apinene) and also a sesquiterpene compound.

Description of the SOA mechanism

Provide all necessary information on SOA formation: precursors, inclusion of IVOC, treatment of POA as SVOC, aging mechanism

Accounted biogenic SOA precursors: isoprene, monoterpenes (here as a-pinene) and sesquiterpenes.

Accounted anthropogenic SOA precursors: aromatics (benzene, toluene, o-xylene (as surrogate for remaining aromatics), n-C4H10 (as surrogate for heavier alkanes), and C3H6 (as surrogate for alkenes).

SOA: The SOA mechanism is based upon the work of Bergström et al. (2012), with SOA yields in the VBS from Lane et al. (2008) and Tsimpidi et al. (2010). SOA species are formed and react in a VBS bin system $\log_{10}(C^*)$ values ranging from 0.01 to 1000 μg/m^3). Aging reactions are also applied: upon reaction with OH SOA compounds in bin N are moved to bin N-1 with lower volatilty, and a 7.5% mass increase is applied to account for increasing O/C ratios. The rate coefficient for the aging in 4.0e-12 is from Lane et al. (2008).

POA: Although previous studies with the EMEP model have used both semi- and intermediate-volatile VOC for POA emissions (Denier van der Gon, 2015, Simpson et al, 2009, 2022) the resulting OA mass tends to be very close to that achieved with a simple assumption of non-volatile POA, since the initial evaporation of POA is counteracted by rapid oxidation and condensation of formed SOA (Simpson et al, 2012, 2022). It can be noted that similar findings were presented in the first large scale demonstration of the VBS system by Robinson et al. (2007). Given that all

RI-URBANS (www.RIURBANS.eu) is supported by the European Commission under the Horizon 2020 – Research and Innovation Framework Programme, H2020-GD-2020, Grant Agreement number: 101036245

assumptions concerning volatility of POA are very uncertain (Simpson et al., 2020), our default modelling uses the non-volatile POA ("NVPOA") approach. In this exercise, we have made use of the extra emissions detail available through the CAMS-REG_v6_1_for_CAMEO_v1 files provided by TNO, and have tracked POA from road transport GNFR-F (POA_F), biomass residential GNFR-C (POA_Cb), fossil fuel GNFR C (POA_Cf), agricultural sources GNFR K, L (POA_ag), forest fires (POA_ff), and remaining POA (POA_rem). For PMF below we include POA_ff in the OOA category, since plumes are usually highly oxidised, and POA_ff displays very different space and time variation to the BBOA factor from PMF analysis.

BGND: The EMEP model assumes a constant background OM level of 0.4 μg/m^3. This OM_BGND is intended to account for sources of OM which are not accounted for in our emission system, such as primary biological aerosols, marine aerosols, and for European-scale modelling also the aerosol associated with transport for outside the domain.

Correspondence to PMF

BBOA: all POA from residential biomass burning

HOA: all POA from other sources except forest fires + 0.5 OM_bgnd

OOA: all SOA compounds + POA_ff + 0.5 OM_bgnd

COA: not included (no cooking emissions available)

7.1 References

Bergström, R., Denier van der Gon, H. A. C., Prévôt, A. S. H., Yttri, K. E., and n, D.: Modelling of organic aerosols over Europe (2002–2007) using a volatility basis set (VBS) framework: application of different assumptions regarding the formation of secondary organic aerosol, Atmos. Chem. Physics, 12, 8499–8527, https://doi.org/10.5194/acp-12-8499-2012, 2012.

Bergström, R., Hayman, G. D., Jenkin, M. E., and Simpson, D.: Update and comparison of atmospheric chemistry mechanisms for the EMEP MSC-W model system — EmChem19a, EmChem19X, CRIv2R5Em, CB6r2Em, and MCMv3.3Em, The Norwegian Meteorological Institute, Oslo, Norway, 1 pp., 2022.

Binkowski, F. and Shankar, U.: The Regional Particulate Matter Model .1. Model description and preliminary results, J. Geophys. Res., 100, 26191–26209, 1995.

van Caspel, W. E., Simpson, D., Jonson, J. E., Benedictow, A. M. K., Ge, Y., di Sarra, A., Pace, G., Vieno, M., Walker, H., and Heal, M.: Implementation and evaluation of updated photolysis rates in the EMEP MSC-W chemical transport model using Cloud-J v7.3e, Geoscientific Model Dev., 2023, 7433–7459, https://doi.org/10.5194/gmd-16-7433-2023, 2023.

Denier van der Gon, H. A. C., öm, R., Fountoukis, C., Johansson, C., Pandis, S. N., n, D., and Visschedijk, A. J. H.: Particulate emissions from residential wood combustion in Europe - revised estimates and an evaluation, Atmos. Chem. Physics, 15, 6503–6519, https://doi.org/10.5194/acp-15-6503-2015, 2015.

Guenther, A. B., Zimmerman, P. R., Harley, P. C., Monson, R. K., and Fall, R.: Isoprene and monoterpene rate variability: model evaluations and sensitivity analyses, J. Geophys. Res., 98, 12609–12617, 1993.

Guenther, A., Hewitt, C. N., Erickson, D., Fall, R., Geron, C., Graedel, T., Harley, P., Klinger, L., Lerdau, M., McKay, W. A., Pierce, T., Scholes, R., Steinbrecher, R., Tallamraju, R., Taylor, J., and Zimmerman, P.: A global model of natural volatile organic compound emissions, J. Geophys. Res., 100, 8873–8892, https://doi.org/10.1029/94JD02950, 1995.

RI-URBANS (www.RIURBANS.eu) is supported by the European Commission under the Horizon 2020 – Research and Innovation Framework Programme, H2020-GD-2020, Grant Agreement number: 101036245

Lane, T. E., Donahue, N. M., and Pandis, S. N.: Simulating secondary organic aerosol formation using the volatility basis-set approach in a chemical transport model, Atmos. Environ., 42, 7439–7451, https://doi.org/10.1016/j.atmosenv.2008.06.026, 2008.

Metzger, S., Abdelkader, M., Steil, B., and Klingmüller, K.: Aerosol water parameterization: long-term evaluation and importance for climate studies, Atmos. Chem. Physics, 18, 16747–16774, https://doi.org/10.5194/acp-18-16747-2018, 2018.

Nenes, A., Pandis, S.N., Pilinis, C., 1998. ISORROPIA: A new thermodynamic equilibrium model for multiphase multicomponent inorganic aerosols. Aquat. Geochem. 4, 123–152.

Kakavas, S., Pandis, S. N., and Nenes, A.: ISORROPIA-Lite: A Comprehensive Atmospheric Aerosol Thermodynamics Module for Earth System Models, Tellus B: Chemical and Physical Meteorology, 74, 1–23, https://doi.org/10.16993/tellusb.33, 2022.

Robinson, A.L., Donahue, N.M., Shrivastava, M.K., Weitkamp, E.A., Sage, A.M., Grieshop, A.P., Lane, T.E., Pierce, J.R., Pandis, S.N., 2007. Rethinking organic aerosols: semivolatile emissions and photochemical aging. Science 315, 1259–1262. https://doi.org/10.1126/science.1133061.

Saxena, P., Hudischewskyj, A. B., Seigneur, C., and Seinfeld, J. H.: A comparative study of equilibrium approaches to the chemical characterization of secondary aerosols, Atmospheric Environment (1967), 20, 1471–1483, https://doi.org/10.1016/0004-6981(86)90019-3, 1986.

Simpson, D., Winiwarter, W., Börjesson, G., Cinderby, S., Ferreiro, A., Guenther, A., Hewitt, C. N., Janson, R., Khalil, M. A. K., Owen, S., Pierce, T. E., Puxbaum, H., Shearer, M., Skiba, U., Steinbrecher, R., Tarrasón, L., and Öquist, M. G.: Inventorying emissions from Nature in Europe, J. Geophys. Res., 104, 8113–8152, 1999.

Simpson, D., Yttri, K. E., Bergström, R., and van der Gon, H.: Modelling SOA in EMEP: Experiments with the VBS Approach, in: Transboundary Particulate Matter in Europe, Status Report 4/2004, edited by: Tørseth, K., The Norwegian Institute for Air Research (NILU), Kjeller, Norway, 2009.

Simpson, D., Benedictow, A., Berge, H., öm, R., Emberson, L. D., Fagerli, H., Flechard, C. R., Hayman, G. D., Gauss, M., Jonson, J. E., Jenkin, M. E., Nyíri, A., Richter, C., Semeena, V. S., Tsyro, S., Tuovinen, J.-P., Valdebenito, Á., and Wind, P.: The EMEP MSC-W chemical transport model – technical description, Atmos. Chem. Physics, 12, 7825–7865, https://doi.org/10.5194/acp-12-7825-2012, 2012.

Simpson, D., Bergström, R., Briolat, A., Imhof, H., Johansson, J., Priestley, M., and Valdebenito, A.: v1.0 – a chemical pre-processing and testing system for atmospheric modelling, Geoscientific Model Dev., 13, 6447–6465, https://doi.org/10.5194/gmd-13-6447-2020, 2020.

Simpson, D., Fagerli, H., Colette, A., et al., How should condensables be included in PM emission inventories reported to EMEP/CLRTAP? Report of the expert workshop on condensable organics organised by MSC-W, Gothenburg, 17-19th March 2020, Norwegian Meteorological Institute, Technical Report 4/2020 (available at www.emep.int), 72 pp., 2020.

Simpson, D., Kuenen, J., Fagerli, H., Heinesen, D., Benedictow, A., van der Gon, H. D., Visschedijk, A., Klimont, Z., Aas, W., Lin, Y., Yttri, K. E., and Paunu, V.-V.: Revising PM_(2.5) emissions from residential combustion, 2005–2019. Implications for air quality concentrations and trends., Nordic Council of Ministers, https://doi.org/10.6027/temanord2022-540, 2022.

Simpson, D., van Caspel, W., Benedictow, A., Fagerli, H., Jonson, J. E., Tsyro, S., Valdebento, A., and Wind, P.: Updates to the EMEP/MSC-W model, 2022–2023, in: Transboundary particulate matter, photo-oxidants,

RI-URBANS (www.RIURBANS.eu) is supported by the European Commission under the Horizon 2020 – Research and Innovation Framework Programme, H2020-GD-2020, Grant Agreement number: 101036245

acidifying and eutrophying components. EMEP Status Report 1/2023, The Norwegian Meteorological Institute, Oslo, Norway, 159–179, 2023.

Stadtler, S., Simpson, D., Schröder, S., Taraborrelli, D., Bott, A., and Schultz, M.: Ozone impacts of gas–aerosol uptake in global chemistry-transport models, Atmos. Chem. Physics, 18, 3147–3171, https://doi.org/10.5194/acp-18-3147-2018, 2018.

Tsimpidi, A. P., Karydis, V. A., Zavala, M., Lei, W., Molina, L., Ulbrich, I. M., Jimenez, J. L., and Pandis, S. N.: Evaluation of the volatility basis-set approach for the simulation of organic aerosol formation in the Mexico City metropolitan area, Atmos. Chem. Physics, 10, 525–546, 2010.

RI-URBANS (www.RIURBANS.eu) is supported by the European Commission under the Horizon 2020 – Research and Innovation Framework Programme, H2020-GD-2020, Grant Agreement number: 101036245

8 Annex 4: Factsheet of LOTOS-EUROS simulations for the Organic Aerosol Model/Observation evaluation

Years simulated: 2019

Emissions: CAMS-REG-AP v6.1 REF2.1 for year 2019

Speciation PM: CAMS split CAMS-REG-AP v6.1 REF2.1 for year 2019

Time profiles: CAMS TEMPO

Domain: CAMS domain @ 0.2 deg. longitude x 0.1 deg. latitude

Meteo: IFS

Short description of the model

Describe the configuration of the model and all generalities that can be useful for the comprehension of results (including information on the particle physics, biogenic emissions)

LOTOS-EUROS is an open-source 3D CTM that simulates the processes of emission, concentration and deposition of chemical substances in the lower troposphere. The model was developed at TNO in collaboration with partners such as RIVM and the Free University of Berlin. The model is widely used, both in scientific research and for regulatory assessments, for example, air quality forecasts or scenario calculations in climate studies. The model is part of the regional ensemble Copernicus Atmospheric Monitoring Service (CAMS), which provides operational forecasts and analyses for the whole of Europe. In this context, the model is regularly updated and validated using data from ground and satellite observations. For a detailed description of the LOTOS-EUROS model, its history and applications, we refer to Manders et al. (2017) and references given therein.

Natural emissions are required to correctly describe the ozone and oxidant formation in the gas phase chemistry and provide the natural particulate matter compounds. Biogenic NMVOC emissions are derived from the CORINE land use database which is combined with the distribution maps of 115 tree species over Europe (Köble and Seufert, 2001). During each simulation time step, biogenic isoprene and monoterpene emissions are calculated as a function of the biomass density and standard emission factor of the species or land use class (see Table 5 for most important types; full table see Schaap et al. (2009). Local temperature and photo-synthetically active radiation are used to calculate the hourly biogenic emissions by following the empirically designed algorithms proposed by Guenther et al. (1993) and Tingey et al. (1980). Our implementation of biogenic VOC emissions is very similar to the simultaneously developed approach by Steinbrecher et al. (2009).

The gas-phase chemistry is a condensed version of CBM-IV (Gery et al., 1988), with some modifications in reaction rates and can be found in (Manders et al., 2017). A kinetic pre-processor is used which makes it relatively straightforward to add or modify chemical reactions. In the current version of the model 38 chemical active tracers are calculated with 96 reactions. Photolysis rates are used in the CBM-IV chemistry scheme. Rates are calculated for each grid cell based on solar angle, radiation and cloud coverage. For 14 different tracers in the CBM-IV scheme: O_3, NO_2, N_2O_5, HONO, H_2O_2, HNO_3, NO_3 (2x), HCHO (2x), ALD, MGLY, OPEN and ISPD, off-line derived rates are used. Those rates are based on IUPAC (Atkinson, 1997; 1999) recommendations for different wavelengths. This gas phase mechanism also describes the photochemical gas phase formation of sulfuric acid and nitric acid.

The following heterogeneous chemistry process are included: sulphate production on wet aerosol surface (Wichink Kruit et al., 2012), in-cloud oxidation leading to formation of SO_4 from SO_2, while accounting for the pH of cloud

RI-URBANS (www.RIURBANS.eu) is supported by the European Commission under the Horizon 2020 – Research and Innovation Framework Programme, H2020-GD-2020, Grant Agreement number: 101036245

droplets (Banzhaf et al., 2012), heterogeneous H_2O_5 chemistry, and coarse mode nitrate formation on dust and sea salt particles. These processes are all calculated using mass transfer kinetics.

The thermodynamic SIA module implemented in LOTOS-EUROS is ISORROPIA-II (Fountoukis and Nenes, 2007) scheme. It is applied to calculate the temperature and relative humidity dependent thermodynamic equilibrium between gaseous nitric acid, sulphuric acid, ammonia and particulate ammonium nitrate and ammonium sulphate and aerosol water. Equilibrium between the aerosol and gas phase is assumed at all times. Note that the module is not applied to the coarse mode aerosol as these are externally mixed. Assuming an internal mixture would erroneously transfer a lot of the nitrate to the sea salt and mineral dust fractions.

For particle deposition, the scheme of Zhang et al. (2001) is used. The wet deposition module takes into account the saturation of water troughs (Banzhaf et al., 2012).

The runs are performed with meteorological data from the ECMWF model (European Centre for Medium-range Weather Forecasts).

Description of the SOA mechanism

Provide all necessary information on SOA formation: precursors, inclusion of IVOC, treatment of POA as SVOC, aging mechanism

The chemical transport model LOTOS-EUROS v2.3.000 uses a VBS scheme (Sturm et al., 2023). Primary organic material (POM) emissions are modeled using a 9-bin VBS approach: the logarithmically distributed bins represent semi- and intermediate-volatile organics with effective saturation concentrations ranging from 10^{-2}–10^{6} µg m $^{-3}$ at 298 K. The reported mass of primary emissions is distributed over the lower 4 volatility bins. As in previous work (Shrivastava et al., 2008), an additional 1.5 times this mass is distributed over the highest 5 volatility bins to represent non-reported intermediate volatility organic compounds (IVOCs).

The S/IVOCs undergo oxidation by the hydroxyl radical OH and enter the distinct siSOA VBS class. As material moves from the POA VBS to the siSOA VBS, it also moves to lower volatility bins. The total siSOA is represented by an 8-bin VBS using effective saturation concentrations from 10^{-2} to 10^{5} µg m^3 (defined at 298 K). Each bin uses two tracers, one aerosol and one gas, to represent the partitioning: this results in 18 tracers for the POA VBS class and 16 tracers for the siSOA VBS class. A kinetic of aging of 4.0E-11 $molecules^{-1}$ cm^3 s^{-1} is used. The aging step is assumed to lead to a decrease of volatility by a factor 10.

Formation of SOA from anthropogenic VOCs is represented with a 6-bin VBS class, defined using effective saturation concentrations of 10 $^{-2}$ to 10 ^{3} µg m $^{-3}$ at 298 K. This results in 12 tracers (6 in the gas phase and 6 in the particle phase). VOCs including aromatics, alkenes and alkanes are classified in LOTOS-EUROS as anthropogenic precursors of secondary organic aerosols and upon oxidation are distributed over the 4 highest volatility bins as done by (Tsimpidi et al., 2010), linearly interpolating between a low-NOx and high-NOx case as originally suggested by (Lane et al., 2008). A kinetic of aging of 1.0E-11 $molecules^{-1}$ cm^3 s^{-1} is used. The aging step is assumed to lead to a decrease of volatility by a factor 10.

An analogous 6-bin VBS class is used to model SOA formation from the biogenic VOCs in LOTOS-EUROS: monoterpene and isoprene. Yields from biogenic gaseous precursors are distributed over the 4 highest volatility bins according to Tsimpidi et al. (2010), with yields calculated by a branching ratio continuously dependent on NOx (Lane et al., 2008). Unlike the anthropogenic VBS class, ageing is turned off for the biogenic VBS in LOTOS-EUROS.

Correspondance to PMF

RI-URBANS (www.RIURBANS.eu) is supported by the European Commission under the Horizon 2020 – Research and Innovation Framework Programme, H2020-GD-2020, Grant Agreement number: 101036245

BBOA (name in output files: *tpoa_bioburn)*: all primary SVOC from biomass burning (not aged). Note that biomass burning contribution to POA has been derived from a separate model run in which emissions from anthropogenic residential combustion + wildfire were zeroed out, since the VBS in LOTOS-EUROS does not have a separate basis set for biomass burning OA. Note that this can lead to some inclusion of POA derived from coal burning in the BBOA in regions with heavy use of coal for domestic heating.

HOA (*tpoa_other*): all primary SVOC from other sources (not aged)

(sum of POA is also available as variable *tpoa*)

OOA (*tsoa*): anthropogenic + biogenic SOA compounds + aged POA species

8.1 References

Atkinson, R.: Gas-Phase Tropospheric Chemistry of Volatile Organic Compounds: 1. Alkanes and Alkenes, Journal of Physical and Chemical Reference Data, 26, 215–290, https://doi.org/10.1063/1.556012, 1997.

Banzhaf, S., Schaap, M., Kerschbaumer, A., Reimer, E., Stern, R., van der Swaluw, E., and Builtjes, P.: Implementation and evaluation of pH-dependent cloud chemistry and wet deposition in the chemical transport model REM-Calgrid, Atmospheric Environment, 49, 378–390, https://doi.org/10.1016/j.atmosenv.2011.10.069, 2012.

Fountoukis, C. and Nenes, A.: ISORROPIA II: a computationally efficient thermodynamic equilibrium model for K^+ - Ca^{2+} - Mg^{2+} - NH_4^+ - Na^+ - SO_4^{2-} - NO_3^- - Cl^- - H_2O aerosols, Atmospheric Chemistry and Physics, 7, 4639–4659, https://doi.org/10.5194/acp-7-4639-2007, 2007.

Gery, M. W., Whitten, G. Z., and Killus, J. P.: Development and testing of the CBM-IV (Carbon-Bond Mechanism) for urban and regional modeling. Final report, July 1985-June 1987, Systems Applications, Inc., San Rafael, CA (USA), 1988.

Guenther, A. B., Zimmerman, P. R., Harley, P. C., Monson, R. K., and Fall, R.: Isoprene and monoterpene emission rate variability: Model evaluations and sensitivity analyses, Journal of Geophysical Research: Atmospheres, 98, 12609–12617, https://doi.org/10.1029/93JD00527, 1993.

Köble, R. and Seufert, G.: Novel Maps for Forest Tree Species in Europe, in: A Changing Atmosphere, 8th European Symposium on the Physico-Chemical Behaviour of Atmospheric Pollutants, Torino, Italy, 7, 2001.

Lane, T. E., Donahue, N. M., and Pandis, S. N.: Effect of NOx on Secondary Organic Aerosol Concentrations, Environ. Sci. Technol., 42, 6022–6027, https://doi.org/10.1021/es703225a, 2008.

Manders, A. M. M., Builtjes, P. J. H., Curier, L., Denier van der Gon, H. A. C., Hendriks, C., Jonkers, S., Kranenburg, R., Kuenen, J., Segers, A. J., Timmermans, R. M. A., Visschedijk, A., Wichink Kruit, R. J., Van Pul, W. A. J., Sauter, F. J., van der Swaluw, E., Swart, D. P. J., Douros, J., Eskes, H., van Meijgaard, E., van Ulft, B., van Velthoven, P., Banzhaf, S., Mues, A., Stern, R., Fu, G., Lu, S., Heemink, A., van Velzen, N., and Schaap, M.: Curriculum Vitae of the LOTOS-EUROS (v2.0) chemistry transport model, Geoscientific Model Development Discussions, 1–53, https://doi.org/10.5194/gmd-2017-88, 2017.

Schaap, M., Manders, A., Hendriks, E., Cnossen, J., Segers, A. J., Gon, H., Jozwicka, M., Sauter, F., Velders, G. J. M., Matthijsen, J., and Builtjes, P. J. H.: Regional modelling of particulate matter for the Netherlands, 2009.

Shrivastava, M. K., Lane, T. E., Donahue, N. M., Pandis, S. N., and Robinson, A. L.: Effects of gas particle partitioning and aging of primary emissions on urban and regional organic aerosol concentrations, Journal of Geophysical Research: Atmospheres, 113, https://doi.org/10.1029/2007JD009735, 2008.

RI-URBANS (www.RIURBANS.eu) is supported by the European Commission under the Horizon 2020 – Research and Innovation Framework Programme, H2020-GD-2020, Grant Agreement number: 101036245

Steinbrecher, R., Smiatek, G., Köble, R., Seufert, G., Theloke, J., Hauff, K., Ciccioli, P., Vautard, R., and Curci, G.: Intra- and inter-annual variability of VOC emissions from natural and semi-natural vegetation in Europe and neighbouring countries, Atmospheric Environment, 43, 1380–1391, https://doi.org/10.1016/j.atmosenv.2008.09.072, 2009.

Sturm, P. O., Manders, A., Janssen, R., Segers, A., Wexler, A. S., and Lin, H. X.: Advecting Superspecies: Efficiently Modeling Transport of Organic Aerosol With a Mass-Conserving Dimensionality Reduction Method, Journal of Advances in Modeling Earth Systems, 15, e2022MS003235, https://doi.org/10.1029/2022MS003235, 2023.

Tingey, D. T., Manning, M., Grothaus, L. C., and Burns, W. F.: Influence of Light and Temperature on Monoterpene Emission Rates from Slash Pine, Plant Physiology, 65, 797–801, https://doi.org/10.1104/pp.65.5.797, 1980.

Tsimpidi, A. P., Karydis, V. A., Zavala, M., Lei, W., Molina, L., Ulbrich, I. M., Jimenez, J. L., and Pandis, S. N.: Evaluation of the volatility basis-set approach for the simulation of organic aerosol formation in the Mexico City metropolitan area, Atmospheric Chemistry and Physics, 10, 525–546, https://doi.org/10.5194/acp-10-525-2010, 2010.

Wichink Kruit, R. J., Schaap, M., Sauter, F. J., van der Swaluw, E., and Weijers, E.: Improving the understanding of the secondary inorganic aerosol distribution over the Netherlands., Tech. rep. Utrecht, The Netherlands: TNO, report TNO-060-UT-2012-00334., 2012.

Zhang, L., Gong, S., Padro, J., and Barrie, L.: A size-segregated particle dry deposition scheme for an atmospheric aerosol module, Atmospheric Environment, 35, 549–560, https://doi.org/10.1016/S1352-2310(00)00326-5, 2001.

RI-URBANS (www.RIURBANS.eu) is supported by the European Commission under the Horizon 2020 – Research and Innovation Framework Programme, H2020-GD-2020, Grant Agreement number: 101036245